ACTA FORESTALIA FENNICA

222

TUOMAS HÄME

SPECTRAL INTERPRETATION OF CHANGES IN FOREST USING SATELLITE SCANNER IMAGES

METSÄN MUUTOSTEN SPEKTRINEN TULKINTA SATELLIITTIKEILAINKUVIEN AVULLA

THE SOCIETY OF FORESTRY IN FINLAND
THE FINNISH FOREST RESEARCH INSTITUTE

ACTA FORESTALIA FENNICA

Acta Forestalia Fennica was established in 1913 by the Society of Forestry in Finland. It was published by the Society alone until 1989, when it was merged with Communicationes Instituti Forestalis Fenniae, started in 1917 by the Finnish Forest Research Institute. In the merger, the Society and Forest Research Institute became co-publishers of Acta Forestalia Fennica.

Prior of the merger, 204 volumes had appeared in Acta Forestalia Fennica, and 145 volumes in Communicationes.

PUBLISHERS – JULKAISIJAT

The Society of Forestry in Finland
Suomen Metsätieteellinen Seura r.y.
Unioninkatu 40 B, 00170 Helsinki
Tel. +358-0-658 707 Fax: +358-0-1917 619
Telex: 125181 hyfor sf

The Finnish Forest Research Institute
Metsäntutkimuslaitos
Unioninkatu 40 A, 00170 Helsinki
Tel. +358-0-857 051 Fax: +358-0-625 308
Telex: 121286 metla sf

AIM AND SCOPE – TAVOITTEET JA TARKOITUS

Acta Forestalia Fennica publishes dissertations and other monographs. The series accepts papers with a theoretical approach and/or of international interest. The series covers all fields of forest research.

Acta Forestalia Fennicassa julkaistaan väitöskirjoja ja muita monografiatyyppisiä kirjoituksia. Kirjoitusten tulee olla luonteeltaan teoreettisia ja/tai kansainvälisesti merkittäviä. Sarja kattaa metsäntutkimuksen kaikki osa-alueet.

SUBSCRIPTIONS AND EXCHANGE – TILAUKSET

Subscriptions and orders for back issues should be addressed to Academic Bookstore, P.O.Box 128, SF-00101 Helsinki, Finland. Subscription price is FIM 70 per issue. Exchange inquiries should be addressed to the Society of Forestry in Finland.

Tilaukset ja tiedustelut pyydetään osoittamaan Suomen Metsätieteelliselle Seuralle. Tilaushinta Suomeen on 50 mk/numero. Seuran jäsenille sarja lähetetään jäsenmaksua vastaan.

ACTA FORESTALIA FENNICA 222

SPECTRAL INTERPRETATION OF CHANGES IN FOREST USING SATELLITE SCANNER IMAGES

Metsän muutosten spektrinen tulkinta satelliittikeilainkuvien avulla

Tuomas Häme

To be presented, with the permission of the Faculty of Agriculture and Forestry of the University of Helsinki, for public criticism in Auditorium XII of the University Main Building, Fabianinkatu 33, on 27 March 1992, at 12 o'clock noon.

The Society of Forestry in Finland — The Finnish Forest Research Institute
Helsinki 1991

Häme, T. 1991. Spectral interpretation of changes in forest using satellite scanner images. Seloste: Metsän muutosten spektrinen tulkinta satelliittikeilainkuvien avulla. Acta Forestalia Fennica 222.111 p.

Spectral characteristics of rapid changes in forest and the spectral separability of change categories were studied through the analysis of satellite scanner images. A computational model of the spectral reflectance of a pine stand as a function of time was constructed and compared with empirical data. The study area, centered at 61°51' N, 24°22' E, was located in boreal forest in Southern Finland. Ground truth data consisted of forest stands and sample plots. Spectral data comprised multitemporal Landsat Thematic Mapper and Spot images as well as spectroradiometer measurements. The separability of the changes was tested with statistical tests and classifications. The separability varied according to the change category. A scheme for fully automated change monitoring system was presented.

Tutkittiin metsässä esiintyvien nopeiden muutosten spektrisiä ominaisuuksia sekä muutostyyppien spektristä erottuvuutta satelliittikeilainkuvien avulla. Laadittiin laskennallinen malli männikön heijastussuhteesta ajan funktiona ja verrattiin mallia kokeelliseen aineistoon. Tutkimusalue, jonka keskipiste oli 61°51' N, 24°22' E, sijaitsi Pohjois-Hämeessä. Maastoaineisto käsitti metsiköitä ja relaskooppikoalaoja. Spektrinen aineisto koostui Landsat Thematic Mapper- ja Spot-kuvista sekä spektroradiometrimittauksista. Muutosten erottumista tutkittiin tilastollisilla testeillä ja luokitusten avulla. Erottuvuus vaihteli muutostyypeittäin. Esitettiin täysin automaattisen muutosten seurantamenetelmän peruspiirteet.

Keywords: remote sensing, forests, changes, satellite image, interpretation.
FDC 585

Author's address: VTT (Technical Research Centre of Finland), Instrument Laboratory, Itätuulentie 2 B, SF-02100 Espoo Finland; tel. + 358 0 4561, fax + 358 0 456 4496, e-mail (Internet) hame@ins.vtt.fi

ISBN 951-651-092-2
ISSN 0001-5636

Tampere 1991. Tammer-Paino Oy

Contents

PART II

Symbols and abbreviations

Age	Mean age of the trees (years) using basal area as the weighing factor.
Basal area	Basal area of the stems (m^2/ha). Measured from the height of 1.3 m.
Density	Number of trees higher than 1.3 m/hectare.
Diameter	Mean diameter (cm) at the height of 1.3 m using basal area as the weighing factor.
Height	Mean height of the trees (m) using basal area as the weighing factor.
H0:	Null-hypothesis. Context tells which of the following hypotheses has been applied: H0: $r = 0$, H1: $r \neq 0$, where r is the correlation coefficient H0: $a = 0$, H1: $a \neq 0$, where a is the parameter
MIR	Middle infrared radiation
NFI	National Forest Inventory
NIR	Near infrared radiation
Red	Red light
SSI87	Spot HRV1 three channel image. Date of acquisition July 20, 1987.
SS1	Channel 1 of the multichannel Spot summer (SSI87) image. Spectral range 0.50—0.59 μm.
SS2	Channel 2 of the multichannel Spot summer (SSI87) image. Spectral range 0.61—0.68 μm.
SS3	Channel 3 of the multichannel Spot summer (SSI87) image. Spectral range 0.79—0.89 μm.
SWI87	Spot HRV1 three channel image. Date of acquisition March 11, 1987.
SW1—SW3	Like SS1—SS3 but from the Spot winter image.
TM	Landsat Thematic Mapper
TMI84	Landsat Thematic Mapper image. Date of acquisition September 15, 1984.
TMI85	Landsat Thematic Mapper image. Date of acquisition June 21, 1985.
TMI86	Landsat Thematic Mapper image. Date of acquisition June 17, 1986.
TM1	Channel 1 of the Thematic Mapper of the Landsat satellite. Spectral range 0.45—0.52 μm, blue-green light. The two optional numbers after the channel number refer to the special image — e.g. TM184 means channel 1 of the TMI84 image.
TM2	Channel 2 of the Thematic Mapper of the Landsat satellite. Spectral range 0.52—0.60 μm, green light.
TM3	Channel 3 of the Thematic Mapper of the Landsat satellite. Spectral range 0.63—0.69 μm, red light.
TM4	Channel 4 of the Thematic Mapper of the Landsat satellite. Spectral range 0.76—0.90 μm, near infrared radiation.
TM5	Channel 5 of the Thematic Mapper of the Landsat satellite. Spectral range 1.55—1.75 μm, middle infrared radiation.
TM6	Channel 6 of the Thematic Mapper of the Landsat satellite. Spectral range 10.4—12.5 μm, thermal radiation.
TM7	Channel 7 of the Thematic Mapper of the Landsat satellite. Spectral range 2.08—2.35 μm, middle infrared radiation.
*	The H0 is rejected with the significance level of 5.0 percent.
**	The H0 is rejected with the significance level of 1.0 percent.
***	The H0 is rejected with the significance level of 0.1 percent.

TERMS

Bitemporal	Data or information from two dates.
Changed	Change that is not "normal", i.e. growth or seasonal variations, has occurred in the forest. Possible other meanings should become clear from the context.
Image	Single or multichannel numerical image. Also, analogous image from numerical data.
Imagery	Multichannel image. Used only if context requires emphasizing that image has several channels.
Intensity, Intensity value	The numerical value of a pixel in one wavelength channel.
Irradiance (E) (Spectral irradiance)	E_λ (W/m^2) Radiant flux incident upon a surface per unit area of that surface. Subscript λ indicates that the irradiance depends on the wavelength.
Monotemporal	Data or information from a single date.
Multitemporal	Data or information from more than a single date.
Overall performance	Proportion of observations (e.g. test stands or plots) which are placed in image classification to their true class, from the total number of tested observations in percent.

Pixel — Picture element, smallest unit of a digital image.

Radiance (L) (Spectral radiance)

L_λ ($W/sr/m^2$) Radiant intensity per unit of projected source area in a specified direction. Subscript λ indicates that the irradiance depends on the wavelength.

Reflectance (R) (Reflectance factor)

$$R = \frac{L_\lambda}{E_\lambda} \cdot 100 = \frac{\text{Radiance}}{\text{Irradiance}} \cdot 100$$

The word reflectance is used to mean the reflectance when measured in nadir or close to nadir (reflectance factor) and not the hemispherical reflectance where the reflected radiation is registered from hemisphere. Subscript λ indicates that the irradiance and radiance depend on the wavelength.

Satellite image — Satellite image acquired using a scanner-type instrument.

Stand — Smallest area unit in forest management. Relatively homogeneous in respect to the main stand variables.

Tritemporal — Data or information from three dates.

Unchanged — Seasonal changes and growth. Other meaning should become clear from the context.

Undergrowth — Field layer (dwarf shrubs — *Vaccinium* spp., *Calluna* spp., *Empetrum* spp. — and herbaceous plants) plus Bottom layer (mosses, lichens, debris, soil)

Visible light — Electromagnetic radiation, wavelength 0.4 — 0.7 μm

Preface

This study began as a subproject of "Stand Based Forest Inventory Using Satellite Images", a project carried out by the Technical Research Centre of Finland (VTT) in 1984—1988. It was later continued as part time and spare time work at VTT and at the Computer Graphics Center of North Carolina State University.

Professor Simo Poso and Assoc. Prof. Risto Päivinen carefully read several versions of the manuscript, giving constructive criticism, and so did Dr. Erkki Tomppo who also helped in processing the National Forest Inventory (NFI) data.

Professor Kullervo Kuusela and M. Sc. (For.) Antti Ihalainen from the Finnish Forest Research Institute (FFRI) organized the remeasurement of the NFI sample plots. The staff at the Korkeakoski district of the National Board of Forestry provided the stand material for the study. M. Sc. (For.) Pekka Alajärvi measured the field plots for the damage study and also prepared the measurement data for analysis. Professor Timo Kurkela and his staff at FFRI provided seedling material for the spectroradiometer measurements.

My dear colleagues at VTT helped in very many ways: Mrs. Brita Veikkanen performed a major part of the computer operation, Dr. Arto Salli and Lic.Tech. Kai Mäkisara advised in statistical analysis, M. Sc. (Tech.) Eija Parmes in image segmentation and clustering, Mr. Markku Rantasuo helped in spectroradiometer measurements, and Lic. Tech. Yrjö Rauste, Mrs. Elma Paulakannas, and Mrs. Hillevi Nikka gave miscellaneous help. During 1989, I enjoyed the company of Prof. Siamak Khorram and his staff in North Carolina. The following individuals also adviced me in my work: Assoc. Prof. Thomas Burk, Prof. Pertti Hari, Dr. Antti Uotila, B. Sc. Floyd Whitley, and Lic. Phil. Hannu Rita. Mrs. Aila Bolton patiently and carefully proofread the English.

During this study I have obtained funding from many sources: Ministry of Agriculture and Forestry, Foundation for Research of Natural Resources in Finland, National Board of Forestry, Central Union of Agricultural Producers and Forest Owners, Forestry Center Tapio, Central Association of Finnish Forest Industries, The Academy of Finland, and VTT; Niemi Foundation and Finnish Culture Foundation have given personal stipends for the study.

I want to give my warmest thanks to all the people and organizations, mentioned above or not, who have advanced this study.

I dedicate this book to Riitta, Yrjö, Lauri, and Juho who all had an influence — the type varying according to their age — on this work having finally been completed.

Helsinki, December 1991
Tuomas Häme

1. Introduction

1.1 The need to detect changes and the use of satellite images

Vegetative succession is the basic natural phenomenon that changes biomass and plant species proportions. Growth bed and climate create the circumstances for the succession, defining which plant species can survive and the potential productivity of the ecosystem. Basic growth factors usually change very slowly (cf. Siren 1955). Biomass growth through succession is a more rapid change. Manmade and natural disasters affect succession, causing rapid changes or disturbances. The most rapid and dramatic change caused by man is clear cutting which initiates succession. In unmanaged forests, fire, storm, animals, and fungi cause changes analogous to those manmade. These natural disturbances exist in managed forests as well, but some natural disturbances, such as fire, are less significant than in natural forests.

Not all forestry related changes occur within forests. A portion of forest is used for other purposes, e. g. building, road construction, gravel pits, and water reservoirs. In many areas of the world, forest is being converted to agricultural land. In Finland, however, some agricultural land is reverting to forest.

Forestry needs information about general growing conditions, forest resources and their changes. Information on the changes is needed to keep the resource data updated and to understand the dynamics of the forest ecosystem. Change information is needed about all characteristics included in a basic inventory. As stated above, the time span of the changes varies. Some changes are predictable. For example, forest growth can be estimated computationally. But to take into consideration rapid, disturbance-type changes, new information is needed to update the forest management system.

Forestry planning requirements can be roughly divided into two categories: strategic planning and operational planning. A typical inventory for strategic planning is a national forest inventory. A typical inventory for operational planning is a stand based inventory for a specific forest management plan. Primarily, strategic planning needs reliable statistics on forest resources, their development, and condition of the forest. For operational planning, statistics are not enough. A stand map is needed and stand characteristic values must be reliable enough for each individual stand to make a correct treatment decision possible. The two planning categories set different requirements for the inventory design, including the inventory of change.

In national forest inventories, change has been seen indirectly by comparing results of successive inventories. Making a map of the change and traditional forest variable values may not be only for operational planning, however. Map type information about damage and natural changes, for example, may help to know the whole forest ecosystem better. This is becoming more important because of increasing concern about pollution and possible global climate change.

During past decades, changes in forest stands were found by using successive inventories, even in operational planning. Between two inventories, some notes about the changes may have been available. Since the 1980's, digital map systems and digital databases have become more commonplace. Total inventory can be taken less often than before due to the updating capabilities of digital map systems. In the new systems, stand files should be updated through field crew reporting. The risk in this procedure is that the reporting may not be reliable. Therefore, a control system may be needed to check the accuracy of the field crew's procedures. Furthermore, reliable mapping of changes due to damage may be very difficult using the field crew reporting system.

Satellite scanner images are a possible source of change detection data, since their intensities and forest characteristic values are related (e.g. Kuusela and Poso 1970, Saukkola and Jaakkola 1983, Häme 1984a, Poso et al. 1984 and 1987, Peng 1987, Tomppo 1988). It has been possible to detect some changes in forest by using satellite data (Wastenson et al. 1981, Saukkola 1982).

Satellite images with reasonable spatial

resolution (80 m by 80 m pixel size, in respect to the normal stand size) have been available since 1972 when Landsat 1 was launched. The special benefits of images from natural resources satellites are that they regularly contain full coverage data from a wide area, they include information invisible to the human eye, they are in digital format, and their price per unit area is low.

There are drawbacks to using these images. The natural resource must be monitored indirectly through interpretation of the reflected or emitted electromagnetic radiation from the target, and the radiation is affected by the atmosphere between the target and the instrument. Another drawback is the moderate spatial resolution, a 10 meter pixel size at best. Interpretation methods for numerical images have been, thus far, so poorly developed that, in reality, the spatial resolution has not been a restrictive factor. The 30 m by 30 m pixel size of Landsat Thematic Mapper (TM) images and the 20 m by 20 m pixel size of multichannel Spot images have been adequate. A very high spatial resolution requires advanced contextual interpretation. New factors, for example the wind, must be taken into account in change interpretation if the resolution unit is very small.

The decrease in the pixel size and the increase in spectral resolution from Landsat multispectral scanner (MSS) images to Landsat TM images has increased the correlation between images and forest characteristics (Poso et al. 1987).

The Landsat Thematic Mapper instrument also has better radiometric resolution than the Landsat MSS instrument, i.e. its sensitivity is higher (Dottavio and Dottavio 1984). But it is unclear, how much the radiometric resolution has really increased, especially in northern latitudes where the incident radiation is weak.

1.2 Aim and definitions

The basic aim of the study is to discover the spectral characteristics of the most interesting and common short time period or rapid changes in forest and the separability of change categories through the numerical analysis of satellite scanner images. Six change types occurring in Finnish boreal forest will be studied. Four of them represent manmade treatments, or "controlled" changes: 1) clear cuttings; 2) selective thinning cuttings; 3) soil preparation for regeneration on clear cut areas; and 4) deciduous shrub removals and/or conifer seedling thinnings on regeneration areas. Changes occurring without manmade treatments, or "uncontrolled" changes, are: 5) pine damage caused by the *Gremmeniella abietina* (Lagerb.) fungus; and 6) deciduous shrub growth on regeneration areas.

The changes to be studied occur in all phases of the rotation period of a stand. New information about the spectral properties of changes will also provide new information about the spectral properties of boreal forest stands in general. These properties have not been discussed extensively in previous studies.

Spectroradiometer measurements of needles will be used to support the satellite image investigation. Needles are an essential source of radiance from coniferous forests.

The focus of the study is on the informational needs of forestry; spectral variation caused by seasonal changes is not of particular interest. Special attention is given to changes where spectral effects are most likely to be minor. Of the six change types listed, all except clear cuttings are such changes. In addition to spectral data, topographical variables will be tested to determine if they could be used as supporting data in damage estimation.

Because the study concentrates on investigating the spectral properties of changes, a cost-benefit analysis of the satellite image oriented method is excluded. How well the form of the changed areas can be interpreted will not be addressed, either.

Part I of the study is directed to achieve the fundamental goal. Part II is a brief discussion about how a satellite image based change monitoring system should be constructed.

PART I

2. Theoretical background of spectral change detection

2.1 General prerequisites to detect and measure changes

Forest canopies are under a constant state of change. Long-term change is growth. Short-term change is seasonal. Typically, in forestry, one is interested in measuring and estimating growth of the stem volume and in detecting and measuring rapid "exceptional" changes, i.e. non seasonal changes.

Detection and measurement of growth requires very precise measurements if the time span is short. Conversely, growth can be coarsely estimated visually if the time span is several decades.

Opportunities to detect rapid changes are largely opposite to the detection of growth. Successive observations with short time spans increase the possibility to detect a rapid change.

Clear cutting decreases the biomass of living trees greatly, possibly to 0 m^3/ha. The change in the biomass is most dramatic because stands with the highest biomass stands are cut. In thinning cutting, the drain in wood is less than in clear cutting. The trees are in a faster growing phase than the mature trees of a clear cut stand, and the trees from the lower crown layer, in particular, are removed. Trees that are left fill the empty space rapidly, and the growth in stem volume after the thinning may exceed the growth before it. In the growth conditions of Central Europe, stands have reached within 3 to 5 years the level of stem volume that existed before the thinning, if the thinning was light (Assman 1970).

For instance, the drain in a thinning cutting may be 40 m^3/ha, and the growth of the stand may be 40 m^3/ha in a three year period from the cutting. To detect the cutting, the stand's stem volumes from the two dates can be compared to stem volumes of other stands.

Cutting detection and drain estimation can be used to update forest inventory data and to determine whether the treatments have been made as planned.

Soil preparation on regeneration areas (plowing or harrowing) barely changes the tree biomass, but destroys temporarily other living vegetation. Also, light colored mineral soil is found under the humus layer. The color changes and decrease in undergrowth are short term changes, the duration depending on the extent of the soil preparation, site type, and the latitude. The changes in local topography last longer.

Deciduous shrub removals on regeneration areas and/or conifer seedling thinnings are comparable to the thinning cuttings. If the deciduous shrub canopy is abundant, changes in tree species proportions may be more radical than in thinning cuttings. The detection of soil preparation and shrub removal serve to control whether the treatments have been successful.

The *Gremmeniella abietina* (Lagerb.) fungus, also known as *Scleroderris* canker, *Scleroderris lagerbergii* (Gremmen) and *Ascocalyx abietina* (Lagerb.), may be the most serious conifer disease in the boreal and temperate forests (Sterner 1984, O'Brien 1984, Gibbs 1984, Yokota 1984, and Kurkela 1984a). Most northern *Pinus* species, and also some *Picea* species, are susceptible to the disease which is also capable of infecting species of *Abies*, *Larix*, *Tsuga* and *Pseudotsuga* (Gibbs 1984). The fungus kills young shoots with the most actively assimilating needles, and also blocks the xylem and phloem through canker formation (Kurkela 1984a).

Kurkela (1984b) has noticed that the potential susceptibility of the host to an attack of *Gremmeniella* is a primary requirement for the development of serious epidemics. The climatic conditions in the topographic depressions are the most favorable for *Gremmeniella*; consequently they suffer the worst damage. Pine stands on sites with unbalanced mineral nutrition and fine-textured soils have also been especially susceptible. Tests have been done to determine whether acid rain increases susceptibility to the disease, but the results have not confirmed any clear relationship (Bragg and Manion 1984, Barklund et al. 1984).

The most striking symptom of *Gremmeniella* damage is the browning of affected needles in the beginning of the growing season in June. The color often turns to grayish-brown,

Fig. 1. Typical Gremmeniella damage in a *Pinus sylvestris* L. stand.

and in July the dead needles begin to fall. In the next growing season, only a few of the dead needles are left. The needle-free dead branches often get a thick cover of lichens, especially *Hypogymnia physodes* (L.) W. Wats. The damaged trees may look quite light in color when viewed from above, e.g. from an aircraft, because of the lichen. The damage starts usually from the lower parts of the crown, and in severe cases, spreads up to the whole tree and kills it (Fig. 1).

Both climatic conditions unfavorable to conifers and the presence of a lot of sexual spores are prerequisites for an extensive epidemic. In 1982, 1985, and 1988 epidemics occurred in Finland. The 1982 epidemic was the worst of the three, and the 1988 epidemic was the lightest (Uotila 1988). All these epidemics were in Scots pine (*Pinus sylvestris* L.) forests. The spruce trees have been damaged only occasionally.

The damage is easiest to detect and identify during an epidemic because of color change in the needles. At that time, one observation date is adequate to delineate the damaged areas of a particular epidemic in the field. Two observations on separate dates are needed if it is not possible to make an inventory during the epidemic. If a single observation is made two to three years after the last epidemic, it is hard to tell which part of the damage has occurred within a certain period of time.

Trees recover from the damage depending, among other things, on the extent of the damage. The larger trees may be noticeably brown due to the *Gremmeniella* damage in June, but recover very well. Obvious signs of a light damage may disappear within a couple of years. A very heavy damage could be noticed for several decades after the trees have died. Often, however, man interferes with the evolution of the damaged areas. The lighter the damage in which one is interested, the shorter the time span that should be used. The damage can be detected best if needle mass estimates from a greater number of field plots, stands, or larger areas are compared. The data set should include both obviously damaged and undamaged forest.

Detection of damage is important to treatment plans and correct growth estimates. It has more general ecological interest, too.

Deciduous shrub growth is a special case of general forest growth. Both the relative increase in biomass and the growth in height may be very fast after a clear cutting. Information about the growth rate shows which areas and soils are likely to get extensive shrub canopies, and helps to focus silvicultural treatments optimally. Growth rate of shrubs is difficult to estimate using a single observation. The growth in height is easy to estimate using successional measurements, but estimating the growth in biomass is difficult. Deciduous shrubs have normally been estimated visually. The optimal time span to detect deciduous shrub growth is somewhat longer, 5 to 10 years, than the time span for the other changes studied.

In this study, plots, stands, and areas with seasonal changes and growth only are called "unchanged". The areas with rapid change and deciduous shrub growth are called "changed".

2.2 Sources of intensity change

The intensity of a pixel of a satellite image can be expressed as:

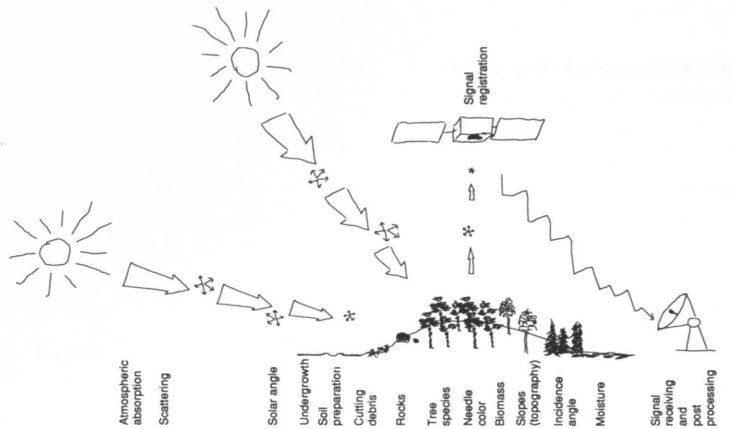

Fig. 2. Possible sources of intensity changes in multitemporal satellite data.

$$\text{Intensity} = f(R_{e\lambda}, T_{e\lambda}, A_{e\lambda}, \text{Area}_{e\lambda}, \text{Mass}_{e\lambda}, \text{Ov}_{e\lambda}, \text{Oh}_{e\lambda}, \text{Sun}_{\lambda}, \text{View}_{\lambda}, \text{Atm}_{\lambda}, \text{Sensor}_{\lambda}, \text{Proc}) \quad (1)$$

where

$R_{e\lambda}$	is reflectance or emittance of element e of the canopy
$T_{e\lambda}$	transmittance of element e of the canopy
$R_{e\lambda}$	absorptance of element e of the canopy
$\text{Area}_{e\lambda}$	area of the reflecting element within a pixel
$\text{Mass}_{e\lambda}$	mass of the element
$\text{Ov}_{e\lambda}$	vertical orientation of the element
$\text{Oh}_{e\lambda}$	horizontal orientation of the element
Sun_{λ}	sun position (elevation and azimuth)
View_{λ}	viewing angle
Atm_{λ}	atmospheric impact
Sensor_{λ}	sensor characteristics
Proc	data processing
λ	indicates that the significance of the factor is dependent on the wavelength

The sources for an intensity change in a pixel can be grouped into four categories (Fig. 2):

1) Relationship between the reflecting and emitting elements of plant canopy
2) Angles between illumination source, canopy and sensor
3) Atmosphere
4) Signal registration and processing

In vegetation studies, only the first category is of interest; the other categories are disruptive.

2.2.1 Relationship between the reflecting and emitting elements

Even each 10 m by 10 m pixel of a panchromatic Spot satellite image contains several tree crowns in a normal boreal forest. If the forest canopy is not closed, the intensity of a pixel is a function of the radiance from the undergrowth, possibly bare soil, rock and cutting debris, tree stems and branches, and the leaves.

Vegetated surfaces have typically a low visible light reflectance and high near infrared reflectance. The reflectances of blue-green light and red light are lower than the reflectance of green light, due to absorption by chlorophylls and other plant pigments (Gates 1970). The reflectance of red light decreases and the reflectance of the near infrared radiation usually increases with increasing biomass (Tucker et al. 1975, Tucker 1979). Conifers, however, have different spectral properties. Growth in the conifer forest must decrease the reflectance in all wavelengths, including the near infrared range, since the correlation between tree stem volume and near infrared is negative (Colwell 1974; Saukkola 1977; Poso et al. 1988).

The reflectance of non-vegetated surfaces and the non-green parts of vegetation typically increases monotonically when the wavelength changes from the green light to the near infrared. The increase was linear from 540 nm up to 1000 nm in a study by Ritari and Saukkola (1985). In the same investigation, the red light reflectance of the A horizon of the podsolized soil in normal moisture was approximately 2.5 times the reflectance of the undergrowth of medium rich site type. The near infrared reflectance of the soil was approximately 0.75 times the reflectance of the undergrowth.

2.2.2 *Angles between irradiance, target and sensor*

Shadows

The existence of shadows, i.e. parts of the image that have received diffuse radiation only, indicates that some object has blocked the radiation. The object has either reflected or absorbed the radiation. There has been no transmittance or it has been very limited.

Proportion of the shaded area in an image is the function of the solar elevation, solar azimuth angle, viewing angle, vertical size and vertical distribution of the geometrical objects, spatial distribution of the objects, and the spectral transmittance of the objects. A decrease in the solar elevation angle, which also means an increase in the angle between the sensor and the sun, increases the proportion of the shaded area in the image, when the observations are made from nadir. Increase in the topographic variation, which can be caused by either the ground topography, manmade objects, or plants, increases the proportion of the shaded area in the image.

Stands with an uneven tree crown surface have more shaded area than stands with an even tree crown surface. Norway spruce (*Picea abies* (L.) Karst.) is an example of a tree species that forms a relatively uneven crown surface layer in an evenly aged stand as well. Many deciduous trees form an even upper surface in the stand. A change in the canopy that increases the roughness of the surface increases the amount of shadows and decreases the reflectance. Such a change can be a thinning cutting or a storm damage.

Changes that increase the roughness of the canopy surface usually also decrease needle or leaf mass. Decrease in the assimilating biomass tends to increase the visible light reflectance. The effect is opposite to that of the roughness. In the near infrared range, decrease in the leaf mass should decrease the reflectance (Gates 1970). The leaf mass change should reinforce the roughness effect.

Shadows have less meaning in the visible light range than in the near infrared range, due to greater scattering of the shorter wavelengths. However, the partial transmittance of tree crowns decreases the impact of shadows in the near infrared range (Colwell 1974).

To conclude, if two stands have the same tree species, same spatial distribution of trees, and same needle mass, the stand with a rougher crown surface structure should have lower reflectance both in the visible and near infrared parts of the spectrum. If the needle mass in the stand with a rougher crown surface is slightly lower, the red light reflectance can be similar. The near infrared reflectance is still likely to be lower. If the canopy is still sparser, the absorptance of the near infrared may decrease, causing an increase in the reflectance. Thus, the near infrared reflectance will first decrease and then increase.

Azimuth angle change relocates the slope shadows. For example, the azimuth angle of the sun is different in Landsat TM and Spot images, since Spot images (vertical) are acquired two hours later than the TM images.

Penetration of the radiation

Not only the shadows but also the form of conifer crowns may cause a reflectance change when the elevation angle of the sun changes. This is due to both the partly specular reflectance properties of the conifers and the amount of tree biomass that receives the incident radiation. Incident radiation with a low elevation angle confronts potentially more tree biomass than the radiation from close to the zenith. However, the power of the low elevation angle radiation is lower than the high angle radiation, due to absorptance by the atmosphere. Decrease in power decreases the transmittance. Also, the penetration properties and reflection properties depend also on the wavelength. For example, the near infrared radiation penetrates the canopy much deeper than the visible light does (Gates 1970, Colwell 1974, Oke 1987).

According to Guyot and Riom (1988), shadows dominate the poorly-penetrating visible light reflectance of forests when the solar elevation is low. The reflectance is low. Near infrared reflectance should be high due to high transmittance and low absorptance. Guyot and Riom's deduction is based on the spectral measurements of crops. Wastenson et al. (1988) state that conifer crowns, especially spruce crowns, are so deep that the near infrared radiation scarcely reaches the ground even when the incident radiation comes from near the zenith. Therefore, the near infrared reflectance is not higher with low solar elevation angles.

Kleman (1986) has measured the reflectance factor of a Scots pine stand in June and September in Sweden. The reflectance factor of red light (channel center 0.68 μm) in September was 80 percent of the reflectance factor in June. The measurements were made from nadir. The respective percentages were 97 percent in the near infrared range (0.85 μm) and 79 percent in the middle infrared range (1.6 μm). Kriebel (1978) has obtained similar results in coniferous forests. In fir (*Abies*) forests, Ranson et al. (1986) also obtained similar results, especially with red light reflectance, which decreased when the solar elevation angle decreased.

A general conclusion about solar angle and reflectance relations is that the reflectance of a conifer stand, with a low solar elevation angle, can be less than 80 per cent of the reflectance with a high solar angle in the visible and middle infrared part of the spectrum. In the near infrared range, the reflectance with low and high solar angles is similar. Research in this topic has been relatively limited.

Viewing angle

Several authors (Kalensky and Wilson 1975; Kadro and Hildebrant 1980; Kimes et al. 1981; Wastenson et al. 1988) have reported how the reflectance factor drastically changed when the viewing angle changed. On most surfaces, the reflectance increases in off-nadir observation. The increase is larger in the visible than in the near infrared area of the spectrum. The reflectance of barley in back light illumination and with a 45 degree sensor angle has been approximately 2.4 times the reflectance to nadir in red light and 1.8 times in near infrared. In front light illumination, the ratio has been 1.4 and 1.3 times, respectively. The solar elevation angle was 38 degrees (Nilson and Kuusk 1989). With conifers, however, the reflectance has decreased in front light illumination, until the tilting angle from zenith is 50 degrees (Kalensky and Wilson 1975; Kriebel 1978). In Swedish studies with a 20 degree viewing angle (Kleman 1986), the lowest reflectance was approximately 90 percent of the reflectance to nadir in front light illumination. When the instrument was tilted 45 degrees from the sun, the reflectance of a spruce stand nearly doubled both in the near infrared and red range. The reflectance of a pine stand increased less, being 1.5 times in red light and 1.3 times in the near infrared of the reflectance to nadir. The solar elevation angle was 50 degrees.

The reasons for the reflectance changes in different viewing angles are the proportion of the shaded area visible to the sensor and the specular reflectance characteristics of the canopies.

The observation angles of the Landsat TM and Spot HRV instruments are so narrow that the spectral effect of the angles is small. Duggin et al. (1985) have found 10 percent higher front light than back light intensities on similar surfaces on the extreme edges of a whole Landsat TM scene (185 km x 185 km). The viewing angle effect should be taken into account if the most oblique viewing images of the Spot satellite are used.

2.2.3 *Atmosphere, signal registration and processing*

Atmosphere

Atmospheric gases, aerosols and dust cause radiation absorption and scattering. Some wavelengths (e.g. 1.4 μm and shorter than 0.3 μm) are absorbed entirely before they reach the sea level. Scattering increases exponentially when wavelength becomes shorter (Manual of Remote Sensing, Vol. I 1983). Atmospheric absorption and scattering cause the original spectral signal, reflected or emitted from the target, to change. The intensity differences become smaller. Increase in the amount of moisture or dust in the air will increase scattering. Thus, if the first observation is made in clear and dry conditions and the second in moist and dusty conditions, the intensities of the low and medium reflectance objects increase although no field changes have occurred. (Assume that the power of the irradiance is the same). The increase in the radiance by scattering is very prominent. The radiance of blue light has been five times as high at the altitude of 14.9 km as at the altitude of 0.92 km. The radiance of red light has been three times as high (Manual of Remote Sensing, Vol. I 1983).

Scattering changes the illumination of the target, too. Heavily scattered radiation (short wavelengths) reaches the whole canopy evenly whereas the amount of longer wavelength radiation (near infrared) is low in shadowed areas.

Signal registration

The Landsat Thematic Mapper sensor has 16 detectors in the flying direction, which means that 16 lines are scanned simultaneously (Landsat 4 data... 1984). Spot has only one row of detectors, but the row consists of four side-by-side detector blocks. It is difficult to calibrate detectors so that the same level of incident radiation gives the same output. The calibration differences cause systematic intensity variation, or striping, to the image. The differences have been adjusted in the data that are delivered to users. However, the errors caused by the sensor block differences were noticeable, particularly in earlier panchromatic Spot images. It has been reported that the problem is being solved with better image calibration (Courtois 1988).

Signal processing

Further signal processing and transmission can cause intensity variation that is not as systematic as the striping, i.e. the sequence of the variation is not constant. That kind of variation, which was apparent in earlier Spot images, is harder to correct than the ordinary striping.

If one is interested in possible field changes between image acquisitions, the images must be connected to the same coordinate system. The basic geometrical correction of an image is normally made in the receiving station, using the track parameters of the satellite. A precise correction or rectification to the map coordinate system needs control points which are selected from the map and the image. Using the control points, a rectification model is constructed (Hirvonen 1971). A new, rectified or geometrically corrected image can be computed by applying the model.

In the rectified image, the true location of a pixel is not exactly the same as the computed location. The shift from the true location is due to: 1) measurement errors in the control points; 2) a difference between the applied model and reality; and 3) the pixel shift that is caused by pixel resampling.

In multitemporal data sets, the detector calibration errors and signal transmission and processing cause intensity changes that have nothing to do with field changes. The atmosphere, image acquisition, and changes related to processing generate image noise and do not usually form uniform areas, or at least not areas which resemble forest stands. Some cloud types may, however, be confused with clear cuts (Saukkola 1982). Cloud shadows may look similar to lakes in visual inspection, but confusion rarely exists in numerical interpretation with multiple spectral channels.

2.3 Computational model of "spectral life cycle" of a stand

The available information about the spectral properties of different elements of canopies are applied to compute a simplified model of the reflectance of a pine stand during its life cycle (Table 1, Fig. 3a and b). Some coarse assumptions have been made. The basic assumption is that the weight of an element is the area of that element as viewed from above. The transmittance of the leaf canopy and the reflectance of elements under the leaves have not been properly taken into consideration. The model includes only the summer seasonal aspect. The reflectance is assumed as being measured from nadir. The shadows in the canopy have been taken into account indirectly since reflectance data from whole pine stands were available (Saukkola 1977). The reflectance is computed:

$$R(k) = \sum_{i=1}^{n} w_i \cdot R_i(k) \qquad (2)$$

where

- $R(k)$ is reflectance of a canopy type in channel k
- w_i proportion of element i of the canopy of the total area
- $R_i(k)$ reflectance of element i in channel k
- n number of elements

The applied reflectances of the canopy elements (Table 1) are selected subjectively with the help of literature (Saukkola 1977; Kilpelä et al. 1978; Häme 1984b; Ritari and Saukkola 1985 and Tucker 1980; Rautiainen and Päivinen 1990; and Peterson 1989) and should be regarded as examples of likely reflectances. Also, the proportions of the reflecting elements are examples only.

In the red light range, the model is very sensitive to the proportion of bare soil due to its high reflectance which is three times as high as the reflectance of the pines. In the near infrared radiation range, deciduous trees, grass, and herbaceous vegetation have

Table 1. Computation of reflectances of different canopy types.

Time	Canopy type	Pine		Deciduous tree		Dry needles		Dwarf shrubs, moss		Grass, herbs		Soil		Reflectance of the canopy	
		w	Refl. R / NIR	w	Refl. R / NIR	w	Refl. R / NIR	w	Refl. R / NIR	w	Refl. R / NIR	w	Refl. R / NIR	R	NIR
0.9, 90.0	Mature pine	0.90	4 / 30	0.05	4 / 55	0.00	7 / 23	0.05	6 / 34	0.00	5 / 55	0.00	13 / 24	4.1	31.5
1.0, 1.9	Clear cutting	0.00	4 / 30	0.00	4 / 55	0.00	7 / 23	1.00	6 / 34	0.00	5 / 55	0.00	13 / 24	6.0	34.0
1.4	Dry needles	0.00	4 / 30	0.00	4 / 55	0.20	7 / 23	0.80	6 / 34	0.00	5 / 55	0.00	13 / 24	6.2	31.8
2.0	Soil preparation	0.00	4 / 30	0.00	4 / 55	0.00	7 / 23	0.80	6 / 34	0.00	5 / 55	0.20	13 / 24	7.4	32.0
9.9	Dec. shrubs	0.02	4 / 30	0.25	4 / 55	0.00	7 / 23	0.52	6 / 34	0.23	5 / 55	0.00	13 / 24	5.2	44.0
10.0	Dec. shrub removal	0.02	4 / 30	0.00	4 / 55	0.00	7 / 23	0.75	6 / 34	0.23	5 / 55	0.00	13 / 24	5.7	38.8
34.9	Thinning cut. aged forest		—		—		—		—		—		—	5.2[1)]	36.5[1)]
35.0	Thinning cutting	0.80	5.2 / 36.5	0.00	4 / 55	0.15	7 / 23	0.05	6 / 34	0.00	5 / 55	0.00	13 / 24	5.5	34.3
35.0	Undisturbed development	0.10	5.2 / 36.5	0.80	4 / 55	0.00	7 / 23	0.07	6 / 34	0.03	5 / 55	0.00	13 / 24	4.3	51.7
70.0	Undisturbed development	0.50	4 / 30	0.40	4 / 55	0.00	7 / 23	0.07	6 / 34	0.03	5 / 55	0.00	13 / 24	4.2	41.0

[1)] Computed using linear interpolation

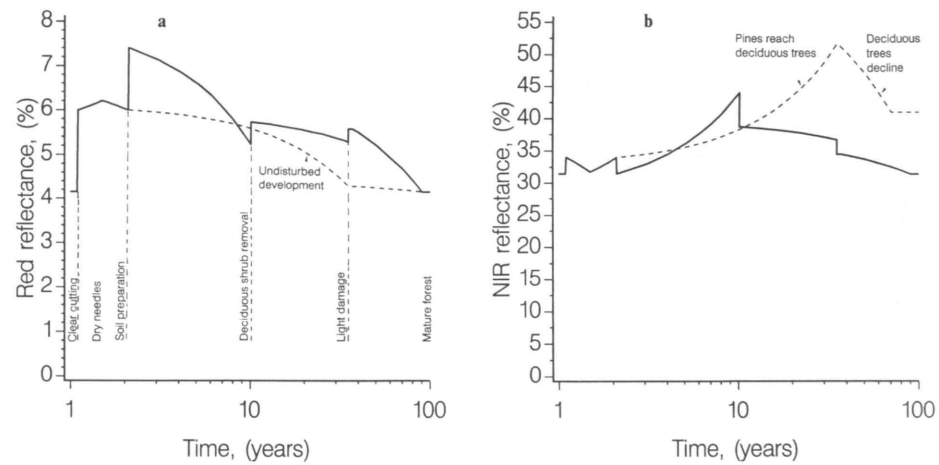

Fig. 3. Computational model of reflectances of a pine stand during a rotation. Vegetation in summer seasonal aspect. a) Red light. b) Near infrared radiation.

almost twice as high reflectance as pine trees.

The output of the computations in Table 1 is presented graphically (Fig. 3). The reflectance change between the rapid changes is assumed to be linear. Thus, the reflectance of a forest of thinning cut age (Time = 34.9 and pine reflectance in Time = 35.0) has been computed using linear interpolation 1) of the reflectance of the canopy after deciduous shrub removal (Time = 10.0) and 2) of the reflectance of the mature pine stand (Time = 0.9 and Time = 90.0). It is very likely that the reflectance change is not linear but that reflectance drops rapidly until the closure of the canopy (approximately 30 years). At that time, reflectance may be close to the reflectance of a mature stand. After the closure, reflectance drops slowly. Linear interpolation was applied because too little information was available to apply nonlinear relationship.

The frequency of the rapid changes is much higher in the early development phase of the stand than after the closure of the stand (Fig. 3). The model suggests that changes could be detected in the following order, from the easiest to the most difficult: 1) clear cutting; 2) soil preparation; 3) deciduous shrub removal and deciduous shrub growth; and 4) thinning cutting and damage.

The general trend for a conifer stand is decreasing reflectance both in the visible light and near infrared range of the spectrum (as well as in the middle infrared range) during succession from an open clear cut area to a mature stand. Dry needles of the cutting debris reflect *red light* effectively. Red light reflectance decreases slightly when the needles fall and when the undergrowth recovers because of increased irradiance.

Soil preparation destroys part of the undergrowth and exposes some highly-reflecting non-organic soil. This causes the reflectance to increase. The spectral characteristics of rapid changes and the development of the reflectance after the changes are similar in all change categories since the amount of green vegetation temporarily decreases in all cases.

In many damage types, the proportion of chlorophylls decreases and the leaves (needles) turn yellowish or brownish before they fall. The color change means significantly increased red light reflectance (Gates 1970, Koch et al. 1990).

The reflectance level of the untreated and undamaged stand is, on average, lower during succession than the reflectance of a stand with rapid changes because the aboveground biomass is higher in the untreated stand.

The general pattern of the reflectance curve may be similar to the red light in the middle infrared spectral range since the visible and middle infrared spectral ranges have high positive correlation (e.g. Peng 1987).

Spectral effects of rapid changes in the *near infrared* range are somewhat uncertain. The general decreasing trend of the reflectance of a conifer canopy (Colwell 1974, Saukkola 1977, Poso et al. 1988) is due to increasing absorptance of the canopy. In the canopies of deciduous trees, the absorptance of the near infrared is up to 6 percent units lower than the absorptance of coniferous canopies (Williams 1991).

The model indicates that, in clear cutting, the reflectance increases relatively less in the near infrared than in the red light range (Saukkola 1982). Soil preparation may not have a great impact on the reflectance. The preparation is usually made so soon after the cutting that the undergrowth has not yet become especially luxuriant (Häme 1984a).

Deciduous shrub growth definitely increases the reflectance. The removal of shrubs decreases it. Häme (1984b) stated that, in the near infrared range, the Landsat MSS intensities of the regeneration areas containing harmful amounts of shrubs were even twice as high as the intensities of the regeneration areas with some shrubs only. The near infrared reflectance stays high if shrub removal is not done. The increase stops when the poorly reflecting pines reach the deciduous trees in height (Fig. 3b). The reflectance drops when deciduous trees (birches), whose life is shorter than the life of pines, start to decline.

Because the near infrared reflectance decreases when the stem volume of a stand increases, thinning cutting should have an opposite effect. The near infrared reflectance should increase. The roughness of the canopy surface may increase in a thinning cutting, which increases the shadows. This, on the contrary, tends to decrease the reflectance. The most usual thinning cutting practice in Finland may not change the upper canopy surface greatly because predominantly shorter trees are thinned.

Damage either destroys needles that have a higher reflectance than the other parts of the trees or it can decrease the needle reflectance (Gates 1970). The effect is supposed to be a decrease in the near infrared reflectance of the canopy (Häme 1988b). An uneven needle loss increases the canopy roughness, which should decrease the reflectance as well. Needle loss allows a larger proportion of the incident radiation to penetrate to the lower parts of the canopy. More radiation reaches the ground and the undergrowth has more impact on the reflectance (Colwell 1974).

In some studies (Guyot and Riom 1988, Williams 1988), damage has increased the near infrared reflectance by 5 to 10 percent units. Buschmann et al. (1989) have not found big differences in the near infrared reflectance of damaged and non-damaged Norway spruce needles. In most studies, however, the reflectance has decreased due to damage (e.g. Colwell 1970, Boehnel 1976, Ajai et al. 1983, Vogelman and Rock 1986, Brockhaus et al. 1988).

The near infrared may not be the best wavelength region to use to separate the damage. Factors with opposite spectral impact determine the final intensity. Even a single reflecting element, leaves, can have a different spectral behavior in different damage types. Spectroradiometer measurements of pine needles are utilized in this study to obtain more information about the ambivalent behavior of the near infrared radiation in the conifer canopy.

2.4 Factors affecting the selection of the interpretation technique

The optimal approach keeps the intensity differences of the changes of interest in the data but minimizes the impact of the other intensity changes. The essential factors in the selection are:

1. Image acquisition
2. Preprocessing
3. Spectral features
4. Ground truth
5. Algorithms

2.4.1 Image acquisition

Seasonal variation causes the most evident and wide-area changes in the nature. Images should be acquired in the same season, if possible, to avoid the intensity differences caused by the seasonal cycle. Vegetation and background should be in a relatively stable phase. The middle of the growing period, from late June to the end of August, is such a period (Peterson 1989). Dry winter season may be another suitable period. However, the amount of snow and frost on the branches can vary a lot. Low solar elevation angle and low power of the irradiance are also problematic.

Because of clouds, the time of image acquisition can seldom be chosen optimally. Good ground truth data can diminish the harm from images acquired in different seasons.

Spectral properties of conifer canopies are so poorly known that the use of images with different viewing angles is very difficult and should be avoided.

2.4.2 Preprocessing

Errors in the rectification model can be minimized by selecting enough (at least 30) control points and measuring their image coordinates and map coordinates carefully. The interval in measuring the image coordinates should be smaller than one pixel, e.g. one half of a pixel. Using Finnish basic maps (1 : 20 000), the mean square error of the rectification model is usually less than one pixel (less than 30 m for Landsat TM images). The maximum residual errors of the control point coordinates are close to one pixel.

In change interpretation, the first priority is that the multidate images overlap well. The second priority is the overlapping with the maps. The rectification can be made in two phases to minimize the overlapping error. First, the images are rectified to a coordinate system of a reference image. Second, the reference image is rectified to a map coordinate system. The same rectification model to the map coordinate system is applied to all images since they already are in the coordinate system of the reference image. The second rectification does not change the relative locations of pixels between the images.

Nearest neighbor resampling (Bernstein 1976, Campbell 1987) causes a shift in pixel

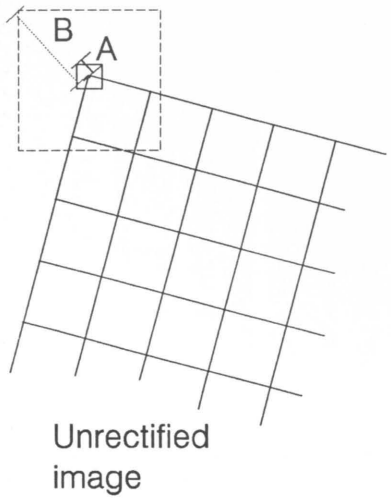

Fig. 4. Maximum intensity shift in nearest neighbor resampling. A with a small pixel size in the rectified image, B with a large pixel size.

location whose size is, at maximum, one half of the diagonal dimension of the pixel of the rectified image. The larger the pixel size of the rectified image the larger the maximum shift (Fig. 4).

The intensity shift caused by the resampling can be diminished using interpolating resampling methods. The most common interpolating resampling methods are bilinear interpolation and cubic convolution (Bernstein 1976). The drawbacks of these methods are that they filter the image or reduce spatial resolution. Also, interpolating the intensities of the standard satellite image products is somewhat questionable since the intensities of the raw data are already processed when the image product is made.

A better way to minimize the resampling error is to use a relatively small pixel size in the rectified image; at least in the case where raw data are not available.

The elimination of striping in the commercial images is very difficult since the standard geometric correction, made at the receiving station, changes the sequence of the striping. Noise is often reduced using image filtering. A simple noise-reducing filtering technique is to compute the mean of the intensities in an n x n pixel window which is moved across the whole image (Peng 1987). Also the mean filtering reduces the spatial resolution and makes the image smoother. Edge-preserving filtering methods have been developed (Nagao and Matsuyama 1979). A drawback of such filtering is that it manipulates the original radiance measurements, i.e. the pixel intensities.

Spatial and supervised interpretation methods are some other means to lessen the impact of the noise. In spatial methods, the environment of a pixel is taken into account in the interpretation. Smaller variation due to noise is not as harmful as when pixels are handled separately.

Supervised classification methods, where the parameters of the estimator are computed using real training areas, are an effective way to take noise into account. The spectral model has all the elements of the registered electromagnetic radiation: spectral differences due to field variation and noise. If the noise is uniform across the image, the supervised method may be a most effective approach to diminish the harmful impact of the noise.

2.4.3 *Spectral features*

Change interpretation can be based on original channels, or image transformations can be computed before the actual interpretation.

Original channels have all the registered information. The majority of the intensity variation may, however, be caused by factors other than the change. Also, the amount of data grows high if all the spectral data are included in the analysis.

The purpose of image transformations is usually to extract the essential information and/or to compress the data. Some irrelevant information is lost by purpose. Intensity transformation to *reflectances* (MacFarlane and Robinson 1984) is an exception. If it is fully successful, the amount of information increases since external information about the irradiance and atmosphere are brought in (Rosengren and Ekstrand 1988).

Adequate information about the atmosphere is hard to obtain, thus making the transformations uncertain. The surface itself is another problem. Reflection properties of non-diffuse surfaces, like conifer forests, change when the solar angle changes.

Furthermore, a slight seasonal change will give somewhat different reflectance values, although all input data and computations were correct. This may be the aim, if one is interested in the changes of the vegetation cover in different seasons. If the objective is to detect forestry treatments and damage using the transference of the old statistics to new images, the seasonal variation is disruptive.

Reflectance transformation or other types of image calibration are important if, for example, general changes in the vegetation cover are studied over a wide area. This is true especially when using unsupervised methods. Without corrections, the results of analyses are hard to interpret. It is more difficult to justify image calibration if specific ground truth is still needed.

Another alternative is not to try to calibrate the images but to develop interpretation algorithms which can adjust to images acquired in different illumination and atmospheric conditions.

Principal component or Karhunen-Loeve transformation is one of the most commonly used data dimension-reduction or compression techniques in remote sensing (Poso et al. 1984 and 1987, Peng 1987). The principal components are linear functions of the input variables. The columns of the transformation matrix are the eigenvectors of the covariance matrix. The first principal component (PC_1) is computed:

$$PC_1 = a_{11}x_1 + a_{12}x_2 + \ldots + a_{1n}x_n \qquad (3)$$

where x_k is the value of the k'th spectral channel

The coefficients a_{1k} are selected so that the variance of the PC_1 is as high as possible. Also, $\Sigma a_{ik}^2 = 1$. The second and further principal components are computed similarly so that the principal components are uncorrelated and orthogonal (Seal 1964). An extension of the principal component analysis is to calculate the transformation from the correlation matrix. The basic variation is concentrated in higher components. Lower components can be excluded from further analysis.

Because at least two images are used in change interpretation, the need to compress the data is evident. Principal component transformation has also been used for direct change extraction (Richards 1980). Two Landsat MSS images from separate dates have been superimposed and the transformation has been made into a combined set (eight channels). Then the major variation, which is usually not due to change, has been concentrated in higher principal components. The minor, small area variation can be seen in the lower components. A classification has been made using the 3rd and 4th principal component. The changes were bush burn areas in Australia. The results left unclear whether an equally good or better result would have been obtained using original channels. The direct extraction of the changes using the principal component analysis requires that a large proportion of the area be unchanged.

Canonical discriminant analysis (Seal 1964) is a dimension-reduction technique related to principal component analysis and canonical correlation. Given a classification variable and several quantitative variables, the canonical discriminant analysis derives canonical variables (Can_i) that summarize between-class variation. Canonical discriminant analysis derives a linear combination of the variables that has the highest possible multiple correlation with the classes (SAS Institute Inc. 1988):

$$Can_i = a_{i1}x_1 + a_{i2}x_2 + \ldots + a_{in}x_n \qquad (4)$$

where x_k is the value of the k'th spectral channel

The coefficients (a_{ik}) are selected so that each canonical variable Can_i maximizes the F ratio of between-classes mean square to within-classes mean square. Also, $\Sigma a_{ik}^2 = 1$. The first canonical discriminant function is based on the highest F ratio. The Can_i variables are uncorrelated. The canonical discriminant analysis may be more relevant to the interpretation problem than the principal component transformation since the principal component analysis only maximizes the explained variance in the components. The performance of the canonical discriminant analysis depends on the validity of the classification variable — on the ground truth in the satellite image analysis.

The aim of *difference channel* computation is to extract the change diminishing the intensity variation, which is common to both channels. Usually, spectral features that represent the same wavelength area, but are acquired on separate dates, are subtracted from each other (Saukkola 1982). The intensities of the difference channels are then

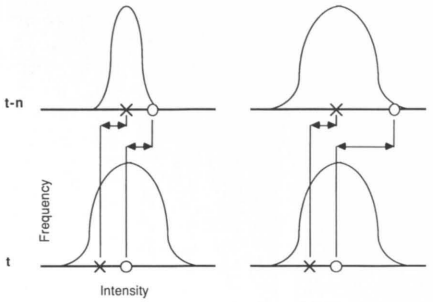

Fig. 5. Intensity differences of two observations (cross and circle) without (left) and with (right) histogram matching. Channels with same wavelength and acquisition dates t-n and t (Häme 1987).

understandable. All values that deviate from the original represent a change. The features may be calibrated before the subtraction (Fig. 5) (Singh 1989).

A drawback of the difference channel computation is the lack of a real, unchanged element in the forest ecosystem. Also, the fading of variation caused by tree cover differences may cause confusion among change classes which would otherwise be very easy to separate using original channels.

Residual images are special types of difference channels. A linear regression model is computed where one spectral feature, i.e. wavelength channel or transformed feature, is the dependent variable. Another feature from the same wavelength area, but from a different date, is the independent variable. The residual is then computed between the dependent variable and the model. If the original channels are successfully calibrated before the model has been computed, the regression equation shows the general trend of the change (Frank 1984). If the proportion of area with major field changes is small, the regression technique can be employed to calibrate corresponding multitemporal channels (Olsson 1991).

Differences of *channel ratios* have also been applied. Channel ratio differences have usually been differences of near infrared radiation/red light ratios, "vegetation indices". Near infrared/middle infrared ratios have also been applied (Vogelmann 1989). The vegetation indices have been computed as a simple ratio of near infrared/red or by using normalized vegetation indexes (NDVI) (Nelson 1983, Sader 1988):

$$NDVI = \frac{NIR - Red}{NIR + Red} \quad (5)$$

where

NIR is near infrared intensity
Red red light intensity

Different ways to calculate the vegetation indices all seem to lead to similar results (Williams et al. 1979).

Instead of subtracting the *bitemporal* channels having the same wavelength, their *ratios* can be computed (Singh 1989).

Rosengren and Ekstrand (1988) suggest that change caused by forest decline should be detected calculating *chromaticity index differences.* In their study, a chromaticity index (CI) was:

$$CI = \frac{R_{TM4}}{R_{TM4} + R_{TM5} + R_{TM7}} \quad (6)$$

where

R is reflectance.

The chromaticity indexes have been applied since it has been assumed that the ratio of near infrared/middle infrared is effective in damage detection and that the use of the ratio diminishes the spectral effect caused by the topography. The method has been applied so far to monotemporal data only. Wastenson et al. (1988) have pointed out that the exact delineation of spruce forests is a prerequisite for useful results by the chromaticity method. Damaged spruce stands give similar chromaticity values to healthy pine forests.

2.4.4 Ground truth

The ground truth is needed as training data to compute the parameters of spectral models in the supervised interpretation approach. It is also needed to test the interpretation results.

Two basic types of ground truth are available in forest applications: stand and plot data. In forestry, stand data are collected for operational planning and plot data for strategic planning. Several spectral vectors, i.e. pixels, can be selected for every stand. Smaller localization errors of the pixels are not very harmful for construction of a model between field and spectral data. Stand data normally permit an adequate number of observations for statistical spectral models.

A drawback of the stand data is that the field variable values may not be very carefully measured. Stand data seem to be the natural ground truth if the aim of the interpretation is to get results for stands.

Measurements from plots are usually very reliable because the objective of the sampling is to give credible statistical information. The plots are located so far from each other that the relationship of the neighboring plots is much less than the field content of adjacent pixels. The National Forest Inventory (NFI) of Finland is a plot (point) sampling survey. One of the advantages of the NFI data is that they are measured at regular intervals from the whole country in a standardized method.

A drawback is that only a few pixels can be selected for each plot. It may be hard to get enough observations, especially for statistical interpretation models. Location errors of pixels are more dangerous than in the case of stand data. The problem is somewhat less if the distance from the plot to the closest stand boundary is registered in the field.

2.4.5 Algorithms

Goldberg et al. (1982) divide the change detection methods to *signal-based* and *symbolic approaches.* The signal-based approach means traditional pixel by pixel classification methods. In the symbolic approach, spatially homogeneous areas are extracted before detection of change is attempted. Signal-based approaches have been used in numerical interpretation more often than symbolic approaches. Visual interpretation can be placed in the category of symbolic approaches.

The simplest approach to interpret change may be to *compare individual analogous images visually* (Hall et al. 1983). A more advanced method is to *compare two numerical classifications* (Joyce et al. 1980, Lehto 1981, Burns 1985). The problem with comparison is the errors in the individual classifications. It is hard to know if the class change is due to the field change or to a classification error of the individual image. Goldberg et al. (1982) have presented a scheme to increase the joint performance. An expert system would compare two classifications and decide whether the category changes are logical. Goldberg et al. (1982) have segmented the images from different dates and compared the classified segments.

The post-classification comparison would be suitable for finding clear cuttings, but hardly suitable for any other changes that are investigated in the study. This can be deduced from the accuracies of the stand variable estimation which have been obtained in recent Finnish studies (Poso et al. 1987, Tomppo 1988).

The most frequently used numerical change detection method may be *thresholding of a single spectral feature,* e.g. difference in the red light channels (Saukkola 1982), which should indicate the change.

Principal component transformation to multitemporal data set, direct multidate classification, and *change vector analysis* are methods where several spectral variables are analyzed simultaneously to separate changes.

In direct classification, the features have most often been either original channels or compressed monotemporal features, such as principal components. For some reason, the use of "change features", e.g. difference channels, has usually been restricted to single feature thresholding.

Swain (1978) has presented an sophisticated extension, a *cascade classifier,* to the traditional maximum likelihood classification. The method has not actually been developed for detecting changes, but rather for giving updated classification results. Bitemporal field data are used to compute so called "transitional probabilities" which describe the probability that a class has changed from one to another between the dates of image acquisition. In the second stage, transitional probabilities are used in classification of the later image in a similar way as are *a priori* probabilities. A direct classification of a merged, two image set gave an 80.8 percent overall performance. The cascade classification had an 83.8 percent performance. It was assumed (Swain 1978) that limited ground truth was the reason for slightly poorer results with the merged data whose dimensionality was twice as high as the data in the cascade classification. Peng (1987) has applied Swain's method to general-purpose forest inventory in Finland.

A *decision tree classification* method has been used with multitemporal data (Lozano-

Garcia and Hoffer 1985). First, the most obvious classes like tree cover/no tree cover are delineated with a simple classification, while the areas of interest are classified in more detail. The determining of an optimal decision tree may, however, be very difficult. If it is to succeed, the tree structure may easily become very complex (Swain 1978).

The change vector analysis by Malila (1980) is an interesting example of symbolic approaches, but it has not been commonly used since its announcement. This method separates change detection and identification, which makes it a different approach from direct multidate classifications that combine the two phases. Also, spectral and spatial information is combined in change vector analysis. First, two images from separate dates are normalized using the Tasselled Cap operation by Kauth and Thomas (1976). This linear operation gives results similar to the principal component analysis. Two variables, "brightness" and "greenness" are computed from both images in the operation. Then, a spectral-spatial clustering is performed on the four-feature data set to find homogeneous areas.

The locations of the areas, "blobs", at different dates are studied. The change vector is computed between the earlier and later locations of the blob spectral mean in the "brightness" and "greenness" coordinate system. The magnitude of the vector tells the magnitude of the change and the direction the type (e.g. clear cutting or regrowth). Thus, not only the type of the change, but also its size, can be output. This method has been reported to be sensitive to its parameter setting (Malila 1980). However, there is no clear procedure on how to define the parameters (Singh 1989).

Robinson et al. (1982) have studied changes in arid lands, observing the *change of the correlation coefficient.* The area was divided into 2 km by 2 km squares. Correlation coefficients were calculated between red light and near infrared channels for each square individually from two images. The image data were Landsat MSS. The correlation coefficient values of the older image were subtracted from the values of the newer, square by square. The positive differences indicated that the amount of green vegetation had decreased. A negative difference indicated an increase. The authors think that the method easily overestimates the change. This method is based on the fact that the red light reflectance decreases and near infrared increases when the amount of grass vegetation increases.

The change interpretation can also be made utilizing an *analogous image of features describing the change* (Eyton 1983).

The collection of reliable ground truth for change inventory is usually difficult. Therefore, it is an attractive idea to collect the ground truth once and use the computed spectral model to analyze new images. This requires that all images are calibrated similarly. Hall et al. (1988) have modified classification statistics, which were computed for a 1973 Landsat MSS (MultiSpectral Scanner) image to classify a 1983 MSS image, into the same relatively coarse classes.

The most often applied change interpretation methods should be placed in the category of supervised methods. The spectral boundaries of the classes are defined with the help of ground truth information. In very many cases, the spectral class boundary has been set by the individual according to his general knowledge.

The supervised methods may be more suitable than the unsupervised when one is interested only in a small part of the intensity variation. The multitemporal data set is likely to include many types of intensity changes besides those due to the predetermined field changes. The primary use of unsupervised methods is to find phenomena that are poorly known.

2.5 Selected technique

According to the earlier studies, more information is needed about the spectral properties of changes and the optimal spectral features used in change interpretation. Therefore, the main focus in the analyses will be on the spectral behavior of the changes (Chart 1).

Many derived spectral features will be tested and compared with each other and with original channels. The tests will be made both feature by feature and by making experimental classifications and regression analyses using sets of features. Finally, several classifications will be made and tested with ground truth data omitted in parameter estimation of classification models.

Several existing algorithms will be tested to study the role of the algorithm in the formation of an interpretation result. Classification will be applied to study the possibility to extract the changed area. Regression analysis will be employed to estimate the continuous variables, drain of the thinning cuts and the damage.

Image segmentation will be a way to use the symbolic approach (Goldberg et al. 1982) in the interpretation. Also, classifications will be tested utilizing forest stands of a forest management plan as testing units instead of single pixels.

The post-classification comparison of individual classifications has been rejected as too coarse a method. Also, the correlation coefficient methods are not used since they were developed for cases where the largest proportion of the area is changed.

The main interest of this study is not to develop new interpretation algorithms. Existing and available algorithms will be applied. New algorithm development is seen as the next step after reliable information about the spectral properties is available.

Chart 1. Selection of the interpretation technique.

Factor to be taken into consideration	Action
Seasonal effects	1) Elimination of spring and autumn aspect selecting summer images if possible. 2) Choosing several image pairs. 3) Analyzing summer and winter images.
Preprocessing	1) Two-phase rectification to minimize overlapping error. 2) Relatively small pixel size in resampling to avoid resampling shift. 3) Nearest neighbor resampling to avoid intensity changes.
Spectral features	1) Basic spectral information employing spectroradiometer measurements of pine needles. 2) Analyzing intensities of separate satellite image channels and channel sets. 3) Comparing derived spectral features with original channels and each other.
Ground truth	1) Stand data. 2) Plot data.
Algorithms	1) Supervised methods. 2) Unsupervised method. 3) Spatial information using segmentation.

3. Materials

3.1 Study area

The study area, centered at 61°51' N, 24°22' E, is a 40 km by 40 km square in the Korkeakoski district of the National Board of Forestry and its surroundings (Fig. 6). The area represents a typical boreal forest in Southern Finland (Kalliola 1973), with small stand sizes (1 to 4 hectares). The area also has some features of the more northern forests, such as a barren upland region. The most common soil type is till. Eskers and other glaciofluvial deposits and silt each represent approximately ten percent of the soil types. The distance to bedrock does not exceed one meter from the soil surface in most of the till area (Geological map... 1982).

The relief of the area is quite flat. Elevation from sea level varies from 85 meters to 190 meters. The higher elevations have not been under water since the last continental glacier melted (Haavisto (ed.) 1983).

The tree canopies were quite young and slightly pine dominated, as seen in Table 2. The data for the table are from forest land plots of the National Forest Inventory (NFI) (forest land: average annual growth in stem volume exceeds 1 m^3/ha using a 100 year rotation). The mean age was 57.0 years, and the mean volume was 59.8 m^3/ha. Scots pines (*Pinus sylvestris* L.) were, on average, younger than the Norway spruce trees (*Picea abies* (L.) Karst.). The most usual or modal age class for pines was 0—25 years (42.5 percent of pine dominated forests) and for the spruce it was 51—100 years (60.0 percent of spruce dominated forests). In

Table 2. Statistics of the study area from NFI data.

Mineral soil and peatlands

Mineral soil	Spruce swamp	Pine swamp	
85.2	6.7	8.1	%

Site type

I	II	III	IV	V	
Rich	Medium rich	Medium barren	Barren	Rock, sand	
20.2	60.1	15.0	3.2	1.5	%

Dominant tree species

I	II	III	IV	V	VI	
Treeless	Pine	Spruce	Birch1	Birch2	Alder	
1.0	52.2	43.1	2.2	1.2	0.2	%

Age class

0—25	26—50	51—100	101—150	151—200	(years)
29.8	16.3	41.9	11.3	0.7	%

Volume class

0—25	26—50	51—100	101—150	151—200	201—250	251—300	(m^3/ha)
30.8	19.7	27.3	16.5	5.2	0.2	0.2	%

Site type
I Rich. OMT-type (*Oxalis-Myrtillus*) or corresponding swamp
II Medium rich. MT-type (*Myrtillus*)
III Medium barren. VT-type (*Vaccinium*)
IV Barren. CT-type (*Calluna*)
V Rock, sand.

Dominant tree species
I Treeless.
II Pine. Scots pine (*Pinus sylvestris* L.)
III Spruce. Norway spruce (*Picea abies* (L.) Karst.)
IV Birch1. (*Betula pendula* Roth.)
V Birch2. (*Betula pubescens* Ehrh.)
VI Alder. (*Alnus incana* Moench., Willd.)

All statistics are percentage proportions of 406 sample plots.

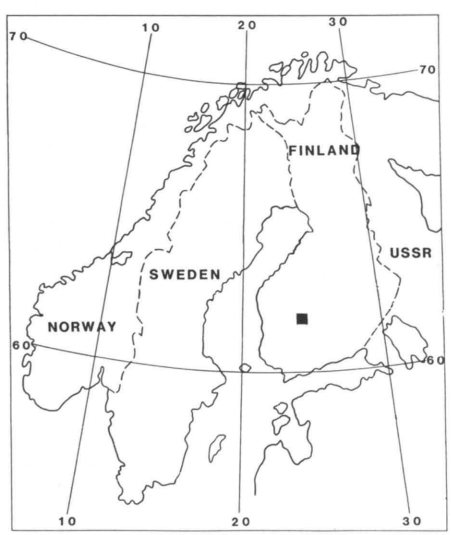

Fig. 6. Study area.

spite of the pine domination, 80.3 percent of the plots were on medium-rich *Myrtillus* or richer site type (Cajander 1913).

The study area was within one of the most important forestry areas in Finland. Consequently, it was also within one of the areas in Finland with the greatest potential for to applying and practicing remote sensing aided change detection.

3.2 Satellite images

3.2.1 *Description of the image data*

Five satellite scanner images were used for interpretation (Table 3). The system-corrected Landsat TM images were obtained through ESA-EARTHNET, and were pre-processed at Esrange, Sweden. The Spot images were obtained through Satellitbild/Spot Image, and were pre-processed to level IB which corresponds to the system correction for the TM images (The catalogue... 1989). The study area was totally cloud-free in the first two Landsat TM images, TMI84 and TMI85, as well as in the two Spot images, SWI87 and SSI87. Thin clouds partially covered the Landsat image TMI86.

Image TMI84 differed from the true summer images because the trees and other plants already had a partial autumn coloration. The relative humidity in image TMI84 was also higher, and the solar elevation angle lower, than in the other summer images. The low elevation angle caused quite low intensities and a narrower dynamic range (Fig. 7). A high relative

Table 3. Satellite images and their pre-processing.

Image name	Satellite	Sensor	No. of chann.	Orig. pixel size (m)	Date	Time (GMT)	Path	Row	Tilt of sensor (°)	Sun elev. (°)	Temp.[1] (°C)	Relat. humid.[1] (%)	Method[2]	No. of contr. points	Max. resid. error (m)	Mean square error (m)
TMI84	Landsat	TM	6(7)	30(120)	Sep 15, 1984	07:45	189	017	0	29	12.6	58	B	49	21	14
TMI85	Landsat	TM	6(7)	30(120)	Jun 21, 1985	07:45	190	017	0	49	22.4	50	A, B	30,49	20,21	14,14
TMI86	Landsat	TM	6(7)	30(120)	Jun 17, 1986	07:45	189	017	0	49	23.7	43	A, B	32,49	21,21	15,14
SWI87	Spot	HRV1	3	20	Mar 11, 1987	10:05	223	069	Left 07.3	24	−7.3	73	A, B	43,49	18,21	13,14
SSI87	Spot	HRV1	3	20	Jul 20, 1987	09:47	223	070	Right11.1	49	20.4	42	B	19	16	10

[1] Measured in Kuorevesi, Halli 09:00 GMT
[2] A: To TMI84 image coordinate system using nearest neighbor resampling method. Pixel size of the rectified imagery 30 m.
B: To base map coordinate system using nearest neighbor resampling method. Pixel size of the rectified imagery 20 m.

humidity had probably increased the scattering of the short wavelengths (Manual of Remote Sensing, Vol I 1983, p. 175). The noise in the first channel of image TMI85 was clearly lower than in image TMI84.

The technical quality of all images was good. The visible light channels of Landsat images had some striping which could not be eliminated since the frequency of the stripes was not uniform due to the preprocessing in the receiving station. In Spot images, striping and noise were very limited on visual inspection. However, the interpretation phase revealed disruptive radiometric errors in the Spot summer image.

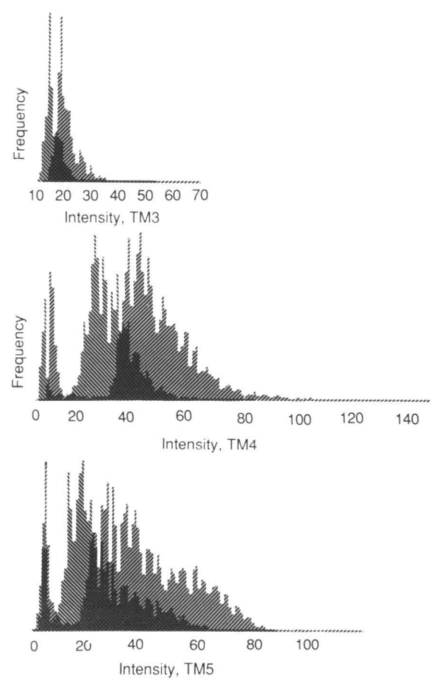

Fig. 7. Intensity histograms of the TMI84 (decreasing lines) and TMI85 (increasing lines) images.

3.2.2 *Geometrical rectification*

The images were rectified to the uniform coordinate system, which is a Finnish coordinate system in the Gauss-Krueger projection. The rectification was based on the linear affine transformation (Hirvonen 1971):

$$l = a_0 + a_1 x + a_2 y$$
$$c = b_0 + b_1 x + b_2 y \quad (7)$$

where
- l is line image coordinate of a pixel
- c column image coordinate of a pixel
- x map East coordinate of a pixel
- y map North coordinate of a pixel
- a_n parameters which are estimated using control points

The control points were measured from the basic maps of the National Board of Survey, scale 1:20 000. The resampling method was nearest neighbor (Bernstein 1976), which was chosen because it does not change intensities.

Landsat images TMI85 and TMI86 and image SWI87 were rectified to the coordinate system of image TMI84 before rectification to the map coordinate system. The second rectification, to the uniform coordinate system, was based on the rectification function calculated for image TMI84.

Visual inspection showed that the differences between pixel locations were as much as one pixel if the images were rectified independently, but the images fitted well if they were first rectified image on image.

3.2.3 *Correction of the radiometric errors in Spot image*

In preliminary classifications using the Landsat TM/Spot data, a very high proportion of the area went to the class of actual thinning cuts. Visual inspection showed that the class was concentrated on the eastern third of the study area and that the boundary of the class with other classes was very sharp. Also, the intensities of the middle third of the area differentiated

somewhat from the eastern and western parts of the study area.

Homogeneous areas were selected from lakes on both sides of the zone's boundary, and the spectral statistics of the channels were calculated. They showed that the intensities of similar lakes were different on each side of the boundary. The significance of the difference was tested with a t-test. If the null hypothesis (means equal) was rejected with 5 percent significance level, the intensities were corrected. The following integers were added to the intensities of the Spot channels in each part:

Spot channel	Part		
	West	Middle	East
SS1	0	+1	+1
SS2	0	0	+1
SS3	0	0	+1

Later classifications did not show any systematic concentrations of the thinning cut class.

The reason for the radiometric errors may have been the calibration differences of the parallel detector elements of the Spot. (The total number of the detector elements is 4 but data from 3 elements covered the study area). The differences between the detector elements caused such small intensity differences that they were not clearly visible in ordinary visual images. They became apparent in the classification where two classes were spectrally very close.

3.3 Combination of ground truth and intensity data

The ground truth data (Table 4) were obtained from three sources:

1) stands measured by the National Board of Forestry,
2) plots measured for estimating the *Gremmeniella* damage and
3) twice-measured plots of the National Forest Inventory (NFI).

The *Gremmeniella* plots were more stand type than real plot type data since the plots were measured within homogeneous stands. In addition to the forest measurement data, the digital elevation model and the basic maps were used.

3.3.1 Stand material

Field personnel of the National Board of Forestry marked on maps (scale 1:10 000) of the forest management plan the boundaries of all stands where a manmade change had occurred between dates of image acquisition, and the boundaries of reference stands with no change. Date limits were set according to the dates of the satellite image acquisition. Each operational area of the Korkeakoski district, which extended into the area of the satellite images, had stands with changes.

Table 4. Distribution of stands and plots into the change and reference classes.

Type of change or reference (R)	Number of stands or plots											
	Set1			Set2			PNFI			Dam		
	Set1A	Set1M	Set1T	Set2A	Set2M	Set2T	PNFIA	PNFIM	PNFIT	DamA	DamM	DamT
Clear cuts	15	8	9	18	8	6	7	7	0	0	0	0
Clear cuts R[1]	16	8	8	11	6	5	89	41	86	0	0	0
Thinning cuts	57	30	27	25	10	15	25	25	0	0	0	0
Thinning cuts R[2]	41	22	19	32	10	22	28	11	55	0	0	0
Shrub removal[3]	9	9	0	11	10	1	13	13	0	0	0	0
Shrub removal R	33	18	16	31	10	21	—	—	—	0	0	0
Shrub growth	0	0	0	0	0	0	14	14	0	0	0	0
Soil preparation	18	9	9	18	10	8	0	0	0	0	0	0
Soil prep. R	6	3	3	5	5	0	—	—	—	0	0	0
Gremm. dam≤30%	0	0	0	0	0	0	0	0	0	36	16	20
Gremm. dam>30%	0	0	0	0	0	0	0	0	0	25	15	10
Total	195	107	91	151	69	78	176	111	141	61	31	30

[1] Plots with tree stem volume ≥ 40 m³/ha in PNFI data.
[2] Plots with tree stem volume 0—39 m³/ha in PNFI data.
[3] Two classes in Set1M: mechanic treatment 3 stands, mechanic-chemical treatment 6 stands.

Set1 Stands by the National Board of Forestry.
Controlled changes Sep. 9, 1984 — June 6, 1985.
Stand variable data included.
Original number of stands 202, change registered on 105 stands.

Set2 Stands by the National Board of Forestry.
Controlled changes June 22, 1985 — June 16, 1986.
Stand variable data not included.
Original number of stands 168, change registered on 77 stands.

PNFI Relascope plots of the National Forest Inventory of Finland.
Measured summer 1984 and summer-autumn 1987.
Controlled and uncontrolled changes.
Stand variable data included.
Original number of plots 406, change registered on 129 plots.

Dam Relascope plots for the *Gremmeniella* damage estimation.
Measured summer 1986, pure Scots pine plots only.
Stand variable data included.
Original number of plots 61, damage registered on 61 plots.
Plots measured in 29 separate areas.

Set1A, Set2A, PNFIA, DamA — Number of stands/plots used for preliminary spectral analysis.
Set1M, Set2M, PNFIM, DamM — Number of stands/plots used for classification model construction.
Set1T, Set2T, PNFIT, DamT — Number of stands/plots used for testing of classifications.

Thus, the changes were distributed to the entire study area. The reference data consisted of stands in which the treatments would be done immediately after the later date limit.

The main stand variable values for Set1 (Table 4) were selected from the forest management plan of the National Board of Forestry. The plan was based on the field inventory of 1975. The stands in Set1 were, on average, more barren than the forests in the study area as a whole. In the total area, 80.3 percent of the NFI plots belonged to medium rich or rich site types. In Set1, this proportion was 56.4 percent. The clear cuts were concentrated on old spruce dominated forests, and the thinning cuts on young forests. The following statistics have been computed from the stand characteristic values of the clear cut or thinning cut stands in Set1. The data are from forest management plan data (1975 inventory) without any computational updating.

Actual clear cuts
- age class 101—150 years, 46.7 % of clear cut stands
- proportion of pine 0—50 %, 100 % of clear cut stands
- suggested drain 300—400 m³/ha, 40.0 % of clear cut stands

Actual thinning cuts
- age class 0—25 years, 58.6 % of thinning cut stands
- age class 26—50 years, 34.5 % of thinning cut stands
- proportion of pine 0—50 %, 50.0 % of thinning cut stands
- proportion of pine 60—100 %, 50.0 % of thinning cut stands
- suggested drain 0—30 m³/ha, 86.2 % of thinning cut stands

Two of the thinning cut stands (3.4 %) had a deciduous tree as the dominant tree species. Most of the thinning cuts were the stands' first thinning, which caused a low drain. The drain in basal area was only approximately 4 m²/ha on some field-checked stands.

The "shrub removal" class in Set1 may include some stands where the treatment was primarily thinning of the overdense pine canopy and not deciduous tree removal. The type of the treatment is known. Three of the nine "shrub removal" stands had had a mechanical treatment only; whereas, on six stands, the treatment had been mechanic-chemical. In the latter case, the main problem in the stand had definitely been deciduous shrubs. Therefore, two separate shrub removal classes were constructed for the final classifications.

Soil preparation on the regeneration areas had been either plowing or harrowing. Information on the type of the cultivation was not included in the field data.

The boundaries of the stands were digitized on a digitizing table to the format of the image processing software (DISIMP 1987). The spectral means and covariance matrices were computed from the intensities of the stands. The stand means were analyzed using SAS statistical software (SAS Institute Inc. 1985 and 1988).

Impossible or very exceptional field variable or intensity values caused some stands to be eliminated from the original stand data sets when the stand sets for the analyses were formed. The incorrect intensities were caused, among other things, by clouds or cloud shadows (in image TMI86), or by wrong delineation of the stands on the forest stand maps. Note that only stands whose intensities deviated drastically from the intensities of the majority of the plots and whose intensities were illogical were eliminated. The proportion of the eliminated stands was 3.5 percent in Set1 and 10.1 percent in Set2 which was used for the partially cloudy TMI86 image.

An example of the exceptional intensities was five clear cuttings in Set1 which were both cut and plowed or harrowed between the dates of two satellite images. Their intensities were heterogeneous and somewhat different from the stands which were cut only. They were too few to form their own class, and for that reason they were left out from the analysis and estimation of the parameters of the classification model. The stands were, however, used for the testing. Set2 had four special clear cuttings. They were included in the intensity value analysis, but excluded from the parameter estimation for the classification model and, by mistake, also from testing.

Stands for the parameter estimation of the classification models were selected using stratified random sampling where the strata represent the change and reference classes. Approximately one half of the stands in each class were used for model construction in Set1, with the other half used for testing. The classification models using Set1 included a large number of thinning cuttings because securing a representative number in the model was desired. The approach in Set2 was more straightforward: ten stands per class were selected when possible. The rest were left for the testing. Only with spectrally very distinct clear cuttings, a smaller number of stands was regarded as satisfactory. Though one stand may often include an adequate number of pixels for sound spectral statistics, a single stand can seldom represent the whole class satisfactorily.

3.3.2 Gremmeniella data

Ground truth data for the interpretation of the *Gremmeniella* damage were field-measured sample

plots. They were originally selected from aerial photographs for a study on the inventory of damage by means of color infrared photography (Alajärvi 1987). The *Gremmeniella* data were collected from two sub areas within the study area, each approximately 3 km by 3 km.

During aerial photo interpretation, smaller stand-type areas that had been classified as being damaged were delineated. A systematic plot sample was placed in each stand. Each stand had 1 to 5 plots, depending on the size. The field distance between the sample plots within a stand was on average 50 m, varying slightly according to stand size. The field inventory was performed in the summer of 1986, a year after an epidemic. Consequently, the needles that died because of the damage had already fallen.

Each sample plot was a combination of a circular plot (100 m^2 in area) and a relascope point (basal area factor 1). For each tree, the diameter of the stem was measured, and tree species was registered. The age and needle loss were estimated visually. The needle loss (L_i) for an individual tree i was estimated:

$$L_i = 0.4 \cdot T_i + 0.4 \cdot M_i + 0.2 \cdot B_i \quad (8)$$

where

- T_i is needle loss in percent in the section of two uppermost whorls of branches for trees under 30 years, 1 m from top for older trees
- M_i needle loss in the residual part between T and B
- B_i needle loss in the four lowest branch whorls

The estimation procedure had been developed at the Finnish Forest Research Institute, Department of Forest Protection. In the procedure, the uppermost part of the tree had the highest weight. The use of such weighing was aimed at taking into consideration the significance of the damage to the future life of the tree. The year of the damage was not registered.

Visual estimation of needle loss has the danger of subjectivity. The most difficult problem in both visual estimation and measurement methods may be to set the reference level with no needle loss. To minimize the subjectivity, the loss was estimated in three parts.

Table 5. Statistics of the *Gremmeniella* data.

Mineral soil and peatlands							
Mineral soil	Pine swamp						
83.6	16.4	%					
Site type							
I	II	III	IV	V			
Rich	Medium rich	Medium barren	Barren	Very barren			
0.0	29.5	47.5	21.3	1.6	%		
Age class							
11—20	21—30	31—40	41—50	51—130	(years)		
6.6	62.3	18.0	3.3	9.8	%		
Volume class							
0—25	26—50	51—100	101—150	151—200	201—250	251—300	(m^3/ha)
4.9	29.5	52.5	9.8	1.6	1.6	0.0	%
Mean diameter							
5.1—10.0	10.1—15.0	15.1—20.0	20.1—25.0	(cm)			
32.8	45.9	19.7	1.6	%			
Mean height							
1.1—5.0	5.1—10.0	10.1—15.0	15.1—20.0	(m)			
3.3	67.2	27.9	1.6	%			
Density							
251—1000	1001—1750	1751—2500	2501—3500	(stems/ha)			
23.0	16.4	39.3	21.3	%			

Site type
I Rich. OMT-type mineral soil (*Oxalis Myrtillus*) or corresponding swamp
II Medium rich. MT-type (*Myrtillus*)
III Medium barren. VT-type (*Vaccinium*)
IV Barren. CT-type (*Calluna*)
V Very barren CIT-type (*Cladina*)

All statistics are percentage proportions of 61 sample plots.

The degree of damage (d_{ba}) for a plot was:

$$d_{ba} = \frac{\left(n_c \cdot \frac{\sum_{i=1}^{n_c} (ba_i \cdot L_i)}{\sum_{i=1}^{n_c} ba_i} + \sum_{n_{c+1}}^{n_r} L_i\right)}{(n_c + n_r)} \quad (9)$$

where

- ba_i is basal area of the stem of the tree i (m^2/ha) at breast height (1.3 m)
- L_i needle loss of the tree i
- n_c number of trees in the circular plot
- n_r number of trees in the relascope point outside the circular plot

Basal area was used as the weighing factor since it is relatively closely related to the tree crown area (Assman 1970).

The basic forest stand characteristics (development class, site type, height) were estimated in the sample plot. The number of stems per hectare was measured. Table 5 shows that the *Gremmeniella* plots were on more barren sites than the forests of the study area on average (Table 2) and that the trees were young.

The plots were located on the satellite image by comparing the plots that were marked on aerial photographs to a three channel color infrared image which was displayed on an RGB-monitor. The image was constructed from the TMI85 image channels. The nearest 4 to 11 pixels surrounding each plot were selected from the Landsat image using a cursor. The selected areas did not overlap. The resulting file was in similar format to the file showing the manmade changes. The intensity values were selected in the same manner as were the intensities of Set1 and Set2. Pure pine plots only were accepted as ground truth for damage interpretation because of the partial autumn coloration in image TMI84.

A digital elevation model was purchased from the National Board of Survey for a 5 km by 10 km area. It had been made by digitizing elevations of the basic maps in a 50 m by 50 m grid. The contour interval in the original data was 5 m. The model was available only from one *Gremmeniella* plot area. The data were changed from the vector to raster format, and rectified to the uniform coordinate system using bilinear interpolation in the resampling (Bernstein 1976). The pixel size in the rectification was 20 meters. An elevation model from the 1 : 200 000 road map was utilized for output of the classification result. The elevation interval in this data was 20 meters.

The study area was inside one of the most damaged forest regions in Finland. Certainly, there were also many other causes of damage, but they were minor compared to the *Gremmeniella*.

3.3.3 *National Forest Inventory (NFI) data*

Initial measurement of the NFI plots in the summer and autumn of 1984 was made as a part of an experimental survey for the eighth National Forest Inventory. In the autumn of 1987, a second measurement was made just for this study. The first measurement corresponded with the eighth National Forest Inventory, except that some measurements from the real National Forest Inventory were left out.

The National Forest Inventory in Southern Finland is a systematic cluster sampling. NFI sample plot clusters are half-quadrangles in Southern Finland where the study area occurred. The length of one side of a half-quadrangle is 2050 m (Fig. 8). The distance between the cluster corners was 8 km by 8 km in the experimental inventory. Every cluster had 21 relascope sample plots. The relascope factor 2 was used. The variables measured or estimated in each plot were: 1) plot identification data; 2) administrative data; 3) land use, soil, and site variables; and 4) measurement data from trees (Valtakunnan... 1986).

Plot data also included plot coordinates, the distance and direction to the nearest stand boundary. In the field plots were located using a compass and chain. If a shift from the correct measurement line was noticed, the amount and direction of the shift was recorded in the field in such a way that computational corrections to the coordinates of the plots could be made. The shift from the line and distance to the stand boundary were measured in 10-meter intervals.

In 1987, all plots were checked, and plots with other than successional changes were remeasured (Hyytiälän... 1987).

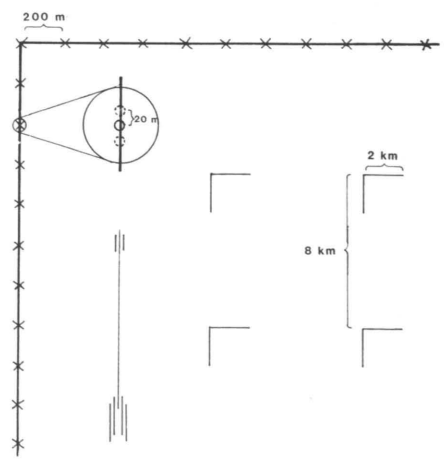

Fig. 8. Location of field plots in the Finnish National Forest Inventory.

The drain from the thinning cuttings was obtained in two different ways: 1) the field crew measured the drain directly by means of stumps; and 2) the basal area in the thinning cut stands was remeasured in 1987, and the drain was calculated by subtracting the remeasured basal area from the previous measurement. The three year growth was not taken into account.

The basal area for a plot was computed using measurements from the principal plot and two auxiliary plots. Auxiliary plots were located 20 meters from the principal plot, and were placed within the same stand as the principal plot. The measurements from the auxiliary plots were used to better represent the basal area of the stand surrounding the principal plot. When the final basal area was calculated, each auxiliary plot had a weight of 0.25. The principal plot was weighted as 0.50. The weights were obtained by empirical experiments (Tomppo 1988).

The deciduous shrubs were recorded only in the 1987 inventory. Thus, the presence of deciduous shrubs in 1984 was surmised during the 1987 field inventory. Both the deciduous shrub removal and growth classes had three categories according to the harmfulness of the shrubs. In the deciduous shrub removal class, deciduous species were registered only in three cases of 13 observations. In the shrub growth class, the main deciduous species was white birch, (*Betula pubescens* Ehrh.), on 13 of the 14 plots. The following statistics describe the deciduous shrub growth class:

	Mean	Min. (m)	Max.
Height of the shrubs 1984	1.3	0.6	3.0
Height of the shrubs 1987	2.6	1.6	4.0
Growth of the shrubs	1.2	0.5	1.7

The spectral intensity value for a NFI plot was obtained by localizing the pixel nearest to the plot, and calculating the value as a mean of five pixels; i.e. the nearest pixel and the four full adjacent pixels shown by the number 1 in the following diagram:

0 1 0
1 1 1
0 1 0

The nearest pixel was localized using the map coordinates of the plot and the map coordinates of the pixels of the rectified imagery. The intensity data were processed using SAS software.

The original distribution of the NFI plots to change classes and unchanged forest was:

Clear cut	21 plots
Thinning cut	41
Deciduous shrub growth	37
Deciduous shrub removal	19
Soil preparation	0
Gremmeniella damage	0
Storm damage	1
Other damage	2
Other change	8
No change	277
Total (principal plots)	406

Thus, almost one third of the field plots reflected some change within the three year period. Not all changed plots, however, could be used for statistical analyses and parameter estimation for classification models due to the following limitation criteria established for the plots:

- the distance to the unchanged area must be equal to or greater than 20 meters from the changed plots
- the distance to the closest stand boundary must be equal to or greater than 30 meters from the unchanged plots
- old basal area minus new basal area must be more than zero square meters per hectare in the cut classes
- old basal area minus new basal area must be less than 15 square meters per hectare in the thinning cut class
- competition from deciduous shrubs must be at least "slightly evident" prior to their removal in the deciduous shrub removal class
- competition from deciduous shrubs should be "not evident" after the removal treatment in the deciduous shrub removal class
- competition by deciduous shrubs must be at least "slightly evident" in the 1987 inventory in the deciduous shrub growth class
- the intensities of all classes must be realistic. High stem volume plots should not have intensities similar to open areas, for instance.

The limiting distance criterion (20 meters) was placed so low for the changed plots because of the small number of plots in most change categories. This led to very improbable intensities in some cases. The plots with erroneous intensities were localized using correlation diagrams of bitemporal red light and near infrared radiation channels and eliminated from the analysis. Because of the small number of plots, they could not be divided into subgroups according to the date of the change, although the date was estimated by the field crew. The limitations are taken into account in Table 6.

The distance-based limitation criteria was placed higher for the unchanged plots since there were more of them. The objective was to avoid plot restriction according to field content/intensity relations. The

Table 6. Statistics of the changed plots from the NFI data.

Type of change	Soil type			
	Mineral soil land	Spruce swamp	Pine swamp	
Clear cuts	85.7	14.3	0.0	%
Thinning cuts	68.0	12.0	20.0	%
Dec. shrubs rem.	100.0	0.0	0.0	%
Dec. shrubs growth	100.0	0.0	0.0	%
	Site type			
	Rich	Medium rich	Medium barren	
Clear cuts	14.3	85.7	0.0	%
Thinning cuts	12.0	80.0	8.0	%
Dec. shrubs rem.	7.7	61.5	30.8	%
Dec. shrubs growth	7.1	71.4	14.3	%
	Main tree species			
	Pine	Spruce		
Clear cuts	28.6	71.4	%	
Thinning cuts	60.0	40.0	%	
Dec. shrubs rem.	92.3	7.7	%	
Dec. shrubs growth	85.7	14.3	%	
	Age class				
	0—25	26—50	51—100	101—150	(years)
Clear cuts	0.0	0.0	100.0	0.0	%
Thinning cuts	4.0	16.0	68.0	12.0	%
Dec. shrubs rem.	100.0	0.0	0.0	0.0	%
Dec. shrubs growth	92.9	7.1	0.0	0.0	%
	Volume class					
	0—25	26—50	51—100	101—150	151—200	(m^3/ha)
Clear cuts	0.0	0.0	14.3	42.9	42.9	%
Thinning cuts	0.0	16.0	40.0	36.0	8.0	%
Dec. shrubs rem.	84.6	15.4	0.0	0.0	0.0	%
Dec. shrubs growth	100.0	0.0	0.0	0.0	0.0	%
	Cutting drain class (difference of bitemporal basal areas)						
	0—5	6—10	11—15	16—20	21—25	26—30	(m^2/ha)
Clear cuts	0.0	0.0	28.6	28.6	28.6	14.3	%
Thinning cuts	36.0	48.0	16.0	0.0	0.0	0.0	%

Statistics are calculated from 7 clear cut, 25 thinning cut, 13 deciduous shrubs removal and 14 deciduous shrubs growth plots.

selected 30 m distance was quite short when compared to the accuracy of the rectification. A longer distance was not possible due to lack of data.

The unchanged plots were divided into two categories for intensity value analysis according to the stem volume (PNFI in Table 4). The volume limit, 40 m^3/ha, was the lowest possible which would allow a larger number of plots in the lower volume category — 28 lower volume and 89 higher volume plots (total 117). Furthermore, for classifications and their testing, the unchanged plots were divided geographically into two parts: a northern half for model parameter estimation (11 lower and 41 higher volume category plots, or a total of 52 plots) and a southern half for testing. This simple division was considered adequate since the study area was large and had similar forest conditions. The relationship between plots used for model construction and testing was also not so close as the case would have been if every second plot had been used for model construction and the rest of the plots for testing. A north-south division was chosen instead of east-west, because Spot imagery had radiometric problems in the east-west direction (Courtois 1988).

Finally, the unchanged plots of the southern part were used for testing without stand boundary distance limitations because the preliminary testings indicated that classification results of the unchanged plots were similar whether the distance limitation was used or not.

3.3.4 *Topographical variables*

Three types of topographical variables were used in the study of the damage:

1) absolute elevation from sea level (digital terrain model)
2) normalized squared magnitude of elevation gradient (g)
3) local elevation

The elevation gradient and the local elevation were calculated to study if *Gremmeniella* damage often occurs in lower parts of slopes and depressions (Kurkela 1984b). The quantity g, characterizing the slope, was computed:

$$g = \frac{y_1^2 + y_2^2}{\Sigma(x_i - m)^2} \qquad (10)$$

where

x_i is an elevation value of a pixel in a 3x3 pixel window and the x_i's are located in the window in the following way

$$\begin{matrix} x_1 & x_2 & x_3 \\ x_4 & x_5 & x_6 \\ x_7 & x_8 & x_9 \end{matrix}$$

$$m = \frac{\Sigma x_i}{9}$$

$$y_1 = x_1 + 2x_2 + x_3 - x_7 - 2x_8 - x_9$$
$$y_2 = x_1 + 2x_4 + x_7 - x_3 - 2x_6 - x_9$$

The purpose of dividing by $\Sigma(x_i - m)^2$ (i.e. "normalizing") is to increase the response from pixels with small intensity differences in homogeneous areas.

The local elevation (le) for each pixel was calculated using Formula (11) (Rauste 1983):

$$le = x_c - m + a \qquad (11)$$

where

x_c is elevation value of the center pixel of the used window (5 x 5 pixels)

$m = \frac{\sum_{i=1}^{25} x_i}{25}$ value of the mean filtered elevation image in center of the used 5 x 5 (1 ha) pixels window

a offset factor used to avoid negative values of le; a = 100 was applied.

3.4 Spectroradiometer measurements

The objectives of the spectroradiometer measurements were 1) to study how *Gremmeniella abietina* (Lagerb.) damage changes the spectral reflectance of Scots pine needles and 2) to investigate the relationship between needle biomass and reflectance.

The seedlings were originally acquired to study the chemical and physiological effects of the *Gremmeniella* damage, alone or combined with frost damage (Department for Forest Protection, Finnish Forest Research Institute). The seedlings were of mid-Finnish origin. The seeds had been sown in spring 1984 in paper pots which were placed in plastic boxes. Each box originally had 15 seedlings. In January 1985, the boxes were placed in growth chambers or kept in a greenhouse. Daytime temperature in the growth chambers was over 15 °C. Night temperature was between 5 and 10 °C. Some of the growth chamber seedlings were submitted to frost damage after their shoots had started to grow. During the frost treatment, the temperature was decreased from −3 to −5 °C. Furthermore, in May-June 1985, some of the boxes were inoculated with a conidial suspension of *Gremmeniella*. Thus, four categories of seedlings were created as shown in Table 7.

Table 7. Needle categories in spectroradiometer measurements for *Gremmeniella* damage.

Gremmeniella	Frost treatment		Tot.
	No	Yes	
No	20	4	24
Yes	19	4	23
Total	39	8	47

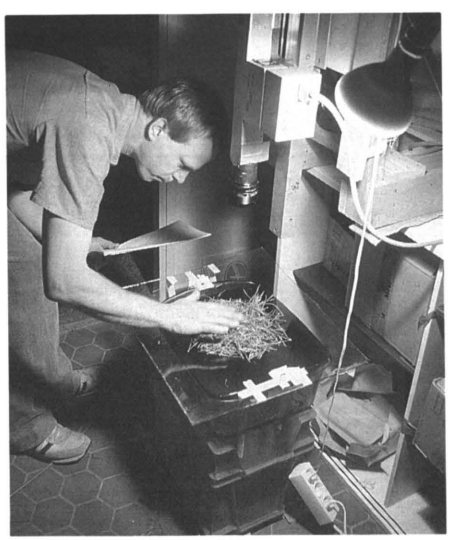

Fig. 9. Organization of spectroradiometer measurements.

After the inoculation the boxes were removed outside where they remained until the day of the measurements.

Spectroradiometer measurements were taken on 17 and 18 May 1986. The measurements were made in a room without windows. The only light source was a 500 W daylight lamp. The spectroradiometer was fixed directly over a black-painted, water-filled plastic dish. On the dish was a clear glass plate. This background was as ideal an absorber of visible light and near infrared radiation as possible. In the middle of the glass plate was a 6.7 cm x 6.7 cm measurement area (Fig. 9). The other arrangements for the measurements were:

Spectroradiometer
- wavelength range: 400—1000 nm with 20 nm bands
- distance between radiometer and sample: 37 cm
- measurement time: approximately 15 seconds

Irradiance
- lamp: Photolita 220 V, 500 W -E27 Type PF 218E/49
- distance from the sample: 70 cm
- elevation angle: 60 degrees

For all measurements, the needles were plucked from the 1985 shoots. The 1986 shoots were missing from many of the damaged seedlings. All samples were taken in like manner. Needles were plucked from one to three boxes until a heap two centimeters high was accumulated on the glass plate.

Healthy seedlings only were selected for the needle biomass measurements. First, the radiance from the plain background was measured. Then, on the glass plate, 0.5 g of fresh needles were weighed and their radiance was measured. Sample weights of the needles were always doubled, so that the subsequent samples weighed 1.0 g, 2.0 g, 4.0 g, 8.0 g, 16.0 g, and 32.0 g, which was the greatest amount of needles measured. The needles in the smallest samples were spread so that they covered as large a portion of the 6.7 cm x 6.7 cm measurement area as possible. The 16.0 g sample formed an approximately 2 cm high heap, which was similar to the heap of the damaged needle measurements. The measurement series was repeated four times, i.e. the number of observations was 8 x 4 = 32.

The measurements were accomplished immediately after the needles were removed from the seedlings. The time between the measurement and the needle removal was 5 minutes maximum in biomass measurements. In damaged needle measurements, the maximum time was 2 minutes.

The irradiance was measured indirectly from a box filled with $BaSO_4$ powder, both in damaged needle and biomass measurements. The box was placed on the glass plate for the irradiance measurement after approximately every sixth needle sample.

4. Data analysis

4.1 Image operations

The most versatile set of operations (Chart 2) was made for image pair TMI84/TMI85. The results of the analyses were used for the other image pairs. Basic operations were, nevertheless, replicated onto image pair TMI85/TMI86 to make sure that results were not dependent on the images used, i.e. on the seasonal aspect or atmosphere during the image acquisition.

Many operations required the use of channel means, standard deviations, and covariance matrices. They were calculated from a 1 percent systematic sample of the image pixels. The intensity values of waters were eliminated from channels TM4 and TM5 when the statistics were computed. In TM4 and TM5 channels, waters formed their own peak in the histogram. The intensity values of clouds were also cut from the TMI86 image, as were the few exceptionally high intensities from other images.

4.1.1 *Difference channels*

The difference channels were computed:

$$\mathbf{y} = \mathbf{x}_{(t)} - \mathbf{x}_{(t-n)} + \mathbf{a} \qquad (12)$$

where

$\mathbf{y}$ is the difference vector

$\mathbf{x}_{(t)}$ original vector of channels at time t

$\mathbf{x}_{(t-n)}$ original vector of channels at time t − n

$\mathbf{a}$ offset vector to avoid negative values. The value of each element of $\mathbf{a}$ was 100.

The difference channels were computed both by using direct subtraction and by calibrating the intensities of image TMI84 to match image TMI85. No matching was performed

Chart 2. Spectral features in Tukey's tests.

TMkyr	Channel k (1—7) of a Landsat Thematic Mapper image. Optional yr stands for the last two digits of the acquisition year of the image. It is used with all abbreviations but only when the context does not tell the year.
SSk	Channel k (1—3) of the Spot summer image.
Dk	Difference channel k calculated from paired bitemporal channels without histogram matching.
DMk	Difference channel k calculated with histogram matching.
Rkl	Ratio feature from channels k and l of monotemporal TM image.
BitRk	Ratio feature from bitemporal paired original channels k.
BitRMk	Ratio feature from bitemporal matched channels k.
DTex	Local variance channel of D3. Window size for variance calculation 3 x 3 pixels. Used only in one final classification.
PCk	k'th principal component computed from covariance matrix of a monotemporal TM image.
PCRk	k'th principal component computed from correlation matrix of a monotemporal TM image.
BitPCk	k'th principal component computed from covariance matrix of a merged bitemporal TM image pair.
BitPCRk	k'th principal component computed from correlation matrix of a merged bitemporal TM image pair.
Cank	k'th canonical variable computed from a merged bitemporal TM image pair.

on image pair TMI85/TMI86 since its intensity value distributions were similar without scaling.

Franssila et al. (1982) have used the applied matching method originally to scale images for digital mosaicking:

$$y_{kc} = (s_{kb}/s_{kc}) \cdot x_{kc} + (m_{kb} - m_{kc} \cdot s_{kb}/s_{kc}) \quad (13)$$

where

- y_{kc} is scaled intensity of a pixel
- x_{kc} intensity of a pixel of image c in channel k
- s_{kb} standard deviation of intensities of master image b in channel k
- s_{kc} standard deviation of intensities of image c to be scaled in channel k
- m_{kb} and m_{kc} are the intensity means of the respective images

The method assumes that intensity differences between images are due to different irradiance and/or general differences in atmospheric conditions. It is also assumed that no large-area field changes have occurred between the dates of image acquisition. For instance, clear cuttings cover only 1 to 1.5 percent of the forest area annually.

To compute the difference channels from image pair TMI84/SSI87, the TMI84 intensities were scaled using linear regression analysis (Frank 1984, Vogelmann 1988):

$$SS_k(87) = a_k + b_k\, TM_k(84) + e_k \quad (14)$$

where

- SS_k is channel k in SSI87 image
- TM_k channel k in TMI84 image
- e_k residual of the model (difference channel)
- a_k and b_k are parameters of the regression model

The regression method was applied to image pair TMI84/SSI87 since the NFI plot data were measured around the acquisition dates of the two images. The model was calculated from the intensities of the unchanged NFI plots only. The residual values representing the difference image were computed for all pixels.

The corresponding Landsat and Spot channels did not fit very well in the visible area of the spectrum. The coefficients of determination (R^2) were 0.46 in the green light (TM2, SS1), 0.56 in the red light (TM3, SS2), and 0.79 in the near infrared (TM4, SS3). The reasons for the low coefficients of determination in the visible channels may be the autumn aspect in the TMI84 image and the three year time span between the images.

In intensity matching, transformation to reflectance values (mentioned in Section 2.4.3) was not used because it is, so far, only a partially understood problem.

4.1.2 Ratio channels

The values of the ratio channels were calculated as a simple ratio of two features. The value was a real number. The monotemporal ratio channels were computed:

$$y_{kl} = x_k / x_l \quad (15)$$

where

- y_{kl} is value of the channel ratio of a pixel
- x_k value of the channel k of a pixel
- x_l value of the channel l of a pixel

The bitemporal ratio channels were computed as:

$$y_k(t, t-n) = x_k(t)/x_k(t-n) \quad (16)$$

where

- $y_k(t, t-n)$ is value of a pixel of a bitemporal ratio channel k
- $x_k(t)$ value of a pixel in channel k at time t
- $x_k(t-n)$ value of a pixel in channel k at time t−n

4.1.3 Principal components

The principal component transformations were calculated from monotemporal images (nonthermal channels) and from combined

Table 8. Correlation coefficients between Landsat Thematic Mapper channels and first five principal components and proportion of the total imagery variance included in the components. Bitemporal principal components, image pair TMI84/TMI85.

Channels	Principal component axes					
	1 Cov. Corr.	2 Cov. Corr.	3 Cov. Corr.	4 Cov. Corr.	5 Cov. Corr.	
TM184	0.71 0.85	0.23 −0.01	0.33 −0.37	−0.34 −0.09	−0.06 0.21	
TM284	0.79 0.90	0.13 0.13	0.39 −0.32	−0.27 −0.09	0.03 0.01	
TM384	0.76 0.90	0.24 0.01	0.37 −0.36	−0.32 −0.05	−0.05 0.06	
TM484	0.77 0.69	−0.33 0.61	0.38 0.07	0.15 −0.08	0.37 −0.34	
TM584	0.91 0.91	0.11 0.25	0.37 −0.07	0.07 0.25	−0.14 −0.06	
TM784	0.86 0.91	0.22 0.12	0.36 −0.18	−0.07 0.25	−0.18 0.00	
TM185	0.74 0.87	0.39 −0.37	−0.04 0.10	−0.04 −0.19	0.16 −0.07	
TM285	0.82 0.91	0.26 −0.23	−0.04 0.16	−0.41 −0.22	0.15 −0.04	
TM385	0.73 0.86	0.47 −0.43	−0.05 0.11	−0.40 −0.12	0.18 −0.12	
TM485	0.78 0.60	−0.60 0.59	−0.14 0.42	−0.07 −0.21	−0.05 0.25	
TM585	0.93 0.87	0.26 −0.07	−0.24 0.37	0.11 0.25	0.01 0.10	
TM785	0.84 0.88	0.46 −0.29	−0.17 0.24	−0.07 0.21	0.07 0.01	
Percent	72.1 72.5	15.3 10.6	6.9 7.0	2.3 3.4	1.9 2.2	Tot. 98.4 Tot. 95.5

bitemporal images (bitemporal nonthermal channels) using both covariance and correlation matrices.

Table 8 (p. 37) indicates that the first principal component from the covariance matrix was a positive sum of all channels, i.e. the "brightness" of the image (upper row of Table 8) (Kauth and Thomas 1976, Badhwar and Henderson 1982). The second principal component reflected the differences between the visible and near infrared channels, and the third reflected differences between the two images when the components were calculated from the covariance matrix. A rough characterization of the remainder of the components is difficult.

The content of the first two principal components from the monotemporal images was similar to the bitemporal principal components, but the third component reflected the sum of the visible channels, and to some extent the differences between TM5 and other channels. Singh and Harrison (1985) have found similar content in the first two principal components from the Landsat MSS data, as have Horler and Ahern (1986) from the TM data. Also, Seal (1964) states that, for most biological data sets, the first component is the positive sum of the original variables because most covariances are positive.

If a correlation matrix was used (lower row in Table 8), the weight of the visible channels increased because, in the original data, they had smaller deviations than the near infrared and middle infrared channels. The first component is still a positive sum of the channels, but interpreting the second component is difficult. The proportion of the total variance, which is included in the component, decreased more slowly when the transformation was calculated from correlation than from covariance matrix.

4.1.4 Canonical variables

The quantitative variables in canonical discriminant analysis were the paired channels TM1, TM3, TM4, and TM5 of image pair TMI84/TMI85. Their intensities were selected by the classes of the ground truth data in Set1. Program CANAL of the DISIMP (1987) software was used to make the analysis. The disk space limited the number of the input channels to eight.

4.2 Acquiring preliminary information about class separability

4.2.1 Tukey's studentized range tests

The paired intensity differences of the change and reference class categories were analyzed using Tukey's studentized range tests. The tests are meant to analyze all possible pairs of means of samples. The following partial hypotheses are tested simultaneously:

$$H0': \mu_i = \mu_j$$
$$H1': \mu_i \neq \mu_j,$$

where μ_i is the true mean of sample (class) i, $i \neq j$, i, j = 1,..., p. p is the total number of classes. Two means are considered significantly different if (SAS Institute Inc. 1988, p. 596):

$$\frac{|m_i - m_j|}{s\sqrt{((1/n_i + 1/n_j)/2)}} \geq q(\alpha\,;\, p,\, pN - p) \qquad (17)$$

where

$$m_i = \frac{\sum_{k \in S_i} x_k}{n_i}, \quad \text{where}$$

x_k is the intensity mean of a spectral feature in stand k (mean of 5 pixels in data set PNFI)
S_i is the set of stands belonging to class i
n_i the number of stands belonging to class i, i.e. the number of elements in S_i
s the pooled standard deviation of the intensities
$q(\alpha\,;\, p, pN\text{-}p)$ is the α-level critical value of a studentized range distribution of p independent variables with pN-p degrees of freedom. $\alpha = 5$ percent was applied. N is total number of stands.

The separation of different deciduous shrub removal classes was not possible in Tukey's tests because of the small number of stands.

4.2.2 Experimental discriminant models

The experimental discriminant models were computed to find the best set of spectral features to separate the changes. Feature sets were compared by testing how well the input data fitted to the discriminant model. The applied formula will be given in the Section "4.4.2 Maximum likelihood classifier". The experimental models included no reject class, and the *a priori* probabilities of the classes were equal. Chart 3 shows the feature sets tested. The feature combinations were chosen based on what was known about the spectral properties of the vegetation and about the relationships between channels. The results of the Tukey's tests obtained in the study were utilized, too.

Because of their known close relationship with vegetation and their quite low mutual correlations (Table 9), bitemporal channels TM1, TM3, TM4, and either TM5 or TM7 were selected when eight original channels were used. (Correlation between TM1 and TM3 is high, but lower than correlation

Chart 3. Tested features in the experimental discriminant models.

Monotemporal data		
+	Orig84	Original channels TM1, TM3, TM4, TM5 from TMI84
+	Orig85	Original channels TM1, TM3, TM4, TM5 from TMI85
Bitemporal data		
	PO1	Paired original channels TM1
	PO2	Paired original channels TM2
	PO3	Paired original channels TM3
	PO4	Paired original channels TM4
	PO5	Paired original channels TM5
	PO6	Paired original channels TM6
	PO7	Paired original channels TM7
+	POSpot	Paired original channels TM2, TM3, TM4
+	PO1345	Paired original channels TM1, TM3, TM4, TM5
+	PO1347	Paired original channels TM1, TM2, TM3, TM7
	POVI	Paired ch. TM3, TM4, TM5 and paired ratio TM3/TM4
	D1	Difference ch. from unmatched channels TM1
	D2	Difference ch. from unmatched channels TM2
	D3	Difference ch. from unmatched channels TM3
	D4	Difference ch. from unmatched channels TM4
	D5	Difference ch. from unmatched channels TM5
+	DUnM	Difference ch. from unmatched non thermal TM channels
	DMacth	Difference ch. from matched non thermal TM channels
	PRatBest	Paired ratio ch. TM1/TM3, TM3/TM4, TM1/TM5, TM3/TM5
	PRatWorst	Paired ratio ch. TM2/TM3, TM3/TM4, TM3/TM5, TM4/TM5
	RatD	Diff. features R1385-R1384, R3485-R3484, R1585-R1584, R3585-R3584
	DRat	Ratio D1/D3, D3/D4, D1/D5, D3/D5
	Miscell	TM184, TM385, TM485, paired TM5, R2384, BitRM3, BitRM4
+	PPC123	Paired princ. comp. 1, 2, 3 from covariance matrix
+	PPC124	Paired princ. comp. 1, 2, 4 from covariance matrix
+	PPC1234	Paired princ. comp. 1, 2, 3, 4 from covariance matrix
	PPCVI	Paired princ. comp. 1, 3, 4 and paired ratio TM3/TM4
	PPCR123	Paired princ. comp. 1, 2, 3 from correlation matrix
	PPCR124	Paired princ. comp. 1, 2, 4 from correlation matrix
	PPCR1234	Paired princ. comp. 1, 2, 3, 4 from correlation matrix
	BiTPC	Bitemporal princ. comp. 1—5 from cov. matrix of merged TMI84 TMI85 data set. Non thermal TM channels
	BiTPCR	Like BitPC but princ. comp. from correlation matrix
	BiTCan	Bitemporal canonical variables from merged TMI84 TMI85 data set. Non thermal channels

+ Corresponding features have been tested in image pair TMI85/TMI86, too.

Table 9. Correlation coefficients between channels of image TMI85.

	TM1	TM2	TM3	TM4	TM5	TM7
TM1	1.00					
TM2	0.91	1.00				
TM3	0.92	0.94	1.00			
TM4[1)]	0.37	0.51	0.32	1.00		
TM5[1)]	0.75	0.79	0.77	0.59	1.00	
TM7	0.84	0.85	0.88	0.41	0.93	1.00

[1)] Intensities of water closed out of computing.

between TM2 and TM3). TM3, which is in the chlorophyll absorption area and has a close relationship with green biomass, and TM4 which also reflects the amount of green biomass, have been the two most important wavelengths in vegetation interpretation (Gates 1970, Tucker 1979, Tucker 1980, Tucker et al. 1975). It was determined that one channel should also be chosen from the middle infrared, the leaf water absorption area (Gates 1970, Hopkins et al. 1988). TM5 had somewhat lower correlations with the visible channels than did TM7.

The maximum number of features in the experimental models was eight. The limit was set because some classes had so few observations that the required matrix operations could not have been calculated using a greater number of independent variables. Furthermore, regarding the classifications of image data, the available disk space set the limit to eight features.

4.3 Regression estimates

The drain in the thinning cuts was estimated using the images TMI84 and SSI87. This pair covered the time between the two field measurements of the NFI. The NFI data were used to estimate the drain because data in the stand sets were less reliable.

The regression estimates were calculated using two input data sets from PNFI. The first set included 25 thinning cut plots and the 65 unchanged plots from thinning-aged stands. The second set covered the thinning cut plots only. The estimation method was regression analysis using SAS software with the MAXR option. The method fits the best one variable model, the best two variable model and so on. Variables are switched so that the R^2-value is maximized. SAS uses the least squares estimation (SAS Institute Inc. 1988).

Drain, the dependent variable, was obtained calculating the difference between the stem basal areas in 1984 and 1987. Preliminary correlation analysis had shown that the correlation between calculated drain and spectral variables was higher than the correlation between the measured drain and spectral variables. The reason may be that some stumps were unrecorded by the field crew.

The number of independent variables was restricted to two due to the small number of thinning cut plots. Similarly, the data set was not divided into subpopulations by means of age or tree species. Independent variable groups were:

1) all original channels
2) difference channels without histogram matching
3) difference channels with histogram matching.

Damage was divided into two categories for the classifications. The study also investigated whether the damage grade in these categories could be estimated. A regression analysis procedure similar to the drain estimation was applied. The dependent variable was the percent of damage on the plot. The independent variables were the three topography related variables and spectral features. The analysis was made using procedure REG with the maximum R^2 improvement technique of the SAS/STAT software (SAS Institute Inc. 1988).

Several (1—5) *Gremmeniella* plots had been measured within a same stand type area; therefore, the following regression model was also tested:

$$EDam = a + b_1x_1 + b_2x_2 + \ldots + b_nx_n + s + e \quad (18)$$

where

EDam	is	estimate for the degree of damage (%) for a pixel
a		intercept of the model
b_k		parameter for spectral feature k
x_k		value of a pixel in spectral feature k
s		offset factor for the stand where the pixel belongs
e		residual of the model
H0 hypotheses were:		
H_a:		$a = 0$
H_b^a:		$b_k = 0$
H_s:		between-stand variance of damage = 0

The model was a combined fixed effect and random effect model, where the fixed effects were the spectral features and the random effects the stands. The number of separate stands was 20 in the light damage category which had 36 sample plots, and 15 in the heavy damage category which had 25 plots (24 were used in the regression analyses because of exceptional intensity values in TM185 in one plot). The analysis was made using the GLM procedure of the SAS/STAT software with the "random" option for a variable that indicated the stand number of a plot (SAS Institute Inc. 1988).

Using the formula from Kellomäki et al. (1980) for pine crown biomass estimation, the damage percentages in the field inventory were transformed into the damaged biomass. The experiments, however, showed that the original damage grade estimation method was more suitable than the transformed.

4.4 Image classifications

Three supervised methods and one unsupervised method were applied. The supervised methods were the non-parametric parallelepiped classification (Lillesand and Kiefer 1987), the Euclidean distance classification, whose only parameter is the class mean, and the maximum likelihood classification (discriminant analysis using the generalized quadratic discriminant functions). The classifications were tested using data which were not included in the parameter estimation. Testing was made for both original and post processed classifications. The unsupervised method was non-parametric.

The first classification experiments were performed using the parallelepiped classification. The results were hampered by the human restrictions to handle more than three dimensional space and subjectivity in class boundary selection. Thus, the parallelepiped classifications were not continued after the first experiments.

4.4.1 Euclidean distance classifier

In the Euclidean distance classification, the intensity vectors are classified in the class to which the Euclidean distance is shortest. The pixel is classified as class c for which the discriminant function g_c gets the highest value:

$$g_c(\mathbf{x}) = \mathbf{x}^T \mathbf{m}_c - 0.5\, \mathbf{m}_c^T \mathbf{m}_c \quad (19)$$

where

$\mathbf{x}$	is	observation vector for a pixel
$\mathbf{m}_c$		mean vector for class c

The Euclidean distance classification did not have any unclassified category or reject class; all pixels were classified.

4.4.2 Maximum likelihood classifier

The ordinary maximum likelihood classification method with equal *a priori* probabilities and the Bayesian approach with altering *a priori* probabilities were applied. Both approaches are later called the maximum likelihood classification. The parameters of the density function of the normal distribution are calculated for all classes using the mean vectors and covariance matrices of the ground truth areas. The form of the density function in the Bayesian maximum likelihood classification is:

$$f_c(\mathbf{x}) = \frac{p_c}{(2\pi)^{nch/2}\,|\mathbf{S}_c|^{1/2}}\; e^{-1/2\,(\mathbf{x}-\mathbf{m}_c)^T \mathbf{S}_c^{-1}(\mathbf{x}-\mathbf{m}_c)} \quad (20)$$

where

$f_c(\mathbf{x})$	is	probability that observation vector $\mathbf{x}$ for a pixel belongs to class c
p_c		*a priori* probability that a randomly selected vector belongs to class c
$\mathbf{m}_c$		the mean vector for class c
$\mathbf{S}_c$		covariance matrix for class c
nch		number of features (channels)

The *a priori* probability is an external factor that affects *a posteriori* probabilities of the vectors to be classified. The vector is placed in the class where the *a posteriori* probability is the highest, or to the reject class. The optional threshold value controls whether the vector is assigned to a real class or to the reject class.

Two classification programs, SMAXLIX and DAN, were used for the maximum likelihood classifications. Both had been developed at the Technical Research Centre of Finland and were based on the DISIMP software. SMAXLIK uses the output of the SIGARE program of DISIMP whereas DAN uses the SAS output. The final *a posteriori* probability is calculated differently in the two programs. SMAXLIX calculates the *a posteriori* probabilities using only Formula (20), but DAN divides the highest *a posteriori* probability from Formula (20) by the sum of all *a posteriori* probabilities for a certain observation vector. Therefore, a quite low unscaled *a posteriori* probability can turn out high if the probabilities for other classes are much smaller. The classification results with both programs are identical if there is no reject class.

The threshold value for the reject class is the scaled *a posteriori* probability in the DAN program. It is possible that vectors which should be classified to the reject class are classified to a real class if the ground truth data does not represent well the spectral variation in the image.

In the SMAXLIK program, the threshold value is a selected value of the quadratic product. The product can be thought of as a squared distance function measuring the distance between the intensity vector and the class mean as scaled and corrected for variance and covariance of the class (Strahler 1980):

$$(\mathbf{x}-\mathbf{m}_c)^T \mathbf{S}_c^{-1} (\mathbf{x}-\mathbf{m}_c) < \mathbf{m}_{1-\alpha_c} \quad [\chi^2(\text{nch})] \qquad (21)$$

where

α_c is the significance level for the class c or probability that a vector really belonging to class c is placed to the reject class. $\alpha_c = 2\,\%$ was applied for all classes and in all classifications.

$\mathbf{m}_{1-\alpha_c}$ $[\chi^2(\text{nch})]$ is the upper $(1-\alpha)$ point of the χ^2 distribution with nch degrees of freedom

For description of other terms, see Formula (20).

If Formula (21) is not valid for any class, the vector is placed in the reject class.

Differences in the SMAXLIK and DAN programs were seen in water areas. Waters without their own spectral classes were assigned to the reject class by SMAXLIK, but were assigned to the real classes by DAN program. Possible differences in the forested areas were not easily detectable since the ground truth data covered the spectral variation and the proportion of the reject class was very low in all classifications.

If the *a priori* probabilities are used, the classification results are not dependent only on the spectral signatures of the classes. For example, the *a priori* probabilities can be proportional to the presumed areas of the classes in the area to be classified, or they can be calculated using the values of a category variable or elevation data (Strahler 1980, Rauste 1983). The closer the *a priori* probability is to the value one or zero, the smaller is the effect of the spectral signature.

The *a priori* probability may be uniform for a certain class or a function of the values of a continuous external variable. Rauste (1983) found that the general performance of a land use/forest canopy type classification increased by 8 percentage units when the *a priori* probability for each pixel was a function of the elevation gradient magnitude of that pixel. The elevation gradient was calculated from a digital terrain model. The study area was in Southern Finland, and the image data Landsat MSS.

Threshold values and *a priori* probabilities can be used to control the risk of misclassifications. Variables with any distribution can be combined to classifications if they are used as "external" variables to change the *a priori* probabilities.

The maximum likelihood classification is a widely used method in remote sensing since the spectral classes are usually assumed to have a multinormal or nearly multinormal distribution. The average probability for incorrect classification is lower than with any other method based on classification of a single random vector if the intensities of the classes have a multinormal distribution. The maximum likelihood classification also gives good results when the distributions are nearly multinormal (Denissoff 1981).

The classification models were constructed according to the results of Tukey's tests and experimental discriminant analysis. In classifications for Landsat TM images, the mean vectors and covariance matrices for classes were calculated using all the pixels falling in the stands sampled to the model construction.

The parameters of the TM/Spot classification models were computed using NFI data, which included the mean values of the five pixels surrounding the plot. The type of ground truth caused the number of pixels per class in the TM/Spot classifications to be considerably lower than in the TM/TM classifications. Given the restrictions described in Section 3.3.3, changed plots, where the distance to the unchanged forest was at least 20 meters, were accepted in the model.

The histogram matching method, which was based on means and standard deviations of images (Franssila et al. 1982) (Formula 13), was applied to test if the class statistics could be transferred to new images. The TMI84 and TMI86 images were calibrated similarly to the TMI85 image. Then, the mean vectors and covariance matrices were calculated from image pair TMI84/TMI85. Image pair TMI85/TMI86 was classified using these statistics.

The TM/TM classifications were made with the SMAXLIK and the TM/Spot classifications with the DAN program.

4.4.3 Unsupervised method

Clustering was used to test a different approach from the parametric supervised methods. The aim was also to find out how representative was the training data for the supervised classification. To fulfil the requirement for dissimilarity, a non-parametric method was selected from among many different clustering methods.

The scheme for the selected unsupervised method was presented by Narendra and Goldberg (1977), and it has been developed further by Wharton (1983) and Rouge (1987). The method is based on the clustering of the multidimensional histogram or frequency table of the image to be classified. The method has the following steps:

1) The frequency values are linked to neighboring values which have the maximum frequency so that no cycles result. The local maxima members of the frequency table are not linked to any pixel. The co-linked members define the class.
2) Individual labels are assigned to the formed trees or classes. A look-up table is made to show which intensity values of the spectral features correspond to the frequency values.
3) Each pixel of the image is classified according to the look-up table.

The number of formed classes and their content can be controlled only by changing the input features and their scaling. However, the number of output classes can be controlled using a single parameter that tells the required minimum modal frequency value of each class. Classes having modal frequency values lower than the value of the parameter are combined into the reject class.

The algorithm is not sensitive to the absolute intensity values because the classes are determined as clusters in the frequency table. Instead, it is sensitive to the intensity range of the input features. If one input feature has a wider dynamic range than others, it often dominates the class formation. Of course, the domination depends mainly on the distribution of the feature.

The whole n-dimensional histogram had to be in the central memory (6 MB) of the computer (VAX 11/750). That is why the number of features and/or intensity values had to be limited. A compromise between the two methods was made to limit the size of the table. Only three features were used, and the number of intensity values per channel was limited to 30. Values were scaled so that all waters were set to a single value if they formed their own peak in the histogram of the feature. Two percent of the highest values of the cumulative histogram were also combined to a single value. The rest of the values were set by means of a linear scaling. The intensity range of the red light channel was somewhat increased while the intensity ranges of the near and middle infrared channels were decreased. That was done to increase the weight of the red light range in the clustering. The whole image area, 40 km by 40 km, was clustered.

4.4.4 Testing of classifications

Chart 4 summarizes the supervised classifi-

Chart 4. Classifications made and tested.

Name	Images	Classification method	Features	*A priori* probab.	Modal filt.	Statistics	Testing
Euclidean	TMI84/TMI85	euclid. dist	original	not avail.	no	Setl+Dam	Set1+Dam
MLOrigEq	TMI84/TMI85	max. likelih.	original	equal	no	Setl+Dam	Set1+Dam
MLOrigAlt	TMI84/TMI85	max. likelih.	original	altering	no	Setl+Dam	Set1+Dam
MLOrigAltF	TMI84/TMI85	max. likelih.	original	altering	yes	Setl+Dam	Set1+Dam
MLDiffEq	TMI84/TMI85	max. likelih.	differ.	equal	no	Setl+Dam	Set1+Dam
MLDiffEqF	TMI84/TMI85	max. likelih.	differ.	equal	yes	Setl+Dam	Set1+Dam
MLDiffTriEq	TMI84/85/86	max. likelih.	differ.	equal	no	Setl+Dam	Set1+Dam
MLDiffTexEq	TMI84/TMI85	max. likelih.	diff.+var.	equal	no	Setl+Dam	Set1+Dam
Euclidean	TMI85/TMI86	euclid. dist.	original	not avail.	no	Set2+Dam	Set2+Dam
MLOrigEq	TMI85/TMI86	max. likelih.	original	equal	no	Set2+Dam	Set2+Dam
MLOrigAlt	TMI85/TMI86	max. likelih.	original	altering	no	Set2+Dam	Set2+Dam
MLDiffEq	TMI85/TMI86	max. likelih.	differ.	equal	no	Set2+Dam	Set2+Dam
MLOrigTraAlt[1]	TMI85/TMI86	max. likelih.	original	altering	no	Set2+Dam	Set2+Dam
MLOrigEq	TMI84/SSI87	max. likelih.	original	equal	no	PNFI	Set1,2+Dam, PNFI
MLOrigAlt	TMI84/SSI87	max. likelih.	original	altering	no	PNFI	Set1,2+Dam, PNFI

1) Classification statistics from image pair TMI84/TMI85.

cations made and lists the data sets used in model construction and testing. When the test data set consisted of stand type areas (Set1, Set2, and Dam), the class distribution within each stand was calculated. The modal or most frequent class of the stand was considered the interpretation result.

Two classifications, MLOrigAltF and MLDiffEqF, were post-processed using filtering by image segments. After the filtering, the modal class within each stand was computed as in the testing of pixel by pixel classifications.

The NFI data-based classifications were tested using stands and plots. The stands of Set1 and Set2, and plots of damage data, were the changed data. The unchanged NFI plots were the unchanged data. The class for a NFI plot was the modal class of the 3x3 pixel window surrounding the plot.

Only stands and plots with intensities not used to estimate the parameters for the spectral classification models were employed for all tests.

4.5 Image segmentation

Image segmentation was utilized to reduce the impact of the noise and minor variation in the image, and to extract the changed areas as a whole. Also, because the classification was performed pixel by pixel, the segmentation brought spatial information into the interpretation. The segmentation was used for post-classification filtering. The filtering windows were obtained from image segmentation. The image to be filtered was the pixel by pixel classification result. The most frequent or modal class within each segment was calculated, and a new image was computed where the segments were filled with their modal classes. The small adjacent segments formed larger uniform areas, i.e. the changed or unchanged areas.

Filtering of the intensities of the raw data was tested before the classification was done. This lead to relatively large changes in proportions in class areas, when compared to the pixel by pixel classification. Therefore, the post-classification alternative was preferred.

The segmentation method was originally developed by Narendra and Goldberg (1980), and developed further by Parmes and Kuittinen (1988). The method uses an approach similar to the clustering described in Section 4.4.3. However, the input features in the image segmentation are spectral instead of the frequency table which was used in the clustering.

A user-defined threshold value e is required to control the number of the segments. Decreasing the threshold value increases the number of segments, but does not move the location of the boundaries, which would result from the use of a higher threshold value (Narendra and Goldberg 1980).

Narendra and Goldberg's method uses a region detection approach, but it also has characteristics of the edge operation methods which have been the other main approach to segmentation. Their method avoids absolute thresholds, however, and therefore yields well-defined region boundaries even when the transition from one region to the next is slow and varying (Narendra and Goldberg 1980).

The segmentation has four phases (Parmes and Kuittinen 1988):

1) Calculation of the maximum gradient magnitude z(i,j) for the pixel (i,j) from a 3x3 pixel window.

$$z(i,j) = \max_{\substack{n=1,\ldots,nk \\ l=1,\ldots,nl}} \left| \sum_{a=-1}^{1} \sum_{b=-1}^{1} \mathbf{M}_k(a,b) \cdot \mathbf{I}_n(i+a, j+b) \right| \quad (22)$$

where
- **I** is image matrix
- nk number of channels
- nl number of boundary templates **M** (nl = 4). The boundary templates **M** (concolution matrices) were

$$\begin{matrix} -1 & -1 & -1 \\ 0 & 0 & 0 \\ 1 & 1 & 1 \end{matrix} \qquad \begin{matrix} 0 & 1 & 1 \\ -1 & 0 & 1 \\ -1 & -1 & 0 \end{matrix} \qquad \begin{matrix} -1 & 0 & 1 \\ -1 & 0 & 1 \\ -1 & 0 & 1 \end{matrix} \qquad \begin{matrix} -1 & -1 & 0 \\ -1 & 0 & 1 \\ 0 & 1 & 1 \end{matrix}$$

2) Calculation of the maximum difference between the maximum gradient magnitude of the pixel and its neighboring maximum gradient magnitudes, and determination of the evident root and boundary pixels.

$$d(i,j) = \max_{a,b=-1,1} (z(i,j) - z(i+a,j+b)) \quad (23)$$

If $d(i,j) < -e$: Pixel is an evident root pixel; no linking.

If $d(i,j) > e$: Pixel is an evident boundary pixel; linking to the neighboring pixel which has the minimum value of the gradient magnitude.

3) Linking of the remaining pixels to the neighboring pixels which have the minimum value of the gradient magnitude so that no cycles are formed. The linked pixels form the closed segments.
4) Giving individual labels to the formed trees or segments.

The best segmentation results were achieved when the input features were bitemporal TM3 channels and channel TM4 from the later image. Using bitemporal data, finding the normal stand boundaries and the boundaries of the changed regions was attempted. The near infrared channel TM4 extracted regions according to the proportion of deciduous trees and by the site type. Before the segmentation, the means of all three channels were scaled to 100, and the standard deviations of the intensities to 30. The segments would have been extracted nearly according to the intensities of the as root, boundary, or intermediate pixel according to the channel which happened to have the maximum difference of gradient magnitudes.

The threshold value e was set so low that the mean size of the resulting segments was on average only nine pixels. The boundaries of minor changes would not have been discerned if higher threshold values had been used.

5. Results of intensity value analyses and classifications

5.1 Spectroradiometer measurements

The healthy needles were dark green and on average 7 cm long. The needles damaged by the *Gremmeniella* were grayish brown, usually shorter than the healthy ones, and had turned nearly woody. The frost needles from seedlings that were also inoculated with the *Gremmeniella* were reddish brown and short, only 2.5 to 3.0 cm long. They were soft, not woody. Thus, the texture of the needle heap damaged by frost plus *Gremmeniella* was different from the texture of the non-frost heap. The needles from plants with frost treatment, but without *Gremmeniella* inoculation, did not look as heavily damaged.

The radiance measured from the $BaSO_4$ box was transformed to irradiance (Saukkola 1983). The reflectance factors for every 20 nm wavelength channel were calculated as the ratio of the sample radiance and the irradiance. The reflectance factor data were analyzed using the General Linear Model Procedure (GLM) for unbalanced ANOVA of the SAS statistical software. The testing was done using a fixed effects model of a factor experiment. A single spectral measurement of a spectral channel can be expressed as:

$$R_{ijk} = \mu + \alpha_i + \beta_j + \gamma_{ij} + \epsilon_{ijk} \quad (24)$$

where
- R_{ijk} is reflectance factor value of a single measurement
- μ grand mean of all measured reflectances of a spectral channel
- α_i main effect of the *Gremmeniella* damage in level a_i ; i = 1,2
- β_j main effect of the frost treatment in level b_j ; j = 1,2
- γ_{ij} interaction between *Gremmeniella* damage and frost treatment
- ϵ_{ijk} error term ; k = 1,47 (47 is the number of reflectance measurements). ϵ_{ijk} is normally distributed with zero mean.

H0 hypotheses were:

H_α: $\alpha_1 = \alpha_2 = 0$

H_β: $\beta_1 = \beta_2 = 0$

$H_{\alpha\beta}$: $\gamma_{11} = \gamma_{12} = \gamma_{21} = \gamma_{22} = 0$

The null-hypotheses were tested using F-test on each of the 30 spectral channels.

The type III square sum which is meant for the unbalanced ANOVA (i.e. different number of observations in different categories) was computed for the tests (SAS Institute Inc. 1988, p. 588). The ordinary method to calculate the square sum in the variance analysis gave test results similar to the type III square sum. There were some differences, and in all cases the type I square sum would have given a higher F-value.

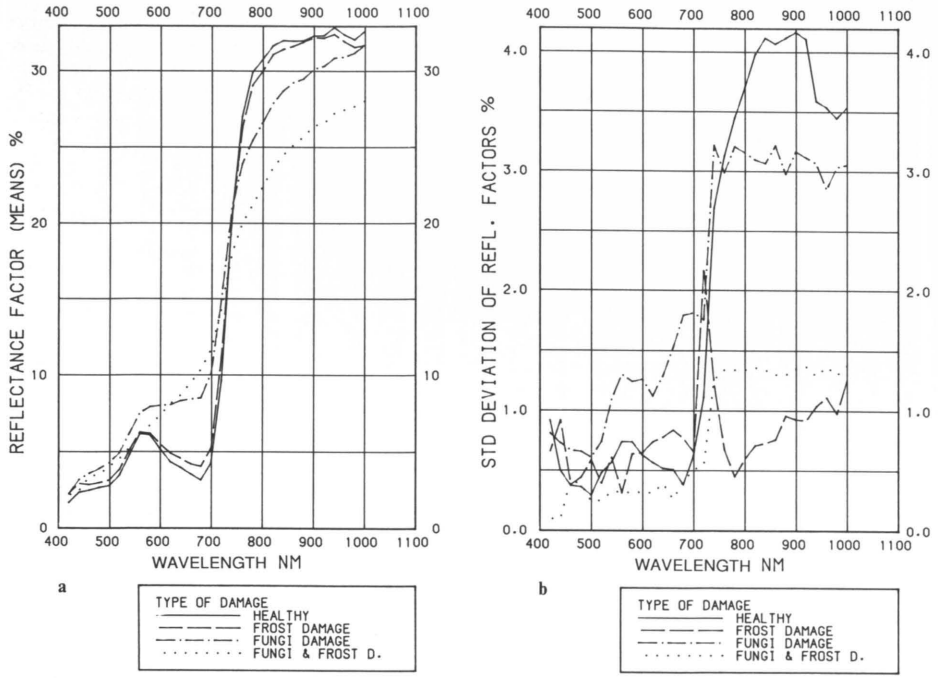

Fig. 10. a) Means of reflectance factors of damaged and healthy *Pinus sylvestris* L. needles. b) Standard deviation of reflectance factors.

The *Gremmeniella* damage increased the visible light reflectance, but decreased the near infrared reflectance (Fig. 10a and b). According to the results of the variance analysis, the damaged needles differed from the healthy, mostly in the red light range (Fig. 11). Note that the F-value peaks at

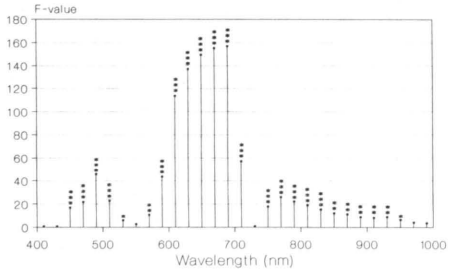

Fig. 11. F-values and rejection of H0: means equal. ANOVA to spectroradiometer measurements. Groups: Healthy needles, damaged needles. Bars represent the center of the 20 nm wavelength area.

480—500 nm and 680—700 nm are at longer wavelengths than the absorption maximum of chlorophylls and other plant pigments (Gates 1970).

The greatest individual differences in the reflectance were found in the near infrared range where the variation was largest. The frost damage alone may have an effect on the reflectance of red light 640—660 nm (*), 660—680 nm (**), 680—700 (**), and on the shorter near infrared wavelengths 740—760 nm (*), 760—780 nm (*), 780—800 nm (*). There seems to be a interaction between the *Gremmeniella* and frost damage on the blue and green light range 420—440 nm (**), 520—540 nm (*) and 540—560 nm (*).

The biomass measurements showed that, when the biomass increased, the values of the reflectance factor in the near infrared increased much more steeply than the reflectance in the visible range (Fig. 12a and b). The reflectance of the 0.5 g sample compared to the reflectances of the 32 g sample was over 0.6 in the blue light and red

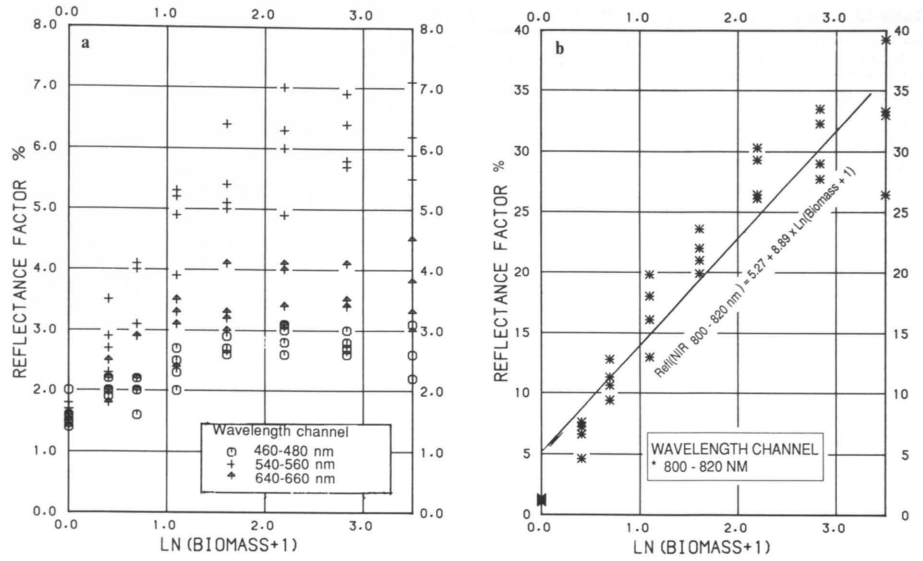

Fig. 12. Reflectance factor vs. needle biomass. Spectroradiometer measurements. a) Visible channels. b) Near infrared channel.

light channels, approximately 0.4 in the green light channel, but only 0.2 in the near infrared channel.

Near infrared reflectance increased during the measurement series. By the 32.0 g sample measurement, the increase appeared to be more even. The heap was probably so thick that only a small proportion of the radiation could reach the lowest layers of the heap and go through the whole heap. The visible light does not penetrate as well as the near infrared radiation. The green light reflectance increased up to the 8.0 g biomass (Ln(Biomass +1) = 2.2), and the blue and red light reflectances increased up to the 4.0 g biomass (Ln(Biomass +1) = 1.6). A regression model was computed to estimate the near infrared reflectance ($Refl(NIR_{800—820\ nm})$):

$$Refl(NIR_{800—820\ nm}) = \underset{***}{5.27} + \underset{***}{8.89} \times Ln(Biomass+1) \quad (25)$$

Asterisks under the function show the significance of the parameters. The number of observations was 32 and the coefficient of determination $R^2 = 0.90$. The reflectance, and not the needle mass was the dependent variable, since the applied estimation reflects the true situation: biomass causes a certain reflectance. If the aim had been to construct a model to estimate the biomass, the dependent and independent variables should have been interchanged. In this case, the aim was to obtain more information about the spectral properties of conifers.

5.2 Spectral properties of changes

5.2.1 Drain estimation in thinning cuttings

Near infrared intensities seem to decrease when the drain from thinning cuttings increases, but the relationship is weak (Table 10, Fig. 13). The estimation of the drain (EDrain) succeeded modestly if thinning cut plots only were accepted to the model (Formula 26, Fig. 14):

$$EDrain = \underset{***}{16.87} + \underset{*}{1.28} \times (SS2\text{-}TM384) - \underset{**}{0.74} \times (SS3\text{-}TM484) \quad (26)$$

The $R^2 = 0.39$. The model was computed using 25 observations. The difference channels were computed without histogram matching. The drain estimation did not

Table 10. Drain and spectral variables. H0: r = 0.

Variable	Mean	Std. dev.	Minimum	Maximum	Corr. with drain	H0:rej.
Drain, (m^2/ha)	7.6	3.62	1.0	14.0	1.00	
SS1	27.4	1.25	25.2	30.0	−0.08	
SS2	14.7	1.39	12.4	18.4	0.10	
SS3	42.0	4.58	32.4	49.8	−0.36	
DGreen	10.6	1.06	9.0	13.2	0.04	
DRed	1.1	1.26	−1.2	4.8	0.25	
DNIR	14.6	2.98	11.0	21.6	−0.46	*
MDGreen	0.7	1.13	−1.2	3.5	−0.06	
MDRed	2.0	1.24	−0.2	5.6	0.25	
MDNIR	0.9	3.73	−5.4	8.1	−0.33	

Total of 25 observations.

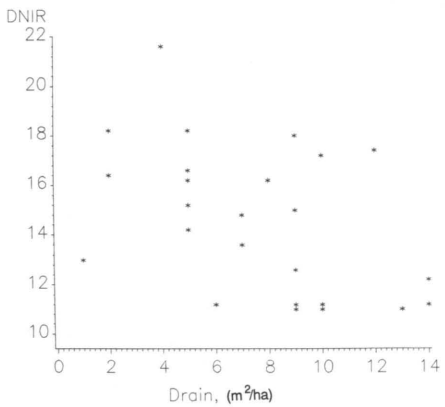

Fig. 13. Near infrared difference (SS387 — TM484) vs. drain from PNFI data.

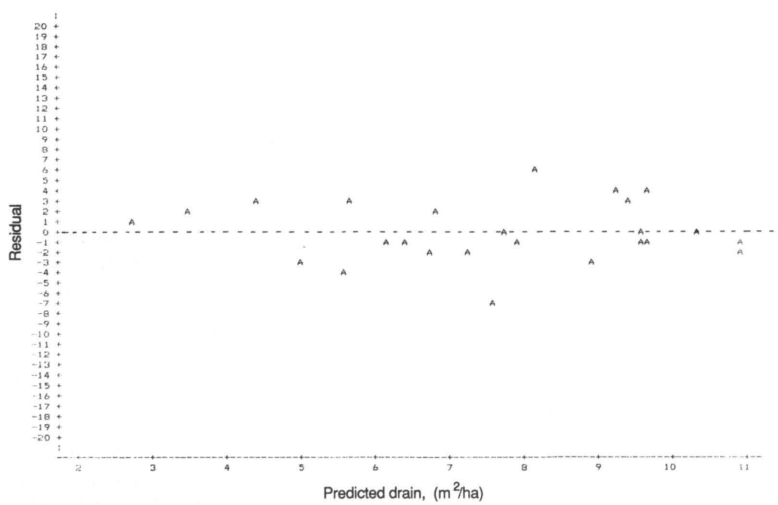

Fig. 14. Residual of the best drain estimation model.

succeed, when the uncut plots were included in the model ($R^2 = 0.18$). Also, the residual of the model showed that separation of the cut from uncut forest was not possible using regression analysis. The channels of the best model for all plots were the same as for the cut plots only.

The drain estimation model for cut plots with the original channels gave $R^2 = 0.23$; difference channels with the histogram matching gave $R^2 = 0.26$.

5.2.2 Damage grade estimation

Topographical data

The absolute elevation was the only topographical variable with significant correlation

Table 11. Damage and elevation variables. H0: r = 0.

Variable	Mean	Std. dev.	Minimum	Maximum	Corr. with dam.	H0:rej.
Damage (%)	29.2	11.49	17.0	64.2	1.00	
Abs. h., (m)	166.2	7.78	153.3	179.1	−0.48	**
Gradient	97.5	12.29	80.9	120.0	−0.07	
Local h. (m)	0.1	0.85	−1.3	2.4	−0.21	

Total of 33 observations.

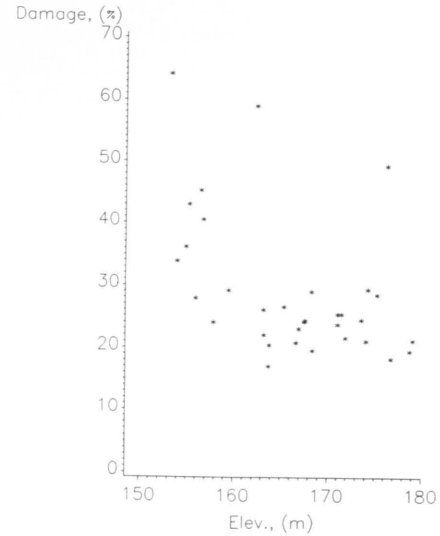

Fig. 15. Damage vs. elevation from sea level.

with the damage grade (Table 11, Fig. 15). The relationship was not actually linear; rather, the damage was heavier in the lowest elevations. Nor did the scatter diagrams between damage and the two other topographical variables give any reason to try to find non-linear relationships. Experimental regression models, where the damage grade was the dependent variable, and the three topographical variables the independent variables, were computed, too. Still, the only significant topographical variable was the absolute elevation.

Correlations between damage grade and spectral variables

Figures 16 and 17 and Tables 12 and 13 show why the damage was divided into two categories in spectral analyses and classifications. Plots with a damage grade of under 30 percent formed the category called "light

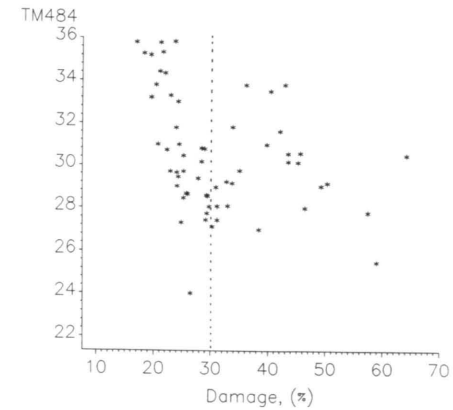

Fig. 16. TM484 intensities vs. damage.

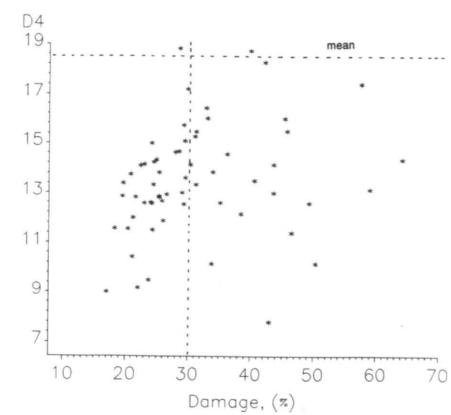

Fig. 17. Near infrared difference (TM485 — TM484) vs. damage. Dotted line shows the grand mean of the difference channel.

Table 12. Light damage, stand and spectral variables. H0: r = 0.

Variable	Mean	Std. dev.	Minimum	Maximum	Corr. with dam.	H0:rej.
Damage (%)	24.4	3.45	17.0	29.8	1.00	
Age (years)	29.6	20.60	18.0	129.0	0.27	
Basal area (m^2)	14.9	4.32	8.0	21.0	0.02	
Diameter (cm)	11.9	3.19	7.9	23.2	0.40	*
Height (m)	9.1	2.64	5.0	18.0	0.36	*
Dens. (stems/ha)	888.9	696.02	500.0	3300.0	−0.30	
TM384	13.8	0.62	12.8	15.1	0.00	
TM484	31.0	2.97	24.0	35.8	−0.74	***
TM385	19.7	0.78	17.8	21.0	0.15	
TM485	44.1	2.52	36.9	49.6	−0.41	**
TM386	18.6	1.22	16.5	21.7	0.30	
TM486	49.4	2.89	41.9	55.5	−0.33	*
D3(TM385-TM384)	5.9	0.81	4.3	7.3	0.14	
D4(TM485-TM484)	13.1	1.99	9.0	18.8	0.59	***
D5(TM585-TM584)	16.1	2.21	10.8	21.4	0.28	
D3(TM386-TM385)	−1.0	0.78	−2.9	0.7	0.32	*
D4(TM486-TM485)	5.2	2.07	−0.9	8.5	0.03	
D5(TM586-TM585)	5.1	3.78	−6.6	13.2	0.33	*
D3(TM386-TM384)	4.8	1.03	3.2	8.0	0.36	*
D4(TM486-TM484)	18.4	2.32	12.4	24.6	0.49	**
D5(TM586-TM584)	21.3	4.56	10.4	30.2	0.40	**

Total of 36 observations.

Table 13. Heavy damage, stand and spectral variables. H0: r = 0.

Variable	Mean	Std. dev.	Minimum	Maximum	Corr. with dam.	H0:rej.
Damage (%)	41.5	9.31	30.3	64.2	1.00	
Age (years)	32.4	23.55	18.0	127.0	−0.46	**
Basal area (m^2)	13.0	5.18	7.0	30.0	−0.41	*
Diameter (cm)	12.1	3.48	7.3	18.0	−0.62	***
Height (m)	8.6	2.82	4.3	14.0	−0.50	**
Density (stems/ha)	1652.0	774.12	300.0	2800.0	0.21	
TM384	14.5	1.62	12.6	20.4	−0.11	
TM484	29.7	2.15	25.5	33.8	−0.05	
TM385	20.3	1.93	16.7	25.4	−0.13	
TM485	43.7	3.30	38.6	49.9	−0.07	
TM386	19.3	2.60	15.4	26.2	−0.28	
TM486	49.7	4.54	41.6	59.1	−0.25	
D3(TM385-TM384)	5.7	1.02	3.6	7.4	−0.08	
D4(TM485-TM484)	14.0	2.56	7.8	18.7	−0.06	
D5(TM585-TM584)	16.9	3.24	10.4	21.8	−0.12	
D3(TM386-TM385)	−1.0	1.13	−3.2	1.1	−0.41	*
D4(TM486-TM485)	6.0	2.32	0.4	10.2	−0.37	
D5(TM586-TM585)	5.26	−5.2	14.1	−0.42	*	
D3(TM386-TM384)	4.8	1.47	2.4	7.8	−0.37	
D4(TM486-TM484)	20.0	3.36	14.6	28.1	−0.30	
D5(TM586-TM584)	23.0	7.51	10.4	36.0	−0.35	

Total of 25 observations.

damage". Plots with a damage grade of 30 percent or higher formed the category called "heavy damage". With less than 30 percent damage, there is a relatively high correlation between the damage grade and intensities. Above 30 percent, however, no clear relationship exists. The probable reason is that when the damage exceeds a certain level, the sparse crown transmits radiation well. Thus, a larger part of the reflected radiation comes from the undergrowth. This increased incident radiation makes the undergrowth more luxuriant, which tends to increase the near infrared reflection (Häme 1988b). During field visits to the heavily damaged stands, vigorous herbaceous undergrowth was often noticed.

To explain their different spectral behavior, it was tested whether the two damage categories had different stand variable values. Using ANOVA, the means of the stand variables, "basal area", "diameter", "height", and "density", were compared in the two categories. The null-hypothesis about the similar means was not rejected in any test.

The relationship between the damage and the spectral and stand variables was also studied for the whole field data set (61 observations). Damage had the highest correlation coefficient with TM484, r = 0.36. The next highest correlation coefficient occurred with "basal area", r = 0.32. The correlations with damage and the site quality types, "diameter", "height", and "density", were not significant. The correlation diagram between damage and "basal area" indicated that in the highest basal area plots the most severe damage grades were missing.

Figure 16 shows that not only the heavy damage but also the light damage dated to the earlier epidemic of 1982. Near infrared intensities are lower for plots of about 30 percent damage than for plots of less than 20 percent damage. That relationship shows a negative correlation coefficient in Table 12 between the damage and TM484. Note that this correlation is higher than any correlation between the damage and stand variables.

In image TMI85, the relationship between the damage grade and the near infrared radiation (TM485) is still inverse in the low damage category, but the correlation coefficient is closer to zero. The correlation between the damage grade and the near infrared difference channel D4 (TM485-TM484) is positive, and the intensities of the healthiest

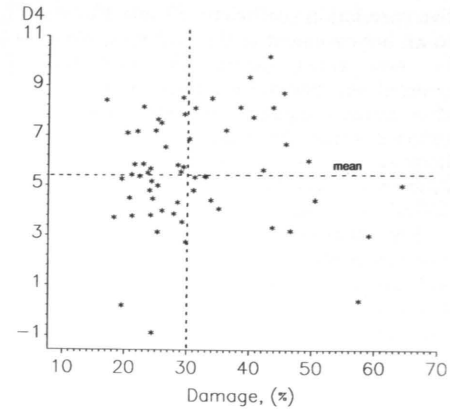

Fig. 18. Near infrared difference (TM486 — TM485) vs. damage. Dotted line shows the grand mean of the difference channel.

plots are furthest from the grand mean. Thus, the change has been greatest in the healthiest forests (Table 12, Fig. 17). The healthiest plots have obviously been affected by the damage for the first time in 1985, whereas the less healthy were already affected in 1982. The change is bigger because they had more needles left during the 1985 epidemic than had the less healthy plots. The near infrared change has barely continued from TMI85 to TMI86 — at least in the light damage category (Fig. 18).

The correlations between the damage grade and spectral variables are low in the heavy damage category. The correlations between damage and the stand variables are higher in heavy damage than in the light damage category (Table 13). The trees on the less healthy plots of the light damage category were usually thicker and higher than the trees on healthier plots. In the heavy damage category, the less healthy plots had younger, thinner, and shorter trees. In other words, the smallest trees were at both ends of the damage scale.

The D3 (TM386-TM385) and D5 (TM586-TM585) have a positive correlation with damage percent in the light damage category (Table 12). The correlation coefficients suggest that in image TMI85, damaged needles, still partially green, have absorbed red light. In TMI86, the red light reflectance from the bare branches was high.

In the heavy damage category, the nega-

tive correlation coefficients (Table 13) points to an improvement in the healthiest plots — i.e. new green shoots. The new shoots covered the herbaceous undergrowth. This also caused a negative correlation in the near infrared range. It must be kept in mind, however, that all correlation coefficients by difference channels from image pair TMI86/TMI85 are quite low.

The correlation coefficients between the damage grade and image TMI86 channels indicate that not the color of the needles but the existence of the needles, needle mass, is the main factor affecting the spectral properties.

Modeling intensities using stand data

The spectral variables were modeled with stand data in order to know which part of the intensity variation comes from the stand variables and what the significance of different variables is in modeling. Table 14 indicates that the modeling succeeded poorly with the traditional stand variables if the spectral data were from image TMI84. It also shows how closely the TM4 intensities depended on the damage grade. The coefficients of determination (R^2) for image TMI85 features were similar to those for image TMI84. The exception was TM485 where R^2 was only 0.32.

The figure changed dramatically if the spectral variables were from image TMI86. For example, the following coefficients of determination were obtained (light damage category):

Dependent variable	R^2
TM486	0.15
TM586	0.57
(TM586 — TM585)	0.67

The coefficients of determination for the heavy damage plots were similar to the light damage plots.

Generally, the best independent variables in both damage categories were "density" and "diameter". Damage grade was only significant for TM4. Note, however, that the data did not include undamaged plots.

Table 14. Regression models for spectral variables using light damage plots. Difference channels TMI85-TMI84. H0: a = 0 (a is coeffient for an independent variable).

Dependent variable	Best three independent variables	Significance of independent variables	Total $R^{1/2}$
TM184	Damage Age Density	 *	0.24
TM384	Age Basal area Diameter	* ** **	0.25
TM484	Damage Age Density	*** * 	0.66
TM584	Density Diameter Height	* 	0.22
D1	Damage Basal area Diameter	 ** **	0.32
D3	Basal area Diameter Height	* 	0.25
D4	Damage Basal area Density	*** 	0.38
D5	Damage Basal area Density	 	0.12

Based on 36 observations.

Modeling damage using intensity data

The best regression model for the light damage (EDamL) was:

$$\underset{}{EDamL} = \underset{***}{39.95} - \underset{***}{1.16} \times TM484 + \underset{*}{0.46} \times TM485 \quad (27)$$

$R^2 = 0.60$. The model was computed using 36 observations. The best model for the heavy damage (EDamH) was:

$$\underset{}{EDamH} = -\underset{*}{173.06} + \underset{*}{3.91} \times TM185 - \underset{**}{0.71} \times TM586 \quad (28)$$

$R^2 = 0.28$. The model was computed using 24 observations.

Figures 19 and 20 present the residuals of the models. The independent variables in the light damage model show how the light damage was a combination of 1982 and 1985 damage. The model for heavy damage may reflect not the damage but the close

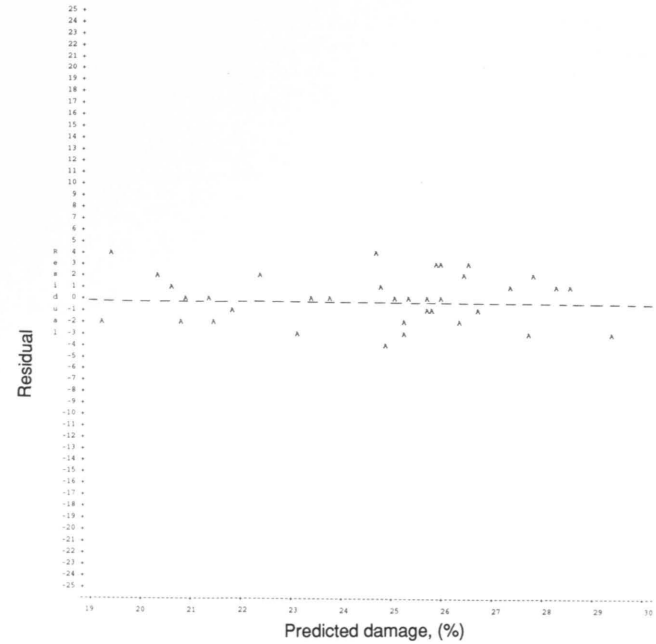

Fig. 19. Residual of the best light damage estimation model.

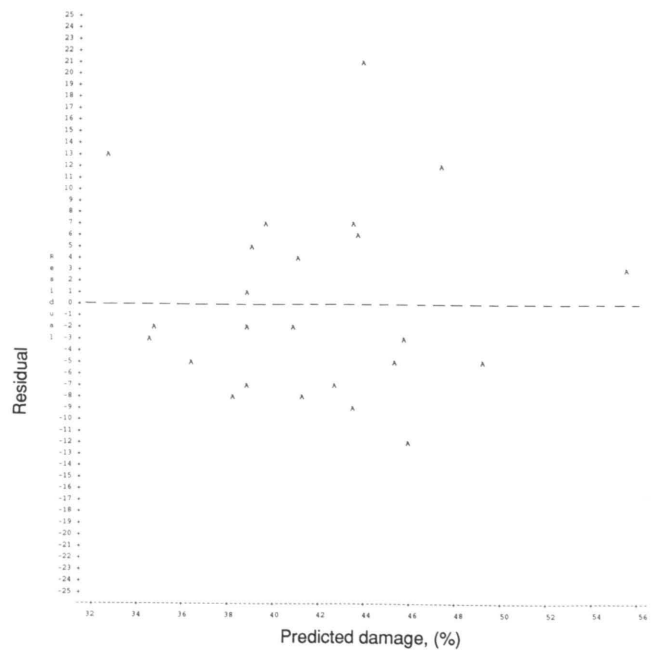

Fig. 20. Residual of the best heavy damage estimation model.

relationship between stand variables and damage in high damage category.

The combined fixed and random effect models without the stand-wise offset values were:

$$EDamL = 36.89 - 0.97 \times TM484 + 0.38 \times TM485 \quad (29)$$

$$EDamH = -164.54 + 3.16 \times TM185 - 0.09 \times TM586 \quad (30)$$

The models are similar to those of the ordinary regression analysis. The biggest difference is in the multiplier for the TM586 channel in the heavy damage model (Formula 30). Testing of the independent variables indicated that the use of the stand as a random variable could not be justified. The null hypothesis (between-stand variance in damage = 0) was accepted in both damage categories. The R^2 values were much higher than in the ordinary regression models but that was due to the large number of independent variables when compared to the number of observations. Each stand was a separate independent variable.

The red light range was not as useful as the near infrared range in the estimation of the damage grade. This does not necessarily mean that the red light range would be poor at discriminating the damaged forest from the healthy. According to the spectroradiometer measurements, red light is very sensitive to the color changes of the needles. However, it may not tell as much about lost needle mass because it does not penetrate deep into the crown.

5.2.3 Tukey's tests

Table 15 shows the summary of the Tukey's tests to image pair TMI84/TMI85. All class pair combinations were tested. The contents of the columns in Table 15 are:

1st column — tested spectral feature
2nd column — number of all tested class pairs where the means were considered significantly different
3rd column — number of tested change/no change class pairs where the means were considered significantly different (change/change and no change/no change class pairs have been excluded)
4th column — number of tested change/reference class pairs (e.g. thinning cut/thinning cut reference) where the means were considered significantly different

Tables 16 and 17 show the corresponding summaries for image pair TMI85/TMI86 and image pair TMI84/SSI87. Complete results are listed in Appendix 1.

In general, the original channels separated the classes better than the transformed features. Only the bitemporal principal components from the correlation matrix (BitPCRn) seemed to be as good as the original channels of image TMI85. The difference channels calculated without image histogram matching gave better results than the difference channels calculated from the matched images.

The matched difference channels were clearly weaker in discriminating classes than the unmatched channels if the classes had high intensities, i.e. if the classes were located on the edge of the histogram. Some results suggested, however, that the matched difference channels could better discriminate classes located near the spectral mean than could the unmatched channels. Such classes were thinning cuts and damage.

The most important spectral ranges were red light (TM3) and near infrared radiation (TM4). The red light range was useful with almost all change types. The near infrared range could discriminate damage as well as shrub removal and soil preparation classes (TMI85/TMI86). The fourth principal component of image TMI85 (PC485), which described differences between the blue-green light (TM1) and middle infrared radiation (TM7), separated the light damage class from other classes better than any other single feature in images TMI84 and TMI85.

The green light difference channel, D2, seemed to be better than all other difference channels in image pair TMI84/TMI85. The autumn coloration in image TMI84 may be the reason. Autumn coloration changes the intensities in the range of TM3 more than of TM2 (Gates 1970). Thus, autumn coloration disturbs the detection of the changes of interest less in the green light than in the red light range.

Ratio channels did not generally prove to be useful because the monotemporal ratios were weaker than the monotemporal original channels, and the bitemporal ratios were weaker than the difference channels. However, the ratio of visible light channels and the red/near infrared ratio seemed to separate light damage from the heavy. The near infrared/middle infrared (R4584 and

Table 15. Summary of Tukey's studentized range test to image pair TMI84/TMI85. Description of spectral features in Chart 2.

Spectral feature	No. of significant differences			Spectral feature	No. of significant differences		
	All class pairs	Change/no change pairs	Change/own ref. class pairs		All class pairs	Change/no change pairs	Change/own ref. class pairs
TM184	21	13	0	R1384	23	13	0
TM284	24	13	0	R2384	23	14	0
TM384	22	13	0	R3484	23	13	0
TM484	21	13	0	R1584	24	13	0
TM584	22	13	0	R3584	24	13	0
TM684	23	13	0	R4584	22	13	0
TM784	23	14	0				
				R1385	25	14	1
TM185	23	14	1	R2385	21	12	1
TM285	23	14	1	R3485	22	14	2
TM385	25	14	1	R1585	22	13	1
TM485	16	11	2	R3585	19	12	1
TM585	25	14	1	R4585	19	11	1
TM685	24	13	1				
TM785	26	15	1	BitR1	10	5	1
				BitR2	12	5	1
PC184	24	13	0	BitR3	18	10	2
PC284	20	12	0	BitR4	15	10	1
PC384	10	7	0	BitR5	12	7	1
PC484	6	4	0	BitR7	12	7	1
PC584	14	8	0				
PC684	2	2	0	BitRM1	9	4	1
				BitRM2	14	6	1
PC185	23	13	1	BitRM3	19	10	2
PC285	20	12	2	BitRM4	14	8	1
PC385	11	6	2	BitRM5	10	5	1
PC485	23	13	1	BitRM7	14	8	1
PC585	10	5	1				
PC685	20	12	1	D3/D4	21	13	2
PCR184	24	13	0	BitPC1	22	13	1
PCR284	18	11	0	BitPC2	18	10	1
PCR384	20	13	0	BitPC3	11	4	1
PCR484	23	13	0	BitPC4	2	2	1
PCR584	24	13	0	BitPC5	12	8	1
PCR684	21	13	0	BitPC6	7	4	0
PCR185	23	14	1	BitPCR1	24	14	1
PCR285	15	10	2	BitPCR2	25	16	2
PCR385	21	12	1	BitPCR3	25	14	1
PCR485	21	12	1	BitPCR4	23	14	1
PCR585	14	11	0	BitPCR5	25	14	1
PCR685	23	14	1	BitPCR6	17	9	1
D1	13	7	1	Can1	19	10	1
D2	23	12	1	Can2	23	14	0
D3	18	9	1	Can3	20	15	2
D4	16	9	2	Can4	12	8	1
D5	17	9	1	Can5	8	6	1
D7	20	10	1	Can6	23	13	1
DM1	9	4	1				
DM2	14	6	1				
DM3	18	9	2	No. of tested class pairs	39	24	4
DM4	14	9	1				
DM5	12	6	1				
DM7	15	7	1				

Data: Set1 + Dam
No. of observations: 256
No. of classes: 10

Table 16. Summary of Tukey's studentized range test to image pair TMI85/TMI86. Description of spectral features in Chart 2.

Spectral feature	No. of significant differences		
	All class pairs	Change/ no change pairs	Change/ own ref. class pairs
TM185	27	18	0
TM285	23	15	0
TM385	28	19	1
TM485	14	9	0
TM585	23	15	0
TM685	18	14	0
TM785	26	18	0
TM186	26	17	2
TM286	28	19	2
TM386	27	16	2
TM486	15	10	0
TM586	28	19	2
TM686	22	16	3
TM786	29	20	2
PC185	23	15	0
PC285	15	10	0
PC385	2	2	0
PC485	16	10	0
PC585	5	4	1
PC685	15	10	1
PC186	26	17	1
PC286	24	18	3
PC386	1	1	0
PC486	15	10	1
PC586	16	10	0
PC686	11	6	1
D1	12	6	1
D2	16	10	4
D3	22	14	5
D4	13	8	1
D5	13	7	1
D6	14	7	1
D7	14	7	1
No. of tested class pairs	45	30	5

Data: Set2, Dam (14 light damage and 15 heavy damage plots), from Set1 21 stands where the thinning cutting had been made between images TMI84 and TMI85.
No. of observations: 201
No. of classes: 11

Table 17. Summary of Tukey's studentized range test to image pair TMI84/SSI87. Description of spectral features in Chart 2.

Spectral feature	No. of significant differences	
	All class pairs	Change/ no change pairs
TM185	9	4
TM384	10	5
TM484	10	6
SS1	11	7
SS2	12	7
SS3	9	5
DGreen	9	6
DRed	10	5
DNIR	10	5
DMGreen	7	4
DMRed	10	5
DMNIR	8	4
No. of tested class pairs	14	8

Data: PNFI
No. of observations: 176
No. of classes: 6

R4585) ratio, which should separate damage well (Vogelmann and Rock 1986), was not effective.

Test results of image pair TMI85/TMI86 were similar to the earlier pair, but better. For example, the thinning cuts were separated from their reference class, as well as from earlier thinning cuts, much better in image pair TMI85/TMI86 than in the TMI84/TMI85 pair.

Tukey's tests were also performed on image pair TMI85/SWI87. The main objective was to find out whether the thinning cuts could be separated from their reference class using a winter image. The only available unchanged forest class was the stands from Set1, where the thinning cuts were made before the acquisition date of image TMI85. Preliminary tests to image pair TMI85/TMI86 had indicated, that the earlier cuts gave similar intensity values to the "real" unchanged classes. The tested features were the original channels and difference channels calculated without histogram matching.

The winter image seemed to separate generally only open or nearly open classes from the classes with tree cover. The differences between the means were often big, but the deviations were big, too. Thinning cuts were not separated.

A general result of all Tukey's tests was that only clear cuts could be distinctly discriminated from all other classes using a single feature. Note that due to the large number of single tests there is a danger of type I errors; i.e. rejecting true null-hypotheses.

5.2.4 *Experimental discriminant models*

The comparisons of the experimental discriminant models verified the results of Tukey's tests. The paired original channels (PO) gave results at least as good as the transformed features (Tables 18 and 19). The first percentage number in the tables is the proportion of the input samples which were assigned to their true class. The second column describes how well the changed and unchanged classes are separated from each other. The low percentage in the second column means that the change classes also include a lot of unchanged forest.

It must be kept in mind that the percentages in the tables should only be compared with the other percentages in the same table because they are based on the input data. The proportions of the classes in the input data were also far from the true proportions in the field.

Three paired principal components plus paired vegetation index features (PPCVI) and paired four ratio channels (PRatBest) yield similar results to the four paired channels as well as to the four paired principal components PPC1234 and PPCR1234. The principal component transformations could not, however, be used to compress the data, which is their basic purpose. Three paired principal components gave poorer results than three paired original channels. The bitemporal operations, BitPC, BitPCR, and BitCan, gave results similar to the three paired principal components.

Variable set Miscell, which included the best original and ratio channels, was somewhat poorer than the paired original channels only. The result of the Tukey's tests (that the ratio channels would better separate thinning cuts from damage as well as damage classes from each other than the original channels) was probably due to two wavelength areas involved with the ratio channels. When multivariable spectral data was processed, the ratio channels were no longer useful.

The results also suggest that Landsat Thematic Mapper images would be better in change interpretation than Spot images because the spectral resolution of the Thematic Mapper is higher. The paired "Spot" channels (POSpot) TM2, TM3, and TM4 gave a somewhat weaker result than if the blue-green light (TM1) and the middle infrared radiation (TM5 or TM7) were included in the model.

Table 18. Comparison of experimental discriminant models to images TMI84 and TMI85. Description of spectral features in Chart 3.

Feature set	Overall performance	Unchanged class. to unchanged
	%	% of unch.
Monotemporal data		
Orig84	54.8	63.3
Orig85	51.2	74.4
Bitemporal data		
PO1	37.2	60.0
PO2	37.6	44.4
PO3	40.8	57.8
PO4	35.2	56.7
PO5	38.4	43.3
PO6	34.4	23.3
PO7	37.2	35.6
POSpot	67.2	85.6
PO1345	74.8	87.8
PO1347	75.6	87.8
POVI	68.8	84.4
D1	18.0	67.8
D2	28.0	44.4
D3	28.4	63.3
D4	28.4	28.9
D5	33.6	46.7
D7	30.4	22.2
DUnM	52.8	80.0
DMatch	46.0	77.8
PRatBest	70.0	86.7
PRatWorst	67.6	78.9
RatD	54.4	75.6
DRat	50.4	71.1
Miscell	70.4	84.4
PPC123	60.0	75.6
PPC124	61.6	78.9
PPC1234	73.6	85.6
PPCVI	74.8	87.8
PPCR123	64.0	77.0
PPCR124	64.0	83.3
PPCR1234	74.4	85.6
BiTPC	59.2	77.8
BiTPCR	57.6	73.3
BiTCan	63.2	77.8

Data: Set1 + Dam
No. of obsevations: 250 of which 90 representing unchanged forest.
No. of classes: 9

The best spectral range was the red light (PO3), and the second best was the near

Table 19. Comparison of experimental discriminant models to images TMI85 and TMI86. Description of spectral features in Chart 3.

Feature set	Overall performance %	Unchanged class to unchanged % of unch.
Monotemporal data		
Orig85	48.5	64.2
Orig86	51.5	73.7
Bitemporal data		
POSpot	75.5	80.0
PO1345	81.1	88.4
PO1347	81.6	87.4
DUnM1345	54.1	80.0
PPC123	70.9	84.2
PPC124	74.0	86.3
PPC1234	78.1	88.4

Data: Set2, Dam (14 light damage and 15 heavy damage plots), from Set1 21 stands where the thinning cutting had been made between images TMI84 and TMI85.
No. of observations: 196 of which 95 representing unchanged forest.
No. of classes: 10

Table 20. Comparison of experimental discriminant models to images TMI84 and SSI87.

Feature set	Overall performance %	Unchanged class. to unchanged % of unch.
Bitemporal data		
PORNIR	65.8	82.7
POSpot	70.3	76.9
DUnM	62.2	65.4
DMatch	56.8	76.9

PORNIR Paired original red light (TM3, SS2) and near infrared (TM4, SS3) channels
POSpot Paired original channels (TM2, SS1 and TM3, SS2 and TM4, SS3)
DUnM Difference channels from paired original channels
DMatch Difference channels from matched paired channels

Data: PNFI
No. of observations: 111 of which 52 representing unchanged forest
No. of classes: 6

infrared (PO4). However, the classification result was very poor, even for the input data of the model, when only one wavelength area was used.

The moderate result with monotemporal features (Orig) and the much poorer overall performance with difference channels (DUnM) than with paired original channels is also similar to the Tukey's tests. The explanation is that the classes were not just change classes. They included different canopy types. Again, the matched difference channels (DMatch) gave a weaker result than the unmatched.

The results from image pair TMI85/TMI86 (Table 19) are surprisingly similar to the results from the earlier pair. In the evaluation of the results, the damage classes were placed in the category of changed forest since the damaged forests still showed some change according to the results presented in Section 5.2.2.

Closer study of the classification result of the input data for TMI84/SSI87 classification suggested that the histogram matching, using regression analysis, helped to separate thinning cuts from unchanged forest, but made the classification results of the shrub removal and shrub growth classes poorer. Table 20 has the summary.

5.2.5 *Properties as a function of time*

Figures 21a and b and 22a and b describe how the intensities of the different data sets have changed during the three year period from the first Landsat image TMI84 to the last Spot image SSI87. The stands which had been used to calculate the statistics for the classifications were also used to compute the intensities for Figures 21 and 22. The calculation unit was a single pixel. The plotted values are the means of the classes. The intensities are standardized by subtracting the mean of each channel from the class mean. Thus, a positive intensity reflects that the class intensity is above the mean. A negative is under the mean.

Due to the large number of pixels and the relatively low standard deviations in each class, the similarities of the class means are not tested using the pixel data. The null-hypothesis about the equal means would have been rejected in almost all tests if the pixel data had been used. For example, if the number of pixels in a class is 150, and the standard deviation of the intensities is 5, then the difference of the intensity means can be smaller than one intensity unit, and still the null-hypothesis is rejected using a 5 percent significance level. In most cases, the standard deviation was smaller than 5, and the number of pixels per class was higher than 150. (The number of pixels in the class for light *Gremmeniella* damage was 136, approx. 60 original pixels). The Tukey's tests described in the previous chapter may have given a

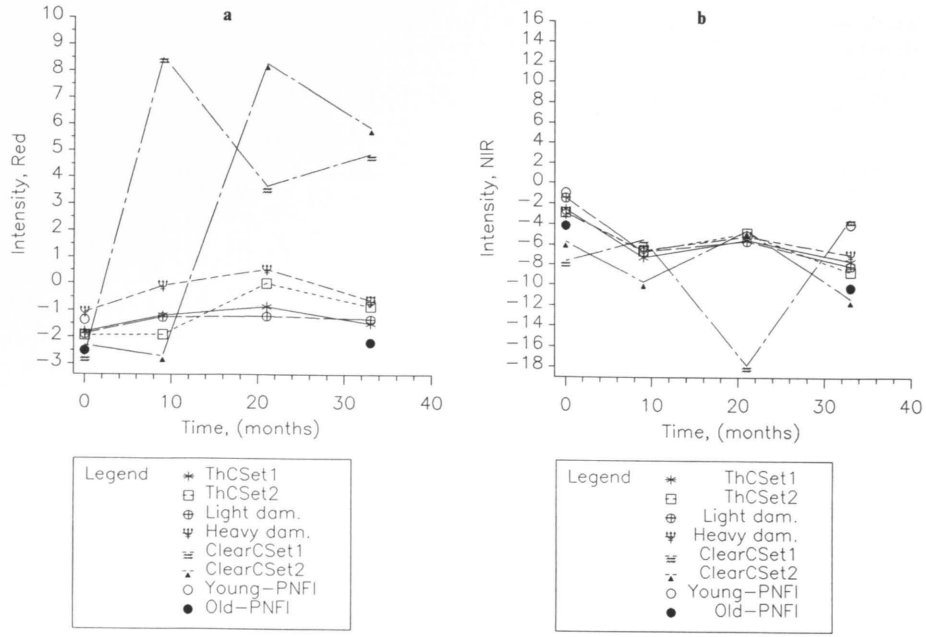

Fig. 21. Intensity means of middle aged, mature and clear cut forests as a function of time. a) Red light (TM3). b) Near infrared radiation (TM4).

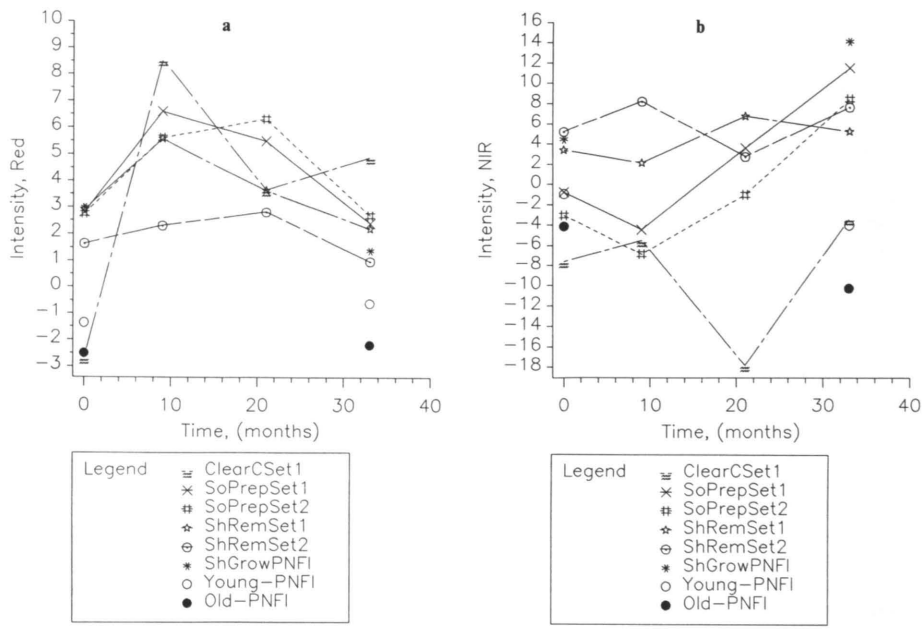

Fig. 22. Intensity means of young and clear cut forests as a function of time. a) Red light (TM3). b) Near infrared radiation (TM4).

much more realistic figure about the class differences, since the calculation unit was the spectral mean of the ground truth stand.

In Figures 21 and 22, the horizontal axis values 0, 9, 21 and 33 equal the dates of images TMI84, TMI85, TMI86, and SSI87, respectively. The Spot winter image was left out of the graphs because Tukey's tests showed that winter images may only be useful in the interpretation of clear cuttings. The following listing may help in the interpretation of the figures:

Class name	Explanation
ThCSet1	Thinning cutting has been made between times 0 and 9 months
ThCSet2	Thinning cutting has been made between times 9 and 12 months
Light dam.	Light damage
Heavy dam.	Heavy damage
ClearCSet1	Clear cutting has been made between times 0 and 9 months
ClearCSet2	Clear cutting has been made between times 9 and 12 months
Young-PNFI	PNFI data, unchanged plots 0—39 m^3/ha
Old-PNFI	PNFI data, unchanged plots 40 m^3/ha and over
SoPrepSet1	Soil preparation has been made between times 0 and 9 months
SoPrepSet2	Soil preparation has been made between times 9 and 12 months
ShRemSet1	Deciduous shrub removal has been made between times 0 and 9 months
ShRemSet2	Deciduous shrub removal has been made between times 9 and 12 months
SGrowPNFI	Deciduous shrub growth, PNFI data

The plots are joined to make reading of the figures easier, although the spectral data were certainly not continuous in respect to time. The plots for the PNFI data are not joined because intensity values for those classes were selected from TMI84 and SSI87 images only.

Thinning cuttings and damage

The red light channel intensities of classes at Time=0 are similar (Fig. 21a). The heavy damage class has somewhat higher intensities in red light during the three year period than the other forests in the same development phase. The crowns of the trees were already sparse due to earlier epidemics (Alajärvi 1991). Damage and thinning cutting have slightly increased the red light intensities. The intensities of thinned and damaged forests appeared to decrease after the change, which may indicate increased biomass, i.e. recovery of the forest. The plots at "time=33" suggest that the spectral tracks of the thinning cuts and damage disappear within a couple of years. In the near infrared range, the differences between class intensities are small.

Clear cutting and soil preparation

After the drastic red light intensity increase due to clear cutting, the intensities decrease (Fig. 21a). The intensities again increase to near the intensities of the clear cut areas after soil preparation. Near infrared intensities increase much less than red light intensities in the clear cutting.

The near infrared intensity changes in soil preparation areas may be caused mainly by the recovery of the undergrowth, since the intensities of SoPrepSet1 and SoPrepSet2 are similar (Fig. 22b).

Shrub removal and growth

Removal of deciduous shrub competition increases red and decreases near infrared intensities (Fig. 22a and b). A similar recovery effect, which could be seen in thinning cut and damage classes, seems to exist in deciduous shrub removal classes.

Deciduous shrub growth increases the near infrared intensities (Fig. 22b).

Figures 21 and 22 presented the class means only, which were computed from the intensities of the single pixels. Figures 23a, b, and c give an idea of the intensity distribution. The only change that clearly differs is in the clear cuttings. The clear cuts increased the intensities much more distinctly in the red light range than in the near infrared range when the deviation is taken into account. The spectral properties of some stands with soil preparation are similar to the unchanged stands. The distributions of the thinned/damaged and the unchanged stands overlap considerably.

The near infrared intensities on many light damage stands decreased when compared to the reference stands. The heavy damage plots are widely distributed, and it is difficult to see whether they form their own cluster. Figure 23b demonstrates the intensity changes of the "unchanged" stands. The

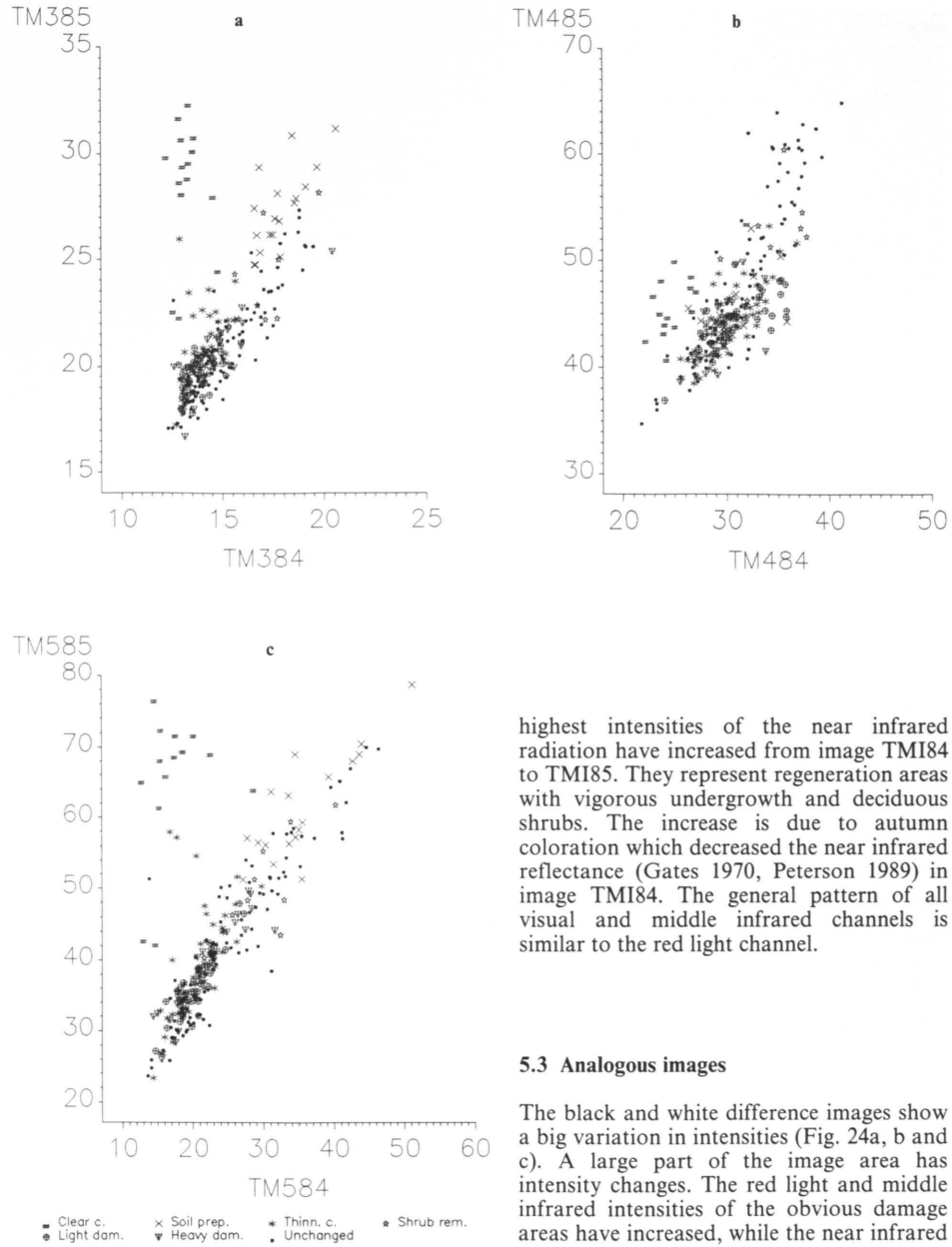

Fig. 23. Bitemporal intensities of the changed and unchanged stands of Set1 and Dam. a) Red light (TM3). b) Near infrared (TM4). c) Middle infrared (TM5).

highest intensities of the near infrared radiation have increased from image TMI84 to TMI85. They represent regeneration areas with vigorous undergrowth and deciduous shrubs. The increase is due to autumn coloration which decreased the near infrared reflectance (Gates 1970, Peterson 1989) in image TMI84. The general pattern of all visual and middle infrared channels is similar to the red light channel.

5.3 Analogous images

The black and white difference images show a big variation in intensities (Fig. 24a, b and c). A large part of the image area has intensity changes. The red light and middle infrared intensities of the obvious damage areas have increased, while the near infrared intensities have decreased (A).

The clear cut areas (B) can be separated well in the red light and middle infrared radiation due to increased intensities, but in the near infrared, however, they are hardly

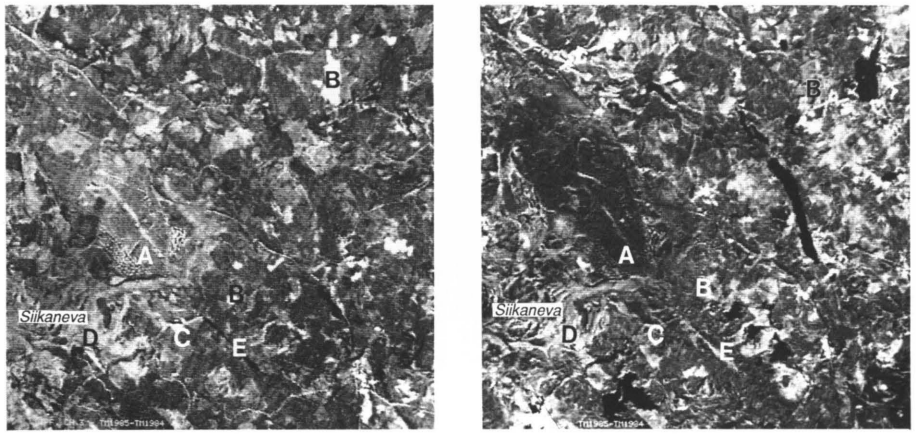

a b

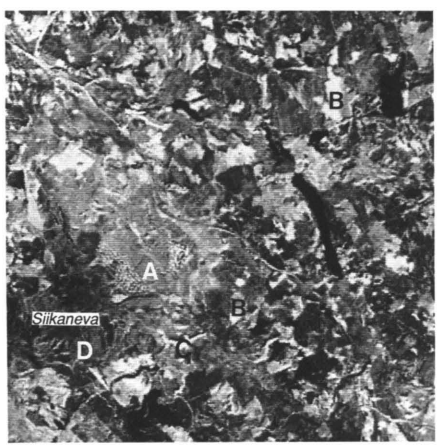

c

Fig. 24. Difference images. Area 10 km x 10 km.
a) Red light difference channel D3 (TM385 — TM384). b) Near infrared difference channel D4 (TM485—TM484). c) Middle infrared difference channel D5 (TM585—TM584).

distinguishable. At least some plowed areas show a change similar to clear cuttings (C).

The open "Siikaneva" bog shows various types of changes which may be seasonal. One of the most conspicuous is the increase in the red and near infrared (D). A partial autumn aspect of the deciduous tree forests in image TMI84 has caused an increase in the red light and a decrease in near infrared in a birch swamp (E). The middle infrared shows no clear changes in this case.

The near infrared intensities of the lakes have changed, but not the red light intensities.

Analogous color images were prepared employing difference channels only (Fig. 25a and b) and original plus difference channels (Fig. 26a and b). The difference channels for Figure 25 were computed in this particular way to achieve a certain visual effect and to make the images more colorful.

Explanation of colors in Figure 25 (additive colors, Lillesand and Kiefer 1987):

yellow	increased red light and decreased near infrared intensities
red/orange	strongly increased red light intensities

Explanation of colors in Figure 26:

magenta	increased red intensities, not increased near infrared intensities
yellow	increased red and near infrared intensities (deciduous shrub growth on regeneration areas)
red/orange	increased red intensities, slightly increased near infrared intensities

Note the difference in the plowed areas (C) between image pair TMI84/TMI85 and TMI84/SSI87 (Fig. 25a and 26a). Note also how the yellowish area in Figure 25b is concentrated spatially as is the magenta area in Figure 26b. The location of the belt is similar to the highland area where the thickness of the soil above bedrock is less than one meter (Geological map... 1982).

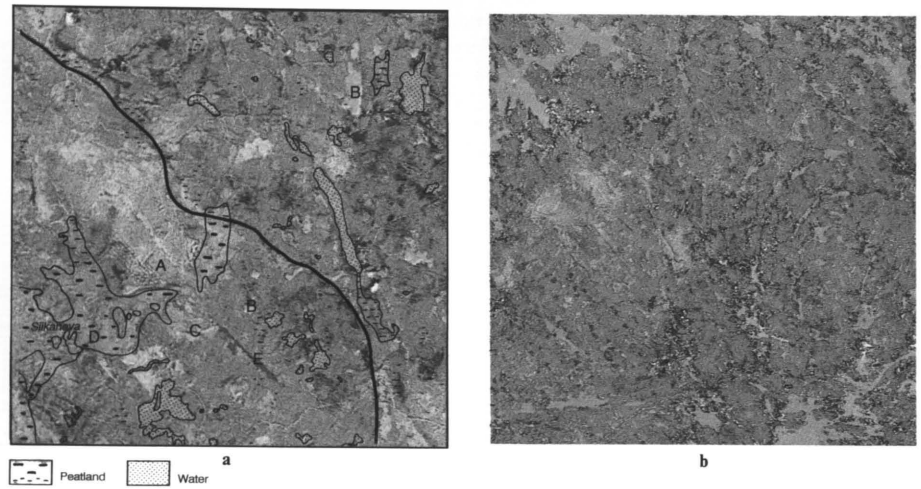

a b

Fig. 25. Color composite of difference channels of image pair TMI84/TMI85. a) Area 10 km x 10 km.
b) Area 40 km x 40 km.
Red: TM385 — TM384
Green: TM484 — TM485
Blue: TM584 — TM585

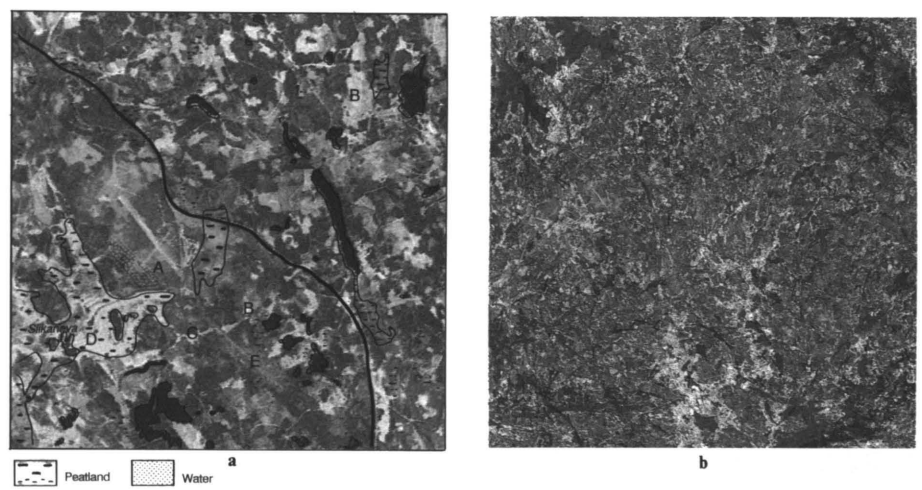

a b

Fig. 26. Color composite of original and difference channels of image pair TMI84/SSI87. a) Area 10 km x 10 km.
b) Area 40 km x 40 km.
Red: SS287
Green: SS387 — TM484
Blue: TM384

5.4 Supervised classifications

5.4.1 Classification statistics

The standard deviation of the spectral classes increased from image TMI84 to image TMI85. The increase may have been caused by the larger irradiance and the summer season in image TMI85 (Table 21). The deviation of the manmade change classes had

Table 21. Means and standard deviations (s) of the classes used in classifications to image pair TMI84/TMI85. The mean and the standard deviation of the whole image in paranthesis.

Feature	Parameter		Class									
			C	CR	T	TR	L	H	S	SR	P	PR
TM184	mean	(48.5)	45.9	46.2	46.7	46.7	46.9	46.9	51.8	48.5	51.7	51.3
	s	(3.7)	1.7	2.0	2.0	1.9	1.5	1.7	2.7	2.4	2.5	2.2
TM185	mean	(64.7)	69.4	62.5	63.0	62.7	63.0	63.9	69.2	64.9	68.9	69.1
	s	(4.6)	3.6	2.9	2.6	2.3	1.5	1.6	4.2	2.9	3.3	2.5
TM384	mean	(15.7)	13.0	13.8	13.9	13.9	13.8	14.6	18.6	16.5	18.5	18.4
	s	(4.3)	1.4	2.0	1.7	1.6	1.0	1.3	3.2	2.4	2.3	1.9
TM385	mean	(21.3)	29.8	19.2	20.1	19.3	20.1	21.2	26.9	22.2	27.9	26.8
	s	(4.9)	5.0	3.2	2.7	2.4	1.1	1.6	4.9	3.2	4.2	2.5
TM484	mean	(32.2)	24.6	26.0	29.6	28.7	30.8	29.3	35.6	35.9	31.4	26.6
	s	(8.5)	4.6	5.7	4.8	4.3	3.7	2.7	5.7	4.5	4.5	4.1
TM485	mean	(50.9)	45.4	39.6	43.7	42.8	44.2	44.4	53.1	57.6	46.4	41.4
	s	(15.2)	5.1	6.9	6.7	5.9	3.0	3.5	7.8	9.6	7.0	6.1
TM584	mean	(25.8)	15.9	19.9	20.0	19.1	20.4	23.5	36.0	32.3	39.0	40.0
	s	(12.5)	4.8	8.2	6.2	5.7	3.6	4.4	8.0	10.6	11.7	8.6
TM585	mean	(41.8)	69.2	34.5	37.0	33.9	37.3	43.2	57.8	50.5	64.9	65.4
	s	(15.8)	18.6	13.6	10.8	10.2	5.3	6.6	18.2	13.7	14.2	12.2
D1	mean	(16.1)	23.5	16.3	16.4	16.0	16.1	17.0	17.5	16.4	17.2	17.8
	s	(3.4)	3.9	2.5	2.6	2.2	1.9	2.0	3.0	2.3	2.8	2.2
D3	mean	(5.4)	16.9	5.4	6.2	5.4	6.2	6.6	8.3	5.7	9.4	8.4
	s	(3.5)	5.1	2.5	2.4	2.0	1.3	1.4	3.2	1.9	3.5	2.0
D4	mean	(16.9)	21.0	13.5	14.0	14.0	13.5	15.1	17.5	21.7	15.1	14.8
	s	(11.6)	5.5	5.3	5.1	4.7	3.1	2.7	5.9	8.2	6.0	4.4
D5	mean	(14.3)	53.6	14.7	16.9	14.7	16.9	19.7	21.8	18.2	25.9	25.5
	s	(10.8)	19.1	10.6	8.5	7.4	3.2	4.0	11.8	7.7	10.7	8.5
No. of pixels/ class			1811	649	4916	3816	136	148	340	1556	508	478
No. of separate areas/class			8	8	30	22	16	15	6	18	9	3

C Clear cut
CR Clear cut reference
T Thinning cut
TR Thinning cut reference
L Light damage
H Heavy damage
S Shrub removal
SR Shrub removal reference
P Soil preparation
PR Soil preparation reference

increased more than the deviation of the reference classes. The TMI84/SSI87 statistics do not show an increasing standard deviation caused by the change (Table 22). The relative increase is largest in the red light difference channel D3, which was used as an input feature to compute a variance channel. The variance was calculated from a 3x3 pixel window. A classification was performed on the variance channel with three difference channels. The standard deviations in TM5 were usually higher than in other channels.

The soil preparation class (P) had higher TM484 intensities than its reference class (PR). In the soil preparation class, the stands had been cut earlier than in the reference class. Thus, the undergrowth had become more luxuriant, increasing the near infrared

Table 22. Means and standard deviations (s) of the classes used in classifications to image pair TMI84/SSI87. The mean and the standard deviation of the whole image in paranthesis.

Feature	Parameter		Class					
			C	OldR	T	YoungR	S	G
TM284	mean	(18.1)	16.3	16.6	16.8	17.3	18.3	19.9
	s	(2.6)	0.7	0.8	0.9	0.8	1.0	1.2
SS1	mean	(29.6)	32.5	26.4	27.4	28.3	29.7	31.0
	s	(4.5)	1.4	0.9	1.2	2.0	0.9	1.5
TM384	mean	(15.7)	12.6	13.2	13.6	14.3	16.3	18.7
	s	(4.3)	0.7	0.8	1.1	1.5	1.5	1.4
SS2	mean	(15.9)	22.9	13.7	14.7	15.3	16.7	17.3
	s	(4.4)	1.8	1.0	1.4	2.2	1.3	1.7
TM484	mean	(32.2)	24.8	28.0	27.5	31.2	35.9	36.7
	s	(8.5)	1.3	4.4	3.9	3.6	5.7	4.1
SS3	mean	(53.4)	46.6	43.1	42.0	49.4	59.7	67.6
	s	(16.3)	9.1	7.5	4.6	8.8	9.3	7.0
No. of plots/class			7	41	25	12	13	14

C Clear cut
OldR Reference class, stem volume ≥ 40 m³/ha
T Thinning cut
YoungR Reference class, stem volume 0—39 m³/ha
S Shrub removal
G Shrub growth

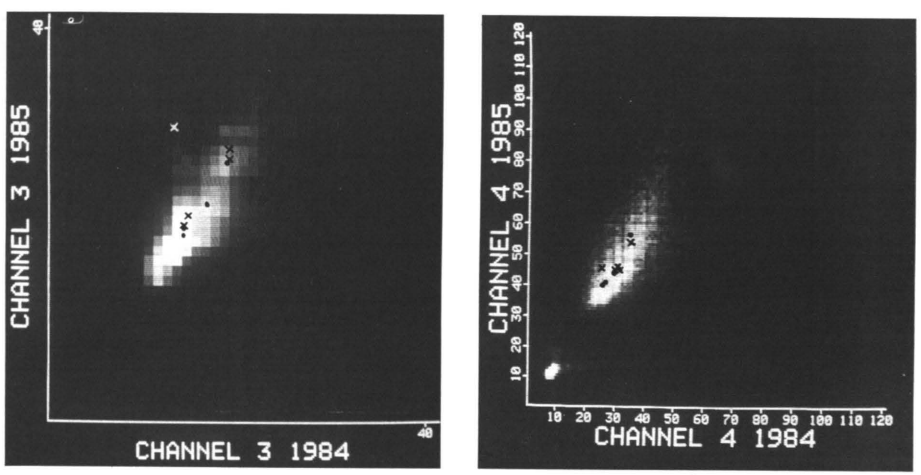

a b

Fig. 27. Location of change (cross) and no change (dot) class means in the frequency table from bitemporal TM channels. a) Red light. b) Near infrared.

intensities. The shrub removal and soil preparation classes had similar intensity values in channel TM385; but in TM485, the intensities of the shrub removal class were higher. Also, the TM184 and TM384 intensities were lower in the change class than in the reference class.

Figures 27a and b demonstrate how uncommon the intensities of the clear cut areas are in the two-dimensional intensity distribution. This should mean easy discrimination of the clear cuts. The thinning cuts are within the most usual intensity values.

5.4.2 *Determining* ***a priori*** *probabilities for maximum likelihood classification*

The area of the changed forest is much smaller than the area of the unchanged forest, if the time period between the images is short. The differences in area were taken into account using lower *a priori* probabilities for the change classes than for the unchanged classes. The aim was to avoid the classification of unchanged forest to change categories, while keeping as much actual changed forest in change classes as possible. One maximum likelihood classification for three different image pairs was performed using altering *a priori* probabilities.

In experimental classifications to image pair TMI84/TMI85, it was tested if the most likely areal proportions of the change and reference classes could be used as the probabilities (Formula 31):

$$p_c = \frac{w_c \cdot A_c}{\sum_{k=1}^{n} w_k \cdot A_k} \qquad (31)$$

where

p_c is *a priori* probability for class c
w_c weighing factor for class c
A_c presumed areal proportion of class c
n number of classes

First, all $w_c = 1$ were tested. This led, however, to far too low areal proportions for the change classes in final classifications. Clear cuts, for example, obtained very low *a priori* probabilities, since the annual area of clear cuts is around 1 percent of the total area. Next, $w_c > 1$ was set for change classes (equal to all change classes) and $w_c = 1$ to all no-change classes. This solution was better than using actual areal proportions. However, it did not take into account the spectral locations of classes. Clear cuts, which were a very distinct spectral class, obtained lower *a priori* probabilities than thinning cuts whose annual area is 2 to 3 times the area of clear cuts. The intensities of thinning cuts were close to the most frequent intensities and very close to the intensities of the reference class. Thus, the confusion of classes was much more probable in thinning cuts than in clear cuts.

Finally, the spectral properties of change classes were noticed in determining their *a priori* probability using deduction and trial and error. The conclusively applied probabilities were:

$$P = \frac{1}{0.7 + 0.5\,n + m} \qquad (32)$$

where

P is *a priori* probability for the unchanged classes. Probability for clear cuts was 0.7 P, and probability for other change classes was 0.5 P
n number of change classes
m number of unchanged classes

5.4.3 *Class distributions*

The TMI84/TMI85 classifications have less change class pixels than the TMI85/TMI86 classifications and more reject class pixels (Fig. 28). The agricultural fields, which were left unclassified (assigned to reject class) due to the autumn image in image pair TMI84/TMI85, are assigned more often to the forest classes, especially the change classes, in the later image pair. The difference between the areas of the unclassified categories in the two image pairs corresponds well with the difference between the percentages of the changed forest category. A distinct exception is the difference image classification MLDiffEq from image pair TMI85/TMI86, where over half of the pixels have been assigned as changed. A large proportion of these changed pixels consists mainly of damage classes. For example, 33.6 percent of the pixels belong to the two damage classes, when the percentage in the earlier image pair is 18.2.

The result verifies the former observations of the study that only a very small change occurred in the damaged forests between images TMI85 and TMI86. Thus, the damage classes have also included unchanged areas.

Note that the Euclidean distance classification originally did not have the reject class. The reject class was masked to the Euclidean classifications from the maximum likelihood classifications which had equal *a priori* probabilities. The masking was done to get the class distributions more comparable.

Lower *a priori* probabilities for the change classes decreased their areal proportion to 70 percent of the proportion of change classes in classifications with equal *a priori* probabilities.

The proportion of thinning cuttings is too small in the TMI84/TMI85 classifications (Fig. 29). The proportion should be higher than the real area, because this type of class, located near the mean and modal intensity

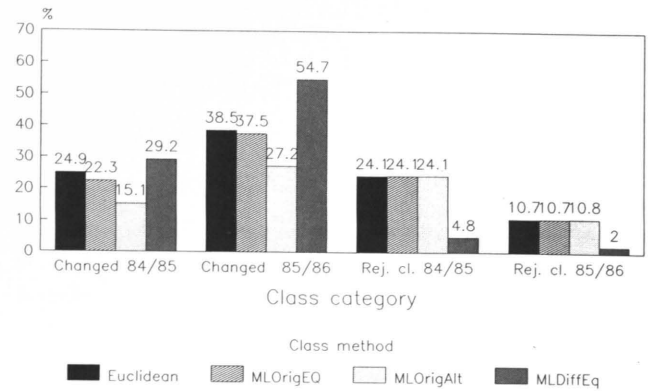

Fig. 28. Proportion of change and reject classes in classifications to image pairs TMI84/TMI85 and TMI85/TMI86.

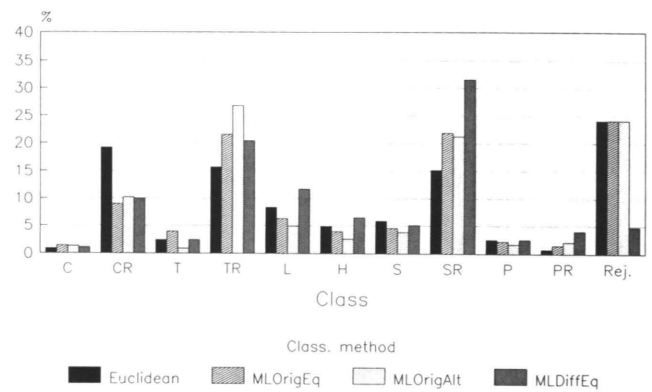

Fig. 29. Class distributions in classifications to image pair TMI84/TMI85.

C Clear cut
CR Clear cut reference
T Thinning cut
TR Thinning cut reference
L Light damage
H Heavy damage
S Shrub removal
SR Shrub removal reference
P Soil preparation
PR Soil preparation reference
Rej. Reject class

values, will contain more individual pixels due to image noise. Similar mean values, but higher deviations when compared to the light damage class, caused the low proportion. The high deviations caused a flatter density function for the thinning cut class than for the light damage class in the maximum likelihood classification.

In the TMI84/SSI87 classifications (Fig. 30), clear cuts cover too small an area. The statistics for the clear cuts were calculated using only seven (7) observations. This caused very low deviations of the channels, and a very narrow density function as well. The proportions of the shrub removal and shrub growth classes are, conversely, quite high. The data did not have enough plots to form good reference classes for open or nearly open areas.

Modal filtering within segments for the map output dropped the proportion of change classes to approximately one half of the proportion in the pixel by pixel classification (Fig. 31). The filtering kept only the uniform change areas, and faded most of the single change pixels. A typical filtering

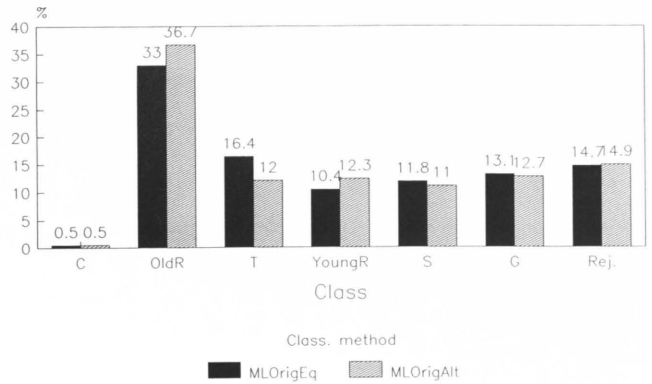

Fig. 30. Class distributions in classifications to image pair TMI84/SSI87.
C Clear cut
OldR Unchanged, tree stem volume 40 m^3/ha or more.
T Thinning cut
YoungR Unchanged, tree stem volume less than 40 m^3/ha.
S Shrub removal
G Shrub growth
Rej. Reject class

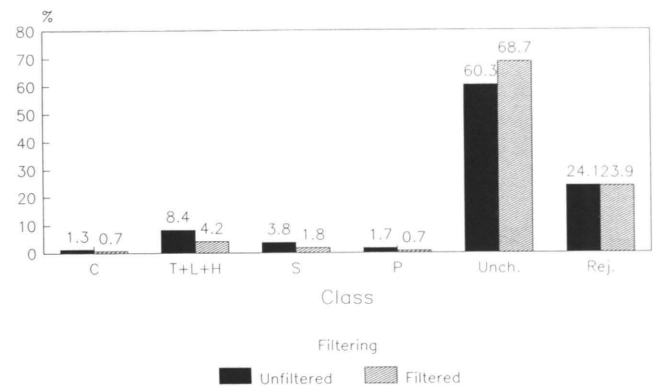

Fig. 31. Impact of modal filtering. Classification MLOrigAlt to image pair TMI84/TMI85.
Unch. Unchanged
Other symbols, see Fig. 29

window, i.e. segment size, was only about ten pixels or less. In certain cases, the size was some tens of pixels (Fig. 32).

The segments within which the proportion of the modal class was 50 percent or more included 96.3 percent of the image area; segments within which the proportion was 75 percent or more included 71.0 percent; and segments within which the proportion was 90 percent or more included 48.2 percent.

Classes with similar field content were combined before filtering. Filtering first and then combining the filtered classifications was also tried, but visual observation showed that the classes should have been combined beforehand. In these two solutions, however, 96 percent of pixels were finally assigned to the same classes. The differences were concentrated in damaged areas which were too small if the filtering had been done first.

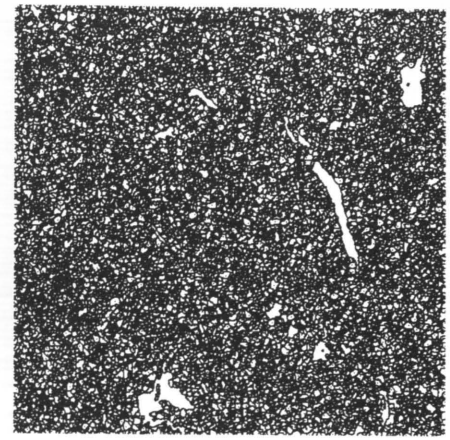

Fig. 32. Filtering windows from image segmentation. Area 10 km x 10 km.

5.4.4 *Results of testing with external test data*

Figures 33 and 34 present the summary of classifications made. Tables 23, 24, 25, and 26 present the confusion matrices of four classifications of image pair TMI84/TMI85. Table 27 presents the result of the tritemporal classification. Table 28 presents the testing result of the TMI84/SSI87 classification, and Table 29 presents the result of the TMI85/TMI86 image classification using transferred statistics. The test results of the rest of the classifications are in Appendix 2.

The class from Set1 representing mechanical shrub removal and/or conifer thinning has been combined into the shrub removal reference class in confusion matrices for TMI84/TMI85 classifications because no spectral value analysis or preliminary classification showed that the class represented a

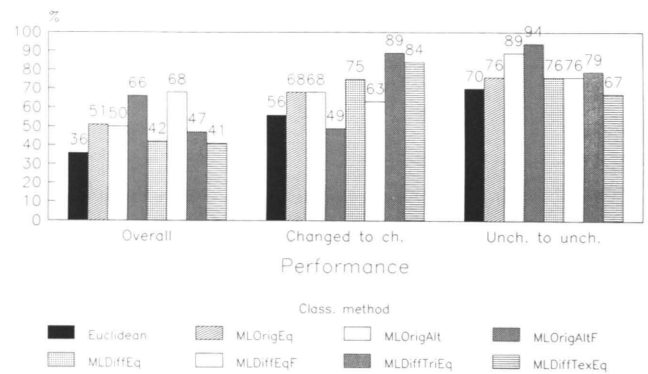

Fig. 33. Summary of testing of classifications to image pair TMI84/TMI85.

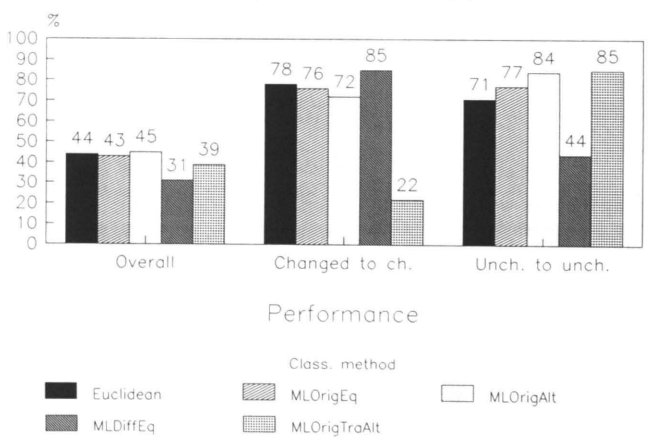

Fig. 34. Summary of testing of classifications to image pair TMI85/TMI86.

Table 23. Test result of the Euclidean classification to image pair TMI84/TMI85.

Field observation	Interpretation Corresponding class in interpretation										
	C	CR	T	TR	L	H	S	SR	P	PR	Tot.
Clear c.	**7**	1	0	0	0	0	1	0	0	0	9
Clear c. R	0	**7**	0	0	0	0	1	0	0	0	8
Th. c.	2	5	**2**	5	5	5	0	3	0	0	27
Th. c. R	0	4	0	**6**	4	2	0	3	0	0	19
Light d.	0	2	3	4	**7**	3	0	1	0	0	20
Heavy d.	0	1	1	3	1	**2**	0	2	0	0	10
Shrub r.	0	0	0	0	0	0	**0**	0	0		0
Shrub r. R	0	0	1	0	1	1	4	**9**	0	0	16
Soil p.	0	1	0	0	0	0	0	1	**3**	4	9
Soil p. R	0	0	0	0	0	0	0	0	1	**2**	3
Total	9	21	7	18	18	13	5	20	4	6	121

Test data: Set1T, DamT

Clear c. Clear cut
Clear c. R Clear cut reference
Th. c. Thinning cut
Th. c. R Thinning cut reference
Light d. Light damage
Heavy d. Heavy damage
Shrub r. Shrub removal
Shrub r. R Shrub removal reference
Soil p. Soil preparation
Soil p. R Soil preparation reference

Table 24. Test result of the MLOrigEq classification to image pair TMI84/TMI85.

Field observation	Interpretation Corresponding class in interpretation										
	C	CR	T	TR	L	H	S	SR	P	PR	Tot.
Clear c.	**8**	0	0	0	0	0	0	1	0	0	9
Clear c. R	0	**6**	0	1	0	0	0	1	0	0	8
Th. c.	3	2	**0**	5	11	4	0	2	0	0	27
Th. c. R	0	1	1	**6**	4	3	0	4	0	0	19
Light d.	0	0	0	1	**15**	4	0	0	0	0	20
Heavy d.	0	1	1	1	3	**4**	0	0	0	0	10
Shrub r.	0	0	0	0	0	0	**0**	0	0	0	0
Shrub r. R	0	0	0	1	0	0	1	**14**	0	0	16
Soil p.	0	0	0	1	0	0	0	0	**8**	0	9
Soil p. R	0	0	0	0	0	0	0	1	1	**1**	3
Total	11	10	2	16	33	15	1	23	9	1	121

Test data: Set1T, DamT
Legend: see Table 23

change. The damage classes were assigned to the group of change classes in the TMI85/TMI86 image pair, although the existence of a change by damage was somewhat unclear between the dates of those images.

The statistics from MLOrigAltF and MLDiffEqF classifications in Figure 33 are not fully comparable with the other classifications, because the thinning cut and damage classes were combined before filtering. The unchanged classes were also combined. The

Table 25. Test result of the MLOrigAlt classification to image pair TMI84/TMI85.

Field observation	Interpretation Corresponding class in interpretation										
	C	CR	T	TR	L	H	S	SR	P	PR	Tot.
Clear c.	**7**	1	0	0	0	0	0	1	0	0	9
Clear c. R	0	**7**	1	0	0	0	0	0	0	0	8
Th. c.	2	3	**0**	8	12	0	0	1	0	1	27
Th. c. R	0	3	0	**9**	2	1	0	4	0	0	19
Light d.	0	0	0	2	**13**	5	0	0	0	0	20
Heavy d.	0	2	0	2	3	**3**	0	0	0	0	10
Shrub r.	0	0	0	0	0	0	**0**	0	0	0	0
Shrub r. R	0	0	0	3	0	0	0	**13**	0	0	16
Soil p.	0	0	0	1	0	0	0	0	**6**	2	9
Soil p. R	0	0	0	0	0	0	0	1	0	**2**	3
Total	9	16	1	25	30	9	0	20	6	5	121

Test data: Set1T, DamT
Legend: see Table 23

Table 26. Test result of the MLDiffEq classification to image pair TMI84/TMI85.

Field observation	Interpretation Corresponding class in interpretation										
	C	CR	T	TR	L	H	S	SR	P	PR	Tot.
Clear c.	**7**	0	0	0	0	0	1	0	0	1	9
Clear c. R	0	**1**	0	6	1	0	0	0	0	0	8
Th. c.	2	0	**0**	3	13	4	0	0	0	5	27
Th. c. R	0	0	0	**8**	6	1	0	2	0	2	19
Light d.	0	0	0	2	**13**	4	0	1	0	0	20
Heavy d.	0	0	0	1	2	**3**	1	1	0	2	10
Shrub r.	0	0	0	0	0	0	**0**	0	0	0	0
Shrub r. R	0	0	0	0	3	0	0	**13**	0	0	16
Soil p.	2	0	0	1	0	0	0	0	**4**	2	9
Soil p. R	0	0	0	1	0	0	0	0	0	**2**	3
Total	11	1	0	22	39	11	2	17	4	14	121

Test data: Set1T, DamT
Legend: see Table 23

Table 27. Test result of the MLDiffTriEq classification using difference channels from image pairs TMI84/TMI85 and TMI85/TMI86.

Field observation	Interpretation Corresponding class in interpretation										
	C	CR	T	TR	L	H	S	SR	P	PR	Tot.
Clear c.	**5**	0	0	0	0	1	0	0	0	0	6
Clear c. R	0	**4**	0	0	0	0	0	1	0	0	5
Th. c.	1	2	**1**	0	6	3	3	0	1	1	18
Th. c. R	0	10	4	**0**	3	0	0	4	0	0	21
Light d.	0	1	0	0	**14**	5	0	0	0	0	20
Heavy d.	0	1	0	0	5	**3**	0	0	1	0	10
Shrub r.	0	0	0	0	0	0	**0**	0	0	0	0
Shrub r. R	0	0	1	0	0	0	1	**18**	1	0	21
Soil p.	0	0	0	1	0	0	0	0	**7**	1	9
Soil p. R	0	0	0	0	0	0	0	0	0	**0**	0
Total	6	18	6	1	28	12	4	23	10	2	110

Test data: Set1T, DamT (11 observations were out of the image area of TMI86 image or affected by clouds)
Legend: see Table 23

Table 28. Test result of the MLOrigEq classification to image pair TMI84/SSI87.

Field observation	Interpretation Corresponding class in interpretation							
	C	R1	T	R2	S	G	Rej	Tot.
Clear c.	**1**	1	0	6	3	1	11	23
Reference 1	0	**46**	22	8	2	6	2	86
Th. c.	0	25	**27**	7	1	3	1	64
Reference 2	0	17	9	**5**	12	6	6	55
Shrub r.	0	1	0	2	**8**	10	1	22
Shrub g.	0	0	0	0	0	**0**	0	0
Total	1	90	58	28	26	26	21	250
Soil p.	0	0	0	2	1	14	0	17
Light d.	0	5	13	0	0	1	1	20
Heavy d.	0	1	5	2	0	1	1	10
Total	1	96	76	32	27	42	23	297

Performance (from 250 observations)
Overall: 35 %
Changed classified to changed: 37 % from changed
Unchanged classified to unchanged: 54 % from unchanged
Test data: Set1A (changed), Set2A (changed), DamT, PNFIT

Reference 1 unchanged, stem volume ≥ 40 m³/ha, from PNFI
Reference 2 unchanged, stem volume 0—39 m³/ha, from PNFI
Shrub g. Shrub growth
Other legend see Table 23

Table 29. Test result of the MLOrigTraAlt -classification to image pair TMI85/TMI86 using statistics from image pair TMI84/TMI85.

Field observation	Interpretation Corresponding class in interp.											
	C	CR	T	TR	L	H	S	SR	P	PR	Rej	Tot.
Clear c.	**10**	1	0	3	1	0	0	0	1	0	0	16
Clear c. R	0	**2**	1	9	0	0	0	0	0	0	1	13
Th. c.	2	7	**2**	10	2	0	1	1	0	0	0	25
Th c. R	0	10	0	**43**	0	0	0	4	0	0	10	67
Light d.	0	3	0	12	**0**	0	0	0	0	0	0	15
Heavy d.	0	5	1	7	0	**2**	0	0	0	0	0	15
Shrub r.	0	1	0	0	0	0	**0**	7	0	0	1	9
Shrub r. R	0	0	0	6	0	0	1	**22**	0	0	2	31
Soil p.	0	0	0	4	0	0	0	2	**0**	12	0	18
Soil p. R	0	0	0	0	0	0	0	1	0	**2**	2	5
Total	12	29	4	94	3	2	2	37	1	14	16	214

Test data: Set2T, DamM, from Set1A 30 thinning cuts which were made before the acquisition of image TMI85.

Rej Reject class
Other legend see Table 23

combination increases the overall performance shown in the figures.

The overall performance was low in all cases. It should, nevertheless, be kept in mind that the class proportions did not correspond to the real field proportions. The proportion of a certain class was also somewhat different in separate test sets. The Euclidean distance classification gave considerably weaker results than the maximum likelihood classifications in image pair TMI84/TMI85 because the deviations of the intensities of classes varied. The Euclidean distance classification does not take intensity deviations into consideration. The result of the Euclidean distance classification was especially poor in the thinning cut and light damage categories, which were the largest groups in the test sets.

The MLOrigAlt classifications may have given the best classification results. The ranking of the methods depends on the aim of the interpretation. The use of smaller probabilities for the change classes has increased the proportion of cases where the unchanged forest was classified correctly. Smaller probabilities did not notably change the test result of changed forests. This is especially worth noticing when we take into account the diminishing area of the change classes in classifications with altering *a priori* probabilities.

The most important difference between the two maximum likelihood classifications using original channels has been the reference class for the thinning cuts. This class was classified more often in the damage class when the *a priori* probabilities were equal than when they were altering.

Tritemporal data also seemed to be useful.

The use of filtering increased the overall performance, but decreased the proportion of the actual changed areas being classified as changed. It must be kept in mind, however, that the boundaries of the test areas may not have been totally correct.

Class distributions had already indicated that the class for thinning cuts did not accurately represent the thinning cuts. Test results confirm that. The light damage class, with its low variance, represented thinning cuts better. Distinguishing the thinning cuts was also studied by classifying the original channels of image pair TMI84/TMI85 without damage classes. Generally, both the damaged test stands and the thinning cuts were assigned to the thinning cut reference class, although the *a priori* probabilities were equal for all classes.

The stand variable values of the actual thinning cuts and the reference class for the thinning cuts were compared to the result of the TMI84/TMI85 difference channel classification. The following observations were made:

Actual thinning cuts

— 3 out of 4 stands classified to heavy damage were in pine swamp.
— 7 out of 9 spruce dominated stands were classified to light damage category.
— The proportion of pine was at least 70 percent on all 5 stands classified to soil preparation reference class; the site type was *Vaccinium* type.
— No clear relationship between stand volume and the successfulness of the classification was found.

Thinning cut reference class

— All 7 stands classified to damage classes were pine dominated, the proportion of pine being at least 80 percent with one exception (60 percent).

The examination of the stand variable values suggested that the change by the thinning cuts is detectable, at least in some cases, because thinning cut spruce trees were assigned to damage classes. Most likely the spruce stands were not damaged. Furthermore, no damage information was available about the seven reference pine stands classified to the damage category.

The thinning cuts in image pair TMI85/TMI86 classifications were less well distinguished than the Tukey's test results indicated. Thinning cuts were not well represented in their own class, but were concentrated in the heavy damage class. The classification results of the other classes, including the damage classes, are similar to the results of the earlier image pair. The class distributions showed, however, that the damage classes also included much forested area other than the damaged. That was particularly the case in the difference image classification.

One classification experiment on image pair TMI85/TMI86 was accomplished without damage classes. The maximum likelihood classification with equal *a priori* probabilities was applied to the original channels. The percentage distribution of the test stands classified to thinning cuts was the following:

Thinning cuts	40
Thinning cut ref.	16
Light + Heavy damage	37

The classification results of clear cuttings and soil preparation were quite good in all Landsat TM image classifications. The errors in the clear cut classifications may be errors in the field data, or they may be by caused by very exceptional clear cuts, such as clear cuttings of young stands due to extensive damage. In the TMI85/TMI86 classifications, all 6 clear cut test stands were classified as clear cuts in three classifications out of four. In one classification, the stand was classified as a thinning cut. Due to lack of test data, the classifications did not answer whether or not it is possible to separate stands where the shrubs have been removed.

The classification results from image pair TMI84/SSI87 are almost useless. The reasons are:

— The data did not allow formation of good unchanged reference classes for the change classes.
— The number of observations was too small in most classes.
— The three years between the images would have required several spectral classes for the same field change class.
— The analogous image from this image pair (Fig. 26a and b) and the changes as a function of time (Fig. 21 and 22) illustrated how vegetative succession, causing its own changes, can fade manmade changes.
— Not all radiometric errors could be corrected.

5.5 Unsupervised classification

The unsupervised classification was first made for imagery which consisted of paired original channels TM384 and TM385 and the near infrared difference channel D4. The red and near infrared spectral ranges were the most important in change interpretation according to the Tukey's tests and classifications with experimental discriminant models. The TM3 original channels should separate the different forest canopy types, in addition to the changes.

The two original channels and one difference channel separated the canopy types but not the change.

The clustering process was continued, employing unmatched difference channels without histogram matching. Use of difference channels also made it possible to add the middle infrared range which was the third important spectral area in the tests. The input channels were D3 (TM385-TM384), D4 (TM485-TM484) and D5 (TM585-TM584) from image pair TMI84/TMI85.

In all, the clustering separated 1144 classes from the data set. The number of classes was restricted to 65 after some experiments. Above that number of classes, the individual classes represented only a very limited number of pixels. The 65 classes contained 76.3 percent of the pixels. The reject class was composed of classes 66—1144, and contained the remaining 23.7 percent of the pixels. The largest class in the 65 classes contained 10.3 percent of the pixels and the smallest 0.1 percent. The first 10 classes contained 44.8 percent of the pixels.

The field content of the clustering classes was clarified by calculating the class distributions within the ground truth areas of the combined Set1 and Dam, which had originally been used to compute the statistics for the supervised classifications.

The largest category in clustering for the treeless or nearly treeless field classes was the reject, or unclassified class. The reason was the class number restriction. Earlier experiments had indicated that the treeless stands often had class numbers above 65, and that they were spread into tens of classes. For instance, 90 percent of the pixels in the clear cutting ground truth class were unclassified, or had the class number 66—1144 in the clustering. The remaining 10 percent included 28 classes. The enormous amount of classes may be a special feature of the multitemporal data. Parmes and Kuittinen (1988) have obtained a proper amount of clusters in clustering of monotemporal Spot imagery.

The analog-to-digital converter of the Landsat TM instrument causes large frequency variation in the successive intensities. In a frequency histogram, those intensities can be seen as local maxima (Kieffer et al. 1985). Because the clustering algorithm searches the local frequency maxima, the radiometric error increases the number of classes greatly.

The unchanged classes with tree cover also had some ten percent reject class pixels. Seasonal changes and noise may have caused this proportion of pixels to have exceptional intensities.

Clustering seemed to distinguish damage. Damage was extensive enough to form classes which were included in the first 65 classes, and the spectral variability was not as high as in the treeless areas. Seven (7) classes reflected damage. A class was assigned to a damage class on the basis of two criteria: 1) their spectral means should harmonize with the other results of this study; and 2) they should form spatially homogeneous areas.

Increased red light, slightly decreased near infrared, and greatly increased middle infrared (TM5) intensities were common to all 7 classes. The 7 classes also formed uniform areas, which was not the case with most of the other clustering classes. The spectral properties of the 7 classes were partially different from the damage classes of the supervised classification.

The 65 classes were combined into six categories: three damage categories, undamaged conifer forests, water, and other classes representing open or nearly open areas.

The most important spectral range was the middle infrared (TM5). For example, the red light and near infrared intensity values of mature spruce forest, a very common forest canopy type, were similar to some damage classes; but the TM5 intensities were only 57 percent or less of the intensities of the assumed damage classes. The three damage categories ("light", "medium", and "heavy" damage) were formed according to the spectral properties of the seven classes. In the heavy damage category, the red light intensities were remarkably increased.

Standard deviations of the change classes were smaller in the clustering than in the supervised classification, although the slightly lower radiometric resolutions of the D4 and D5 channels have been taken into account. In clustering, the highest standard deviations were in the D4 channel which had a maximum of 2.8. The highest D5 deviation for damage classes was 0.74. In the supervised classification, the D5 deviation was 3.2 for the light damage and 4.0 for the heavy damage class. Note, however, that a larger number of classes in clustering automatically decreases the deviations. The TMI84/TMI85 classifications had 10 classes.

Damage separated by clustering was concentrated in older forests. The ground truth areas for the supervised classification were mainly from young forests in the age category of first thinning.

The damage classes from clustering best represented the ground truth class for heavy damage (Fig. 35). The figure also shows that the damage class names from clustering and supervised classifications are not equivalent.

The same segmentation used for the map

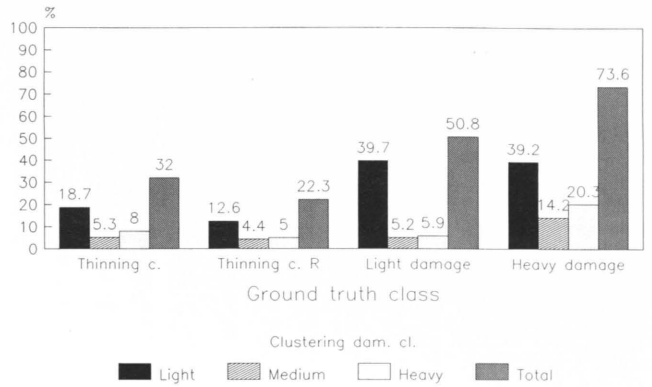

Fig. 35. Distribution of pixels of some ground truth classes of Set1 and Dam to the damage classes of clustering.

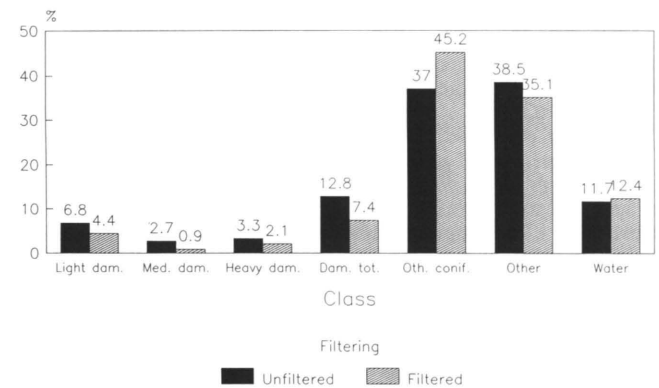

Fig. 36. Class distribution in clustering and impact of filtering.

outputs of the supervised classifications was applied to the clustering result. As in the supervised classifications, modal filtering by segments made the areas of the damage classes smaller (Fig. 36). The proportion of damage classes was smaller than in the supervised difference channel classifications from image pair TMI84/TMI85, but larger than in the supervised classifications with the original channels.

5.6 Change maps

The areas interpreted as damaged form the same spatial pattern (Fig. 37, 38 and 39) that could be seen in the analogous images (Fig. 25b and 26b, Section 5.3). Figure 40 shows how the areas interpreted damaged were concentrated on uplands.

The area classified as damaged in the difference channel classification MLDiffEqF approximately covered the "light damage" class of the clustering. Of that class, 82 percent was classified as damaged in the MLDiffEqF classification in a subarea of 500 x 500 pixels (Fig. 41, Fig. 42). The corresponding figures were 42 percent for the "medium damage" and 21 percent for the "heavy damage" clustering classes. The damage classes of the MLDiffEqF classification also cover the damage classes of the MLOrigAltF classification (Table 30, Fig. 42, Fig. 43).

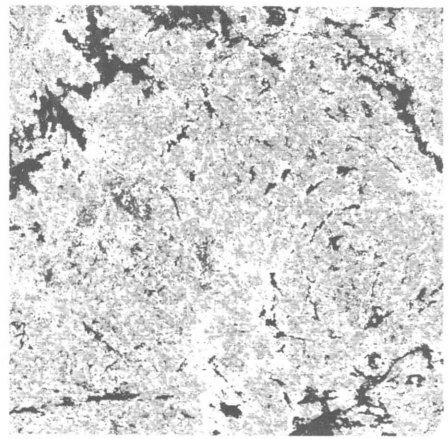

Fig. 37. Damage classes of clustering which is post processed with filtering. Area 40 km x 40 km.
Colors:

Light violet	Light damage clustering class
Reddish violet	Medium damage clustering class
Dark violet	Heavy damage clustering class
Light green	Other coniferous forest
Blue	Water
White	Other

The areas classified as shrub removal classes (orange) are mainly seasonal changes, e.g. the open bog (D) in the lower left corners of Figures 42 and 43 (compare also with Fig. 25a and 26a, Section 5.3). Note how different parts of the bog have been assigned to the shrub removal class in the MLDiffEqF and MLOrigAltF classifications (Fig. 42 and 43). On mineral soil areas, the classifications agree better.

The yellow colored area, soil preparation class, is also clearly larger than the actual forest soil preparation, especially in the MLOrigAlt classification. The area of the larger-scale hardcopy was, however, special in respect to the soil preparation class. In the whole area, the proportion of the soil preparation class was higher in the ML-

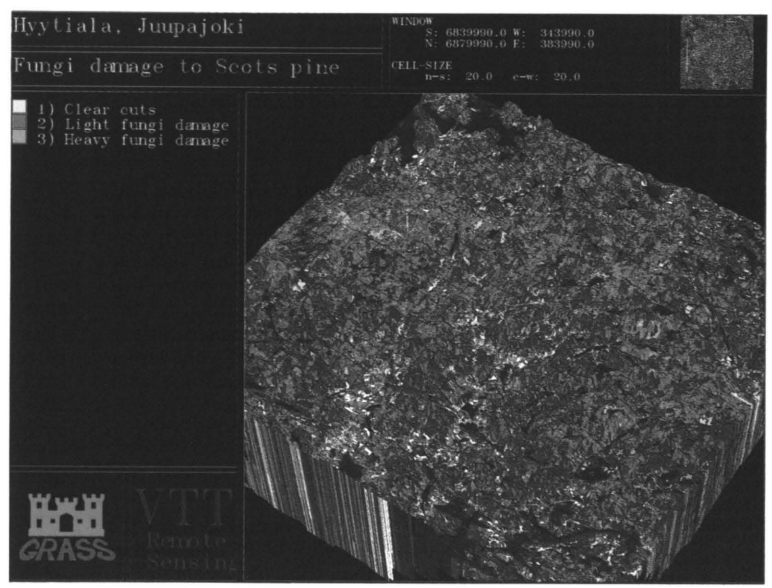

Fig. 38. Combination of MLDiffEqF classification to image pair TMI84/TMI85, Spot panchromatic image and digital terrain model from the 1 : 200 000 map. Viewing point 45 km southeast and 90 km up from the southeast corner of the area. Clear cuts 0.8 %, Light damage 11.0 %, Heavy damage 3.5 % of the 40 km x 40 km image area.

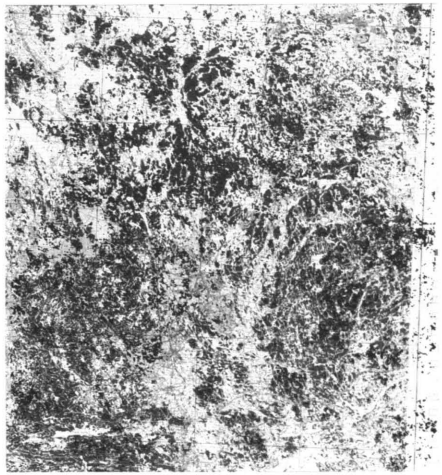

Fig. 39. Damage classes of MLDiffEqF classification to image pair TMI84/TMI85 (black) and outcrops of bedrock-class (grey) of quaternary deposits map of the geological survey of Finland. Area 20 km x 30 km.

Fig. 41. Damage classes of clustering which is post processed with filtering. Area 10 km x 10 km. Colors like Fig. 37.

DiffEq (2.5 %) than in the MLOrigAlt (1.7 %) classification. Some of the incorrect classifications may be seasonal and/or some type of soil preparation other than preparation for forest regeneration.

The use of modal filtering by segments (Fig. 44a and b) has faded the individual pixels of the clear cut class. In certain cases, it seems that some more uniform areas have also faded. This means that the boundaries

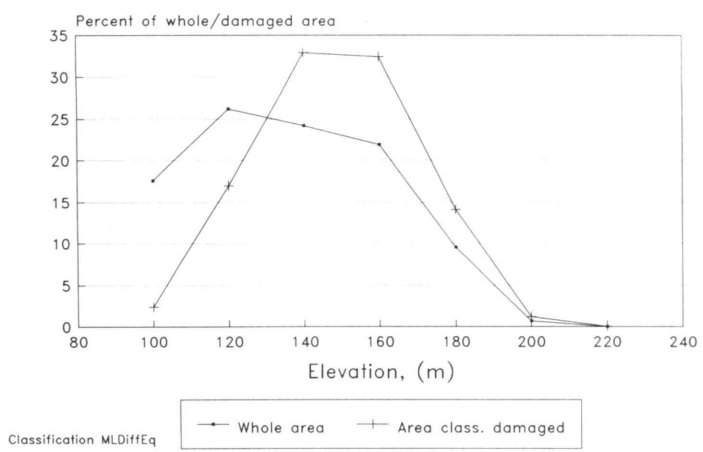

Fig. 40. Elevation distribution of damage classes of MLDiffEqF -classification compared to the elevation distribution of the whole 40 km x 40 km study area. Elevation data from the 1 : 200 000 maps.

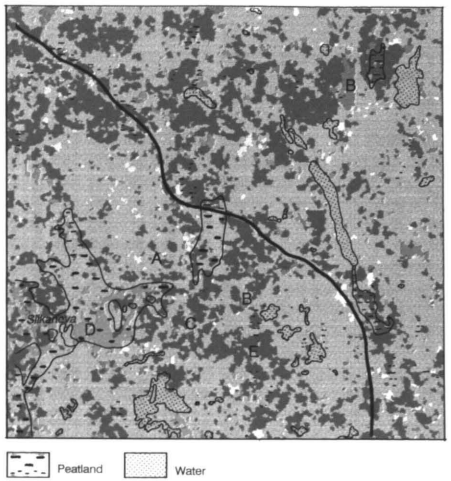

Fig. 42. Classes of MLDiffEqF-classification to image pair TMI84/TMI85. Area 10 km x 10 km.
Colors:

Red	Clear cut
Violet	Thinning cuts + light damage + heavy damage
Yellow	Soil preparation
Orange	Deciduous shrub removal
White	Reject class

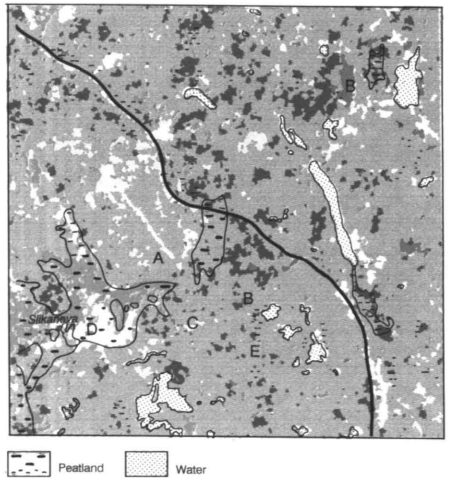

Fig. 43. Classes of MLOrigAltF-classification to image pair TMI84/TMI85. Area 10 km x 10 km. Colors: see Fig. 42.

of the segments have not been optimal. Note, however, that a single pixel represents only a 20 m by 20 m area.

Figure 45 is an example of another type of output. The modal filtered image was relabeled so that all the uniform areas would have their own numbers. Then, the raster-vector transformation was performed. The result was output using a pen plotter.

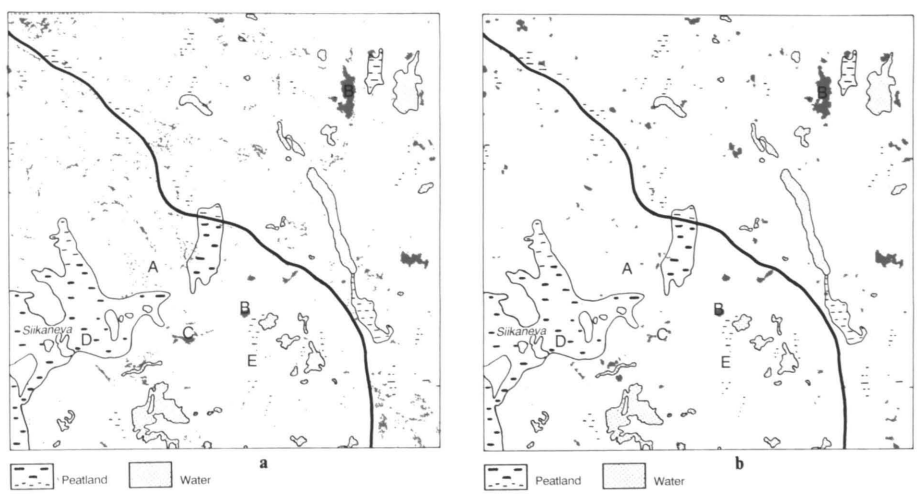

Fig. 44. Impact of filtering to the clear cut class. Classification MLOrigAlt to image pair TMI84/TMI85. Area 10 km x 10 km. a) Unfiltered classification. b) Filtered classification.

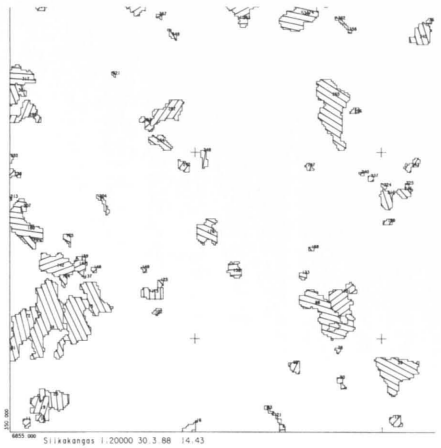

Fig. 45. Line map of change classes. Output in National Board of Forestry. Area 2.5 km x 2.5 km. Original scale 1:20 000.

Table 30. Distribution of classes of MLOrigAltF classification to the classes of MLDiffEqF classification. Area same as in Fig. 41. Classifications to image pair TMI84/TMI85.

MLOrigAltF	MLDiffEqF Corresponding class						
	C	D	S	P	Unch.	Uncl.	Tot.
Clear c.	**66**	1	8	7	17	0	100
Damage	0	**92**	0	0	7	0	100
Shrub r.	3	14	**29**	1	53	0	100
Soil p.	9	2	3	**16**	70	0	100
Unchanged	0	23	1	1	**75**	0	100
Unclassif.	1	1	13	2	78	4	100

6. Possibilities to detect changes

The results gave information about spectral changes caused by the rapid field changes of a stand. Because the field changes occur during different times in the life of a stand, information about the general spectral behavior of stands was obtained. Furthermore, information about the opportunities to spectrally separate field change types was obtained.

Empirical model for spectral life cycle

The class statistics of classes of image TMI85 (classes C, CR, L, TR, S, SR, P, PR, Table 21) were used to compute an empirical model of the reflectances during a rotation (Fig. 46a and b and Fig. 47a, b, and c). To make comparison easier between the empirical model and the computational model (presented in Section 2.3), it was assumed that the reflectance of the clear cutting reference class (CR) was the same as the reflectance of mature forest in the computational model. The rest of the reflectances were computed from the class intensities so that the ratio of the computed reflectances in different development phases of the stand was the same as the ratio of the intensities of the classes.

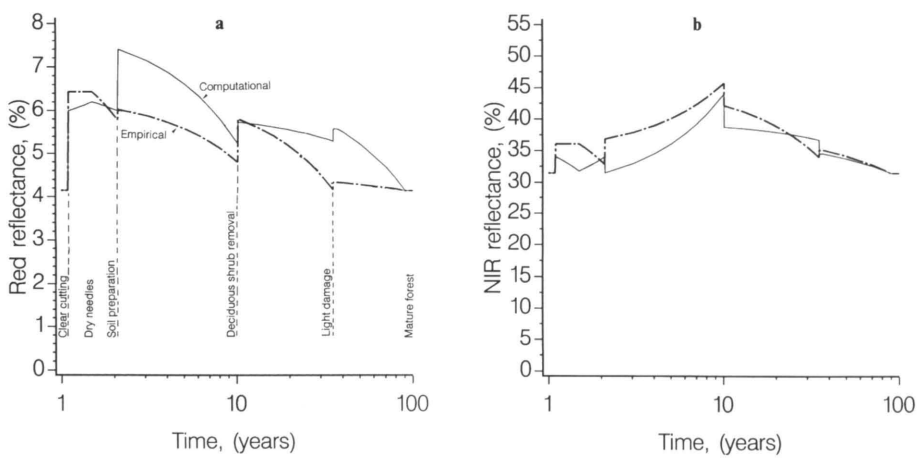

Fig. 46. Empirical model vs. computational model of reflectances of a pine stand during a rotation. Vegetation in summer seasonal aspect. a) Red light. b) Near infrared radiation.

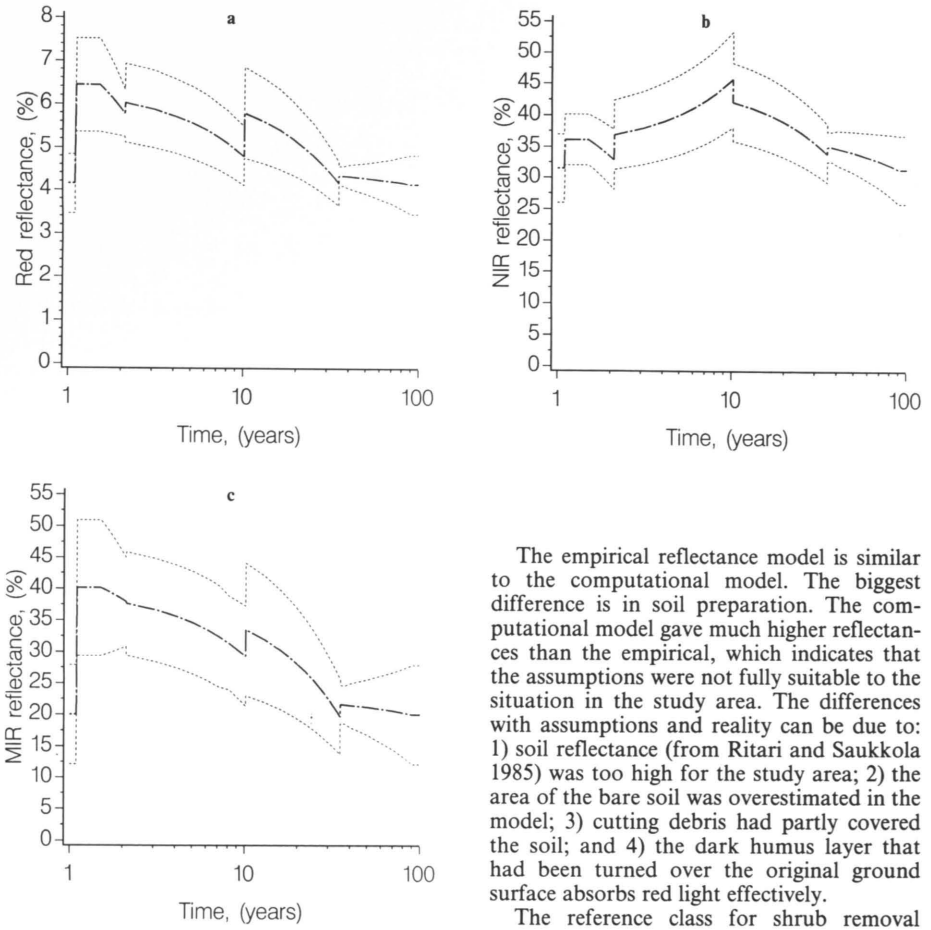

Fig. 47. Empirical reflectance model and standard deviation of the reflectance. Vegetation in summer seasonal aspect. a) Red light (TM3). b) Near infrared radiation (TM4). c) Middle infrared radiation (TM5).

The empirical reflectance model is similar to the computational model. The biggest difference is in soil preparation. The computational model gave much higher reflectances than the empirical, which indicates that the assumptions were not fully suitable to the situation in the study area. The differences with assumptions and reality can be due to: 1) soil reflectance (from Ritari and Saukkola 1985) was too high for the study area; 2) the area of the bare soil was overestimated in the model; 3) cutting debris had partly covered the soil; and 4) the dark humus layer that had been turned over the original ground surface absorbs red light effectively.

The reference class for shrub removal partly represented stands that were older than the typical age for shrub removal. Therefore, the red light reflectance was low before the treatment in TMI85 data.

The reflectance change between Time=35 years and Time=90 years is not linear as was assumed in the computational model. More research should be done to find a better model for the general relationship. These models should be developed separately for different wavelength ranges. Models applied earlier have been created for practical purposes to estimate the tree stem volume in a single study (Tomppo 1988).

The weaknesses in the computational model are not, however, critical to its use as a basis for an automated forest change detection system.

Separability of change types

The number of test stands and plots in many classes was inadequate to answer exactly how well each class can be separated (Genderen and Lock 1977, Cinevan 1979, Hay 1979). However, several classifications to image pairs TMI84/TMI85 and TMI85/TMI86 all gave similar results. The exception was the damage interpretation which gave different results depending on whether one image of the pair was acquired before or after the epidemic in 1985. The results of the image pair TMI84/SSI87 classifications were poor, most probably due to limited ground truth and the three year time span between images. The results of Tukey's tests supported the test classification results.

Different types of changes could be separated with different reliabilities. The order of the separability of the change types was somewhat different in the empirical data from the computational reflectance data (Section 2.3). Soil preparation could not be separated as well as the computational reflectances indicated, and damage could be separated better. The order of the change categories was, from the best separability to the worst: 1) clear cutting; 2) damage; 3) soil preparation; and 4) thinning cutting, deciduous shrub removal, and deciduous shrub growth.

In the study, predetermined changes were investigated. This made it possible to detect smaller spectral changes than can be done if satellite image interpretation is used to update a general forest inventory (Peng 1987). Predefinition is not always possible, however. All the changes may not be known. An example of unknown changes, which was found using clustering, was the obvious *Gremmeniella* damage in older forests.

The clear cuts formed their own distinct spectral class, according to the statistical tests and empirical classifications. Clear cutting increased the intensities in all wavelengths. The relative increase was largest in the red light. Clear cut and deciduous shrub growth classes were the only change classes studied which increased the near infrared intensities (Fig. 22b).

According to the empirical data, thinning cutting, damage, and soil preparation had only a minor effect on the near infrared reflectance. Figure 47b indicates an increase in the near infrared radiation due to soil preparation. The bitemporal intensities of the soil preparation class and its reference class show that the treatment has not changed the near infrared intensities. The intensity differences between the soil preparation and the reference class in Figure 47b are caused by the different phases of the vegetative succession of the classes.

The spectral variability of the clear cut areas was large. For example, if the clear cut areas were both plowed and cut between the dates of the image acquisition, for example, the intensities of the reflected radiation were different than if the area had been cut only. A three year time span between images showed a great amount of spectral variability within clear cut areas, due solely to the succession of the vegetation.

Very small-area clear cuttings can be confused with intensity changes caused by the different shadow lengths. In the study, an image pair was used where the former image was from September and the latter from June. The increased solar angle caused an intensity change similar to clear cutting. These misclassifications could not be completely eliminated using modal filtering by segments. A small segment-size was used. A large filtering window (segment) would have faded the smallest clear cuttings.

Confusion of seasonal and moisture changes in an open bog with clear cuts (Saukkola 1982) was not discovered, probably because multiple wavelengths were used instead of the red light range only.

Thinning cuts and damage by the *Gremmeniella abietina* fungus were interconnected when many cuttings were made because of the damage. But the two changes were also spectrally similar, since many thinned spruce stands were classified into the light damage category. Ground truth for thinning cuts, collected in normal forestry practice, seemed to be too coarse for the interpretation of such tiny spectral changes resulting from the thinning cuts. Stand data did not indicate that the separability of thinning cuts would be better in high volume classes where the drain is usually higher. However, the NFI data did have a relationship between drain and intensities within the class for thinning cuttings. Near infrared intensities decreased with the increased drain.

Gremmeniella damage caused a spectral change which was detectable in satellite scanner images. The separation of the heavy damage category from undamaged forest was not as reliable as the separation of the light damage category.

The damage grade estimation succeeded in the light damage category only. This result looks useless from a practical point of view. The damage categories should be known before the damage grade can be estimated. The 1982 damage had been worse in the heavy damage category than in the light. Because of the earlier damage, the change in the needle mass could not have been large in the heavy damage category in 1985. Consequently, the needle mass change in 1985 in the light damage category may have been larger than in the heavy damage category. The luxuriant undergrowth may have increased the intensities in heavily damaged forests (Colwell 1974).

Damage detection with monotemporal images hardly succeeds. Results of the modeling with Landsat channels suggest that satellite image aided estimation of traditional forest variables would give incorrect results if a damage epidemic is ongoing.

The spectral change due to autumn coloration in image TMI84 was inversely related to the change by damage. The intensities of deciduous trees decreased in the visible light channels and increased in the near infrared channel from image TMI84 to image TMI85 (Gates 1970, analogous images of this study). Thus, the seasonal change could nullify the spectral change due to the damage.

The connection of the infrared radiation to the thinning cutting and damage was unclear, as presented in Section 2.3. The spectroradiometer measurements indicated that the reflectance of the needles decreased due to *Gremmeniella* damage. The decrease in the reflectance was caused either by increased absorptance or by transmittance or by both. The relative decrease was smaller than the increase in the red light range. The satellite image analyses showed a near infrared decrease in medium damage and in thinning cutting. On average, the near infrared radiance of the damaged ground truth stands was similar to the reference stands.

The observations support the theory, presented in Section 2.2.2, that a slight decrease in the biomass would decrease the near infrared reflectance and a heavy decrease would increase the reflectance. The decrease is caused by changes in the spectral characteristics of the needles and by increased roughness of the surface. The increase occurs when the absorbing plant mass drops under a critical limit and the reflectance from the ground surface starts to control the total reflectance.

The near infrared absorptance by the plants is very low. The leaf absorptance of conifers is higher than the absorptance of deciduous trees. Williams (1991) has measured a 1 to 2 percent absorptance by sugar maple leaves in the near infrared region. The absorptance of Norway spruce needles was 5 to 6 percent. The near infrared absorptance of a conifer forest stand increases when the biomass increases, and the reflectance decreases. With crops and grasses, the near infrared reflectance and biomass have had a strong positive correlation (Tucker 1979, Tucker 1980, Tucker et al. 1975).

The difference in the spectral behavior between conifers and grasses has not been discussed much, but some studies indirectly suggest that the plant species themselves would be the reason. The explanation seems to be very simple: the critical factors are the amount of green biomass and the vertical thickness of the plant layer. When the green biomass is low, increase in the biomass increases the reflectance since the leaves reflect the near infrared radiation better than the bare soil. After a certain threshold in the amount of biomass, the near infrared reflectance starts to decrease. The decrease starts when the biomass of the canopy is high enough to begin to prevent the transmittance of the radiation to the soil or dead organic material. Then, the absorptance of the canopy starts to control the reflectance. The decrease continues until all of the incident radiation not reflected from the very surface of the canopy is absorbed. The reflectance of such a canopy is the same as the reflectance of the upper surface. The biomass of grasslands differs dramatically from the biomass of forests. In Tucker (1979), the highest dry mass in a grassland was 3 500 kg/ha, when in a boreal forest in Finland the above-ground dry mass of trees only can more than 100 000 kg/ha, 30 times as much as the mass of grasses (Mälkönen 1974).

The mechanism should be similar with deciduous trees, conifers, and other plant species. The reflectance drop starts earlier with conifers than with deciduous trees since the near infrared absorptance of the conifers

is higher. The spectral characteristics of needles and deciduous tree leaves are similar, however. The higher absorptance of a conifer stand is caused by the layered structure of the crown (Oke 1987). This permits a larger part of the radiation to go directly to the lower parts of the canopy. The radiation, if reflected upwards, hits the needles in the upper parts of the canopy. Those needles can absorb the radiation or reflect it downwards again.

The theory suggests that the near infrared reflectance from deciduous tree forests would level out in lower biomass levels than the reflectance from conifer forests. Thus, the biomass estimation in conifer forests should succeed better than the biomass estimation in deciduous tree forests. On the other hand, the lower near infrared absorptance of deciduous trees may be an opposite factor to the crown cover structure in biomass estimation. In Finnish boreal forests, it is hard to get data that is extensive enough for deciduous tree biomass estimation.

Results of the needle spectroradiometer measurement were in partial disagreement with needle measurement results on *Pinus pinaster* by Guyot and Riom (1988). Guyot and Riom observed an increased reflectance in the near infrared range from damaged needles. The probable reason for their results is that the damaged needles were very dry during the measurement (Williams 1988).

A relationship between elevation and damage was observed in the field plot data, although the area of the plots covered only a few hundred hectares and the total variation in the elevation was only 26 m. Also, comparison of elevation distributions of the areas classified as damaged in the general elevation distribution indicated that elevation and damage are related. Consequently, the topographical data may be very useful in the *Gremmeniella* damage interpretation.

The relationship between *Gremmeniella* damage and topography seemed to have micro and macro scale characteristics. The micro scale characteristic could be noticed in the field. The worst damage occurred in depressions that may have been very small. The resolution of the elevation model was too coarse to separate small depressions when local elevation was calculated. Furthermore, local cold air concentrations were not only caused by the ground's topography but also by the vegetation, e.g. the edge of an older forest. A macro scale characteristic was that most damaged areas were on the lower slopes of the highlands. Still, the damage was concentrated in local depressions, but in this case "local" means an area of some tens of kilometers in diameter instead of some tens of meters.

The slightly colder climate in the depressions of the highlands was only one factor typical of the damaged area. A related factor was the possible impact of the genesis and morphology of the soil. At least part of the area had not been under water since the last continental glacier melted (Haavisto 1983 ed.), which may make those soils different from the other forest soils. Further factors were the closeness of the bedrock, and often the quite poor site type. The closeness of the bedrock can impede rapid water drainage in the root layer, which can cause aeration problems for the roots. Combinating the interpretation result with other existing information helps to understand the interactions better (Fig. 38 and 39, Section 5.6).

Part of the soil preparations on regeneration areas could be detected, although the real spectral change was much smaller than the computational change.

The poorer separability of soil preparation may be, in addition to the spectral characteristics of the elements, due to the heterogeneity of the plowed areas which increased the deviations of intensities. The damaged areas were separated better than expected due to their spectral homogeneity in these data.

Analysis of image pair TMI85/TMI86 data indicated that detection of shrub removal can succeed. Also, the empirical reflectance model showed relatively big spectral changes due to shrub removal. Lack of test data makes the evaluation of the classifications uncertain. Some seasonal changes on open bogs were confused with the shrub removal class.

Tests with the NFI plots and image pair TMI84/SSI87 supported the hypothesis that the appearance of deciduous shrubs on regeneration areas can be detected. Shrubs were detected due to increased near infrared intensities. The classification results were confusing, however. The stands from which the deciduous shrubs were removed were largely assigned into the deciduous shrub growth class. No plots were available to test the shrub growth class. Class statistics for this class were computed using 14 observations only.

Features

In general, the best spectral features were the red light (TM3) and the near infrared radiation (TM4), which did not correlate with other channels especially well. The adding of the middle infrared (TM5 or TM7) and the blue-green light (TM1) increased the performance of the classification for the input data. The high standard deviations of the TM5 intensities in the maximum likelihood classification models suggest that the middle infrared data includes information that does not have a very close relationship with the traditional stand variables. In the unsupervised classification model, deviations for TM5 were not higher than for other channels. In this model, the TM5 channel seemed to be very useful in separating damage classes.

According to the spectroradiometer measurements and the spectral value analyses of the Landsat TM images, the best individual channels to separate thinning cuts and damage from the unchanged forest were red light (TM3), middle infrared (TM5), and near infrared (TM4), in that order (Häme 1988b, Olsson 1989). The TM4 channel was not useful in classification, but it was effective in regression analysis to estimate the damage grade when the damaged forest was separated from other forest. The sensitivity of the near infrared to the damage grade must be due to its good transmittance trough the canopy. The radiation reaches the lower parts of the crown which suffer most of the needle loss.

The role of the middle infrared channel TM5 is somewhat uncertain. It was the best channel to separate the obvious damage classes in clustering. Olsson (1990) has found channels TM5 and TM7 the most useful in the detection of thinning cuts. The usefulness of those channels in his study can partly be due to the calibration of bitemporal images which had succeeded well in the middle infrared range.

An explanation for the relative weakness of the principal components and canonical variables is that the changes of interest covered only a minor part of all intensity value variation. Then, the changes occurred in the lower components together with the noise. The canonical transformation, based on the intensities of the ground truth areas, was only slightly better than the other operations for bitemporal images. Even the training areas seem to have had so much spectral variation, other than what was due to the changes, that the transformation was not helpful. A canonical transformation to difference channels might have worked better, but there is not much need to compress the difference channel data. The calculation of difference channels already reduces the amount of the data to half of the original.

The widely used ratio channels did not work very well. All channels, except the near infrared, reacted similarly to the changes, which does not support the use of channel ratios. Also, when the absolute values are small, relatively small value differences change the ratio a lot. The ratio operation may increase the significance of noise. In some cases, increased red and decreased near infrared intensities were related with damage. This could provide justification to use the red/near infrared channel ratio.

The only textural channel computed, local variance, was disruptive to classification when it took the place of the D1 channel. The spatial resolution of Landsat TM seemed to be, according to this single experiment, too coarse to compute a textural channel for change interpretation purposes. The separation of soil preparation, and perhaps thinning cuttings too, could be better if a textural channel were available from an image having a higher spatial resolution. Spot panchromatic data with 10 m by 10 m pixel size might include valuable textural information. These data were not available for this study.

The most useful arithmetic image operation was difference channel calculation, but matching of the histograms before the difference channels were calculated did not prove useful. Rather, it was slightly disruptive.

A conclusion of the feature testing is that an arithmetic image operation should not be done automatically as is often the case in many forestry remote sensing applications. Also, the same feature set seemed to be suitable for all classes. Consequently, all classes can be interpreted simultaneously.

Temporal aspect, illumination, and atmosphere

The classification with transferred statistics could usually only separate some clear cuts.

The image histogram matching method that was used may not have been optimal. Seasonal factors and the *Gremmeniella* damage made the scaling more difficult. It is, however, probably very difficult to find an image calibration method that makes possible direct evaluation of older class statistics if the detection of change is difficult, even when using ground truth.

The use of tritemporal summer image data gave good results in the classifications, although the middle infrared spectral range was missing. The result supports the theory, presented in Section 5.2.5., about recovery after a rapid change. The input data in the tritemporal classifications were difference channels. Thus, the variation in image data was largely caused by the change.

Temporal information in the form of winter images did not appear useful. The main problem was the dramatic reflectivity difference between trees and snow. Relatively small differences in the canopy structure — which are not necessarily related to the traditional forest stand variables — cause big changes in the intensities. Cutting debris on the snow, bare spots, and snow and frost on the branches make winter images less useful. The snow and frost on branches were recorded every day in March for the study. The information was, unfortunately, lost after recording. Winter images may be used in ecological studies, together with summer data, but the reflectivity difference may always be a problem unless the aim of the interpretation is to map the snow itself (Ritari 1987, Kuittinen 1988).

Different solar elevation angles in images TMI84 and TMI85 may be one reason why the spectral changes in spruce forests were similar to changes by damage in pine forests. The reflectance of long spruce crowns with high needle mass should not be sensitive to the solar angle, because the needle layer in vertical direction is thick enough not to transmit the near infrared radiation. However, the form of the crowns causes specular reflections. In low solar angles, the specular reflection can turn to nadir, causing a high near infrared intensity (cf. Wastenson et al. 1988). In the image pair, used for damage inventory, the older image had a lower solar angle of 29 degrees. The specular reflection to nadir with a 29 degree solar elevation angle would require a branch angle of −30.5 degrees measured from horizon level. The specular reflection with the 49 degree solar angle of the June image would demand a — 20.5 degree branch angle.

In the analogous images of the TM4 difference channel, a decrease of the near infrared could be detected both in pine and in spruce forests. The homogeneity of the decrease was different. An even decrease could be seen in pine forests. The near infrared difference channel intensities varied more in spruce forests. Kleman (1986) measured only pine stands with different solar angles. The effect of the solar angle was not strong in the near infrared.

Different solar angles could also have made the separation of the damage easier. Thus, the visible light reflectance of all pine stands may have increased from September 1984 to June 1985 (Kleman 1986). The damage may have exaggerated the increase.

It was doubtful whether different air and canopy moisture levels had any impact on the results. Decreased moisture from TMI84 to TMI85 could partially explain the increase in TM5 intensities, but according to some recent studies (Ahern 1988), the TM5 intensities do not reflect needle moisture. Rather, they reflect the fraction of damaged foliage and bare and lichen-covered branches within a pixel. Thus, they would indicate similar things in the visible channels. Olsson (1991) has observed no big impact of soil moisture on the Landsat TM intensities in boreal forests.

Radiometric and spectral resolution

Spectral changes by thinning cuttings, soil preparation and deciduous shrub removal were close to the radiometric resolution limit of the Landsat TM and Spot satellite images. Better sensitivity of the sensors could make the separation of those changes easier. The increased noise in the images of better radiometric resolution can be partly eliminated using image segmentation and other contextual techniques. The spatial resolution could not be much coarser either. The opportunity to detect field changes with minor spectral impact is less with Landsat MSS data than with TM data. The field content of each MSS pixel is much more heterogeneous than the content of a TM pixel.

Spectral resolution is less of a problem. Red light and near infrared radiation channels alone give quite good results. Landsat TM channels are almost optimally located for damage detection according to the spectroradiometer measurements. Nevertheless, very narrow, 2 — 5 nm wide channels, would be very interesting in damage inventory. The narrow channels would make it possible to detect the transfer of the inflection point of the reflectance curve between red light and near infrared radiation. Also, the narrow channels could be effective in detection of the radiation absorption by photosynthesis.

Interpretation methods

The supervised classification methods in general, and the maximum likelihood method in particular, were most suitable for interpreting changes. Regression analysis could be used in some cases to estimate the grade of the change, but not to separate changed forest from unchanged. The problem with the unsupervised methods seem to be the enormous amount of different changes between the images. The changes of interest to everyday forestry often cover a small area when compared with the seasonal changes, for example (Peterson 1989). The unsupervised method can not find specific changes, because no supervision exists to specifically separate them. Furthermore, the intensities of scanner images do not form clear clusters. The clustering may mainly just divide data into smaller fractions rather than extract different canopy types.

Targeted changes often occur in stands with limited or no tree cover. This makes the unsupervised method even more difficult. Open areas usually have higher variations in intensities than older forests. A high spectral variation produces many classes in most unsupervised methods. The main benefit of the unsupervised method in this study was that a change in older pine forests was found, which was most probably caused by the *Gremmeniella*-fungus. This type of damage was not separated using the supervised classification since the ground truth was mainly from younger forests.

Although the maximum likelihood classification using change and reference classes was the best method to separate minor spectral changes, it has some weaknesses. First, the main weakness may be that it requires high quality ground truth data. The classification result may be weak and hard to predict if ground truth data do not completely represent field classes, and if no threshold value is used or if it is low. Second, the proportion of a class in the final classification may be low if the variance of the spectral variables is high. The *a posteriori* probability of a class membership can be low even at the mean intensity vector. Third, if the distribution of the class intensities is far from multinormal, the assumptions of the method are not in effect, and the results are suboptimal. The class distribution usually approaches multinormal when the amount of pixels per class grows.

Ground truth

The incomplete ground truth caused problems in the evaluation of the results. The main ground truth data, stands of the National Board of Forestry, were originally collected during operational forestry planning. The field inventory had been made about ten years before the acquisition of the first image. The change information was collected separately by the field personnel of the National Board of Forestry. No field measurements were made. The most serious difficulty with the ground truth was the unreliability of the stand boundary delineation. The delineation was checked visually using the satellite data. The checking indicated obvious errors in stand boundary delineation and also in the geometric performance of the stand map. The boundaries were not corrected on the basis of the intensities because of the danger of manipulating the results. Whole stands with very unlikely intensities were rejected. Further restrictions in the stand data were the coarseness of the stand variable values and lack of damage information.

The *Gremmeniella* damage data was accurately measured. The main restrictions were the small amount of the data and lack of a completely healthy forest. Also, the undergrowth was not estimated. The damage varied greatly within small areas. The degree of damage was assumed to be the same in the radius of 20 — 40 m from the center of the plot. This may not always have been a correct assumption (Alajärvi 1991). The data were concentrated on stands at the age of the

first thinning. They represented this canopy type relatively well.

The NFI data were measured accurately twice. The measurement dates matched the times of image acquisition well. Preliminarily, the NFI data were assumed to be the best ground truth. The analyses showed that there were far too small a number of observations in the change classes. The proportion of changes from the total area was too small to apply sampling of this type.

In the study, the most important rapid changes were studied. Studying of many changes lead to the need to use predominantly existing ground truth data. If only one change type had been selected, the ground truth could have been more accurate. The analyses showed that the spectral characteristics of different field changes were similar. Concentration on a certain field change type would have made it difficult to form a general view of the possibilities for change interpretation. Furthermore, before of the study it was difficult to know what kind of ground truth would have been optimal. A good example is the presumed usefulness of the NFI data.

PART II

7. On the practical use of satellite image aided change detection

The areal proportion of changes that are important to forestry is quite high. Some change was registered on one third of the plots measured in 1984 and 1987 in the National Forest Inventory data. Thus, a change had occurred in about ten percent of the plots per year. About half of the changes were "traditional" cuttings. The proportion of change plots might have been even higher, if the field crew had registered the *Gremmeniella* damage as a change in the 1984 —1987 time period.

Satellite image aided change detection can be used for updating forest map systems, helping normal treatment planning, updating sampling inventory results, and giving information for ecological investigations. Known change types can be localized and mapped, and poorly known changes can be found.

The most straightforward applications are treatment planning and ecological investigations. The interpretation result shows directly, for instance, the general location of damaged areas and areas with fast deciduous shrub growth. Updating a digital map system and sampling inventory results needs field work to support the interpretation. Checking of the interpretation is especially important if a total inventory is not made at regular intervals. The detection of thinning cuttings is so uncertain that in all cases field checking is needed. The value of the interpretation is that field work is only checking instead of total inventory and that the whole area need not be checked. In sampling inventory, proportions of classes are corrected using field measurements. The checking can also be done from an aircraft using video imaging, for example. Big cost savings can be realized when a total inventory can be replaced with checking (Häme 1984a).

Timing of image acquisition

The reasons for the timing of image acquisition are similar to the timing of other types of measurements which aim to detect change (Section 2.1). If the aim of the interpretation is to detect manmade changes and epidemic-type damage, the time span between the images should be quite short, optimally one year. The phase of the growth period should be the same (summer). A short time span gives better results because canopy succession will fade the evidence of the changes surprisingly fast. The marginal utility of a third image should be evaluated in respect to the requirements of the interpretation. The third image, if used, should be acquired one to two years after the basic change. Natural changes, such as vegetative succession, increase in the tree stem volume, and deciduous shrub growth should, of course, be interpreted using a longer time span, and preferably with more than two images.

Ground truth collection

Changes that have only a slight spectral impact and cover a small proportion of the area, require ground truth which is carefully collected for image interpretation purposes. The ground truth collection should be included in the normal operation of a forestry organization.

The ground truth should consist of stand-type data, collected either by using stratified sampling where the strata are the different treatment types in a forest management plan, for example, or by subjective selection. The selection procedure involves the risk that the change classes do not represent all changed areas. Nevertheless, it seems to be the best way to separate classes with small intensity changes. National forest inventory type data are not very suitable for the ground truth of manmade changes. Although the proportion of the changes is quite high, the number of fresh changes, suitable for the ground truth, is often inadequate. Furthermore, plot sampling may prevent selection of very many pixels surrounding the plot and may assume that their field content is similar. Image segmentation could be used to find homogeneous forest surrounding the plot. But in the

case of thinning cuts, for example, it might be very difficult to find the boundary of the cut.

The changed ground truth stands and unchanged reference stands should be located in the same type of forest, possibly next to each other. Care should be taken that the field data is geographically representative (e.g. Poso 1988). To prevent pixels from other stands from disturbing the spectral statistics, the delineated boundaries of ground truth stands should be closer to the stand center than are the true boundaries. The intensities in this study, were selected from the whole stand which may have made the separability of the classes weaker.

An auxiliary result of the study is related to the collecting of ground truth variables. It would be useful from the standpoint of satellite image interpretation if the forest density, stems per hectare, is included in the forest variables measured. It was, together with the stem diameter, the best independent variable when the spectral channels were modeled. It was especially important for the image TMI86 acquired after the *Gremmeniella* damage.

The damage grade estimation method, used in the field inventory, was good. The damage percents had linear correlations with the TM4 intensities. The field method is even more appropriate, since it considered the effect of damage to the future life of the trees. Two damage classes were separated in the study. The applied limit, 30 percent needle loss, should be tested later with new data sets.

Either stand-type ground truth or national forest inventory plots could be used for the interpretation of gradual, long term changes.

Use of different interpretation methods

Maximum likelihood classification, either with original or difference channels, is the best of the commonly available methods to detect rapid small area changes, according to the results of this study. The *Gremmeniella* damage grade can be estimated using regression analysis if the damaged area is first separated from the surroundings and if the canopy is not very sparse. Regression analysis is also suitable for gradual, longer period changes.

The benefit from the difference channels is that ground truth stands may not be needed from every changed stand type. The impact of the normal stand variables disappears, or at least decreases, in the difference channel operation. The confusion between the change classes can be improved by using forest management plan data or an interpretation result of a single date satellite image.

Unsupervised methods should be applied in cases where the objective is to make a general change inventory, and where one is interested in changes over larger areas in which information on the changes is limited. A time series of satellite scanner images and an unsupervised classification method offer interesting tools to investigate vegetative succession and other dynamics in a forested area. The comparison of the clustering classes of several classifications requires image calibration. The unsupervised methods serve also as a first step to more careful change analysis; they can be used, among other things, to select ground truth areas.

Maximum performance versus meaningful performance

Any classification procedure alone, supervised or unsupervised, may be biased by individual classes as long as the classes spectrally overlap and their true proportions of the total field area are different. The classifier overestimates the size of a class whose true area is small and underestimates a large-area class. The reason is that pixels from the overlapping spectral area can fall in a small-area as well as a large-area class. The classification procedures are most likely unbiased over classes, however.

In the maximum likelihood classification, altering *a priori* probabilities can be used to make the proportion of the most undesirable errors smaller and decrease the bias in the estimation procedure. The proportion of the changes of interest may be approximately ten percent a year. Smaller *a priori* probabilities in the change classes than in the nonchanged classes can be used to obtain areal proportions that are closer to the truth than those obtained using equal probabilities. Small *a priori* probabilities cause the pixels from the overlapping area to be more likely assigned to the class with a higher *a priori* probability.

It is, of course, not always meaningful to try to maximize overall performance. Assume, for example, that the aim is to find clear cuttings in a forested area. The true proportion of clear cuttings is one percent. A classification model allocates 60 percent of the area to the unchanged forest class. In this particular class, clear cuttings are not included. The other class includes all clear cuttings and the rest of the unchanged forest. Thus, the overall performance of the whole classification is low, 61 percent. The result is useful, however, because the more careful clear cutting inventory can be concentrated on 40 percent of the total area. A classification model which would have allocated all the area to the class for unchanged forest would have given a 99 percent overall performance, but the result would have been useless.

In the maximum likelihood classification, the probability setting using areal proportions directly (Strahler 1980), does not seem to work well in cases where: 1) some classification errors are more undesirable than others; 2) the separability of the classes is different; and 3) some classes represent a very small part of the area to be classified. The best way to set the probabilities may be a combination of the areal proportions and spectral distances. In this study, it was approximated by choosing the probabilities by deduction and by trial and error. The selected probabilities functioned similarly in two different image pairs. The same probabilities may function generally in managed boreal forests, since the mutual spectral relations of the classes are likely to remain similar.

The *a priori* probabilities were used in the study to get the change classes as reliable as possible. This caused also that part of the area with actual changes was classified as no-change classes. Another solution would be to try to separate the clearly unchanged (only growth and seasonal changes) forests giving low *a priori* probabilities for the non change classes. Growth models could be safely applied to those forests to update the forest variable values, and the rest of the area could be checked in the field or from an aircraft. The performance requirements and available funding would define how the *a priori* probabilities are to be used. The relatively high probabilities for change classes will increase the checking work and costs when only area classified as changed in checked.

Updating maps

An interpretation result with a moderate reliability will be useful if it is used as preliminary information to be supplemented from other sources, e.g. aerial photography and video imaging or field checking. The method could be used to update large-area forest management plans. Visual interpretation or numerical interpretation approaches, or a combination of the two, can be selected.

In the visual interpretation approach, 1) a color composite is made by using difference channels from a bitemporal image set, as described in the study. The color image is displayed as background for the stand map in a GIS system. 2) The field changes are delineated by visual interpretation. A separate layer of the obvious changes is generated to the GIS system. 3) After checking, the original map is updated.

In the numerical interpretation approach, the interpretation result with stand boundaries is obtained automatically (Fig. 48). Some additional rules or a primitive expert system can be utilized to avoid young stands being classified as clear cut areas, for instance. Modal filtering by image segments should be used to delineate the uniform change areas, if

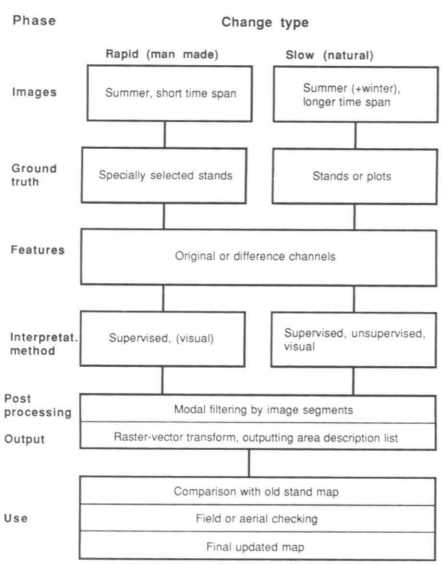

Fig. 48. Phases of satellite image-aided change detection for change mapping.

the aim of the interpretation is more than to check possible change within a known area. The use of the result in a vector-format map system requires generalization since the original pixel by pixel classification gives an enormous number of individual areas. When a very small segment size (about 10 pixels on average) is applied, filtering may not lead to incorrect boundaries of the classes. In the study, the class distributions within segments indicated that the segmentation had usually generalized the interpretation result well.

The third opportunity would be to output the classification probability of the maximum likelihood model for each pixel, separately for each class. The output would be a normal image file. The likelihood image of thinning cuts, for instance, is then displayed as background for a stand map. The final interpretation is done visually.

The checking of the classification result is similar in all approaches:

- — *Unchanged forest.* Checking in experimental phase. Aim: no checking necessary.
- — *Clear cuttings.* No checking usually necessary. Some additional data must be used in some cases, e.g. to separate cuttings for forest regeneration from clearings for road or building construction.
- — *Soil preparation.* Aerial checking.
- — *Deciduous shrub removal.* Aerial checking.
- — *Deciduous shrub growth.* Grade checked from air.
- — *Smaller decrease in biomass than by clear cutting* (fungi damage, storm damage, thinning cutting). Aerial, possibly also ground checking.

If the final requirement of a forest inventory operation is a map that is completely error free, satellite image interpretation of changes is not useful. Some mixture of classes always remains. Total field inventory is therefore required.

Updating national forest inventory type data

Useful statistics about the areas of the changes might be computed for clear cuttings and *Gremmeniella* damage areas directly from the interpretation result. The direct statistical computation procedure would be biased. Part of the thinning cuts will be included in the *Gremmeniella* class. The areal estimates of the deciduous shrub removal class would require the use of a mask for peatlands and agricultural areas. Reliable areal estimates of thinning cuts and plowed forested areas may not be possible.

To make the change inventory procedure unbiased, a field inventory should be combined with the satellite image interpretation. Also, external statistical data, e.g. national cutting statistics, can be applied to reduce the bias. For instance, a procedure by Burk et al. (1988) could be applied. In this "regression sampling" method, the results of the satellite image classification are corrected using measurements of larger clusters. The true proportion of each class, or values of continuous variables, is measured within clusters. Then, a regression model for each class is calculated to correct the satellite image classification results. The location of the clusters can be selected using random, systematic, or stratified sampling. The selection is independent of the image interpretation. Part of the field work on clusters can be replaced using aerial surveying. Shuttered video cameras offer an inexpensive tool to obtain detailed image data both for visual and numerical interpretation (Häme and Rantasuo 1988). Another alternative to the regression sampling is stratified random sampling where the strata are the classes of the image interpretation.

The regression sampling and stratified sampling techniques are especially suitable for change interpretation where the number of variables is quite small (Cunia 1978, Poso et al. 1987, Kilkki 1988). However, a classification based on the most important forestry variables can be useful in giving good estimates of a larger number of variables. This is possible if the correlations between the variables are high.

One alternative is to include all main change types in the classification when the results of supervised and unsupervised classifications are merged (Fig. 49). Another alternative is to use the result of the unsupervised classification to select new training areas for the supervised classification.

In the first alternative, the obvious change classes of the unsupervised classification are combined with the result of the supervised classification if they cover an area not classified as changed in the supervised classification. The change classes of the unsupervised classification are identified by means of spectral statistics.

The supervised classification should be

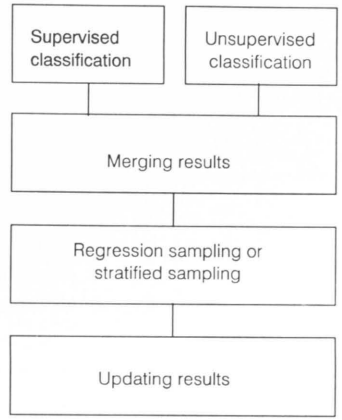

Fig. 49. Use of satellite image-aided information to update national forest inventory type data.

used because the results are in general better than in the unsupervised method, as discussed above. Modal filtering by image segments is applied, since a big part of the "salt and pepper" effect may not reflect field variation or change.

Automated forest change monitoring system

The reflectance model of this study and other knowledge about changes in forest could be applied to create a fully automated forest change detection system (Fig. 50).

In this approach, neither careful image calibration nor comprehensive ground truth are necessarily needed. A coarse estimate of the changed and unchanged (only ordinary forest growth) areas should be available. The method is most suitable for interpretation of rapid changes, such as manmade change and epidemic-type damage. The approach has the following steps (bitemporal data):

1) A bitemporal image set is rectified to the same coordinate system.
2) All 2 x 2 pixel groups which are relatively homogeneous in respect to intensities in all channels and both images are extracted. A 2 x 2 pixel group is the smallest approximation of a circle within which the intensity deviation can be computed.
3) Pixel groups are divided into 20—30 categories by means of an unsupervised classification to the first (earlier) image. Categories are labeled and sorted according to tree species and biomass using their red light and near infrared radiation intensities.
4) The intensities of the 2 x 2 pixel groups are selected from the second (later) image by the categories of the unsupervised classification which was made to the first image. The standard deviation of the categories in all channels of the second image is computed.
5) If the deviation in a certain category is greater in the second image than in the first image, another clustering is made to the second image within this category. In this phase, 2 or 3 categories are separated.

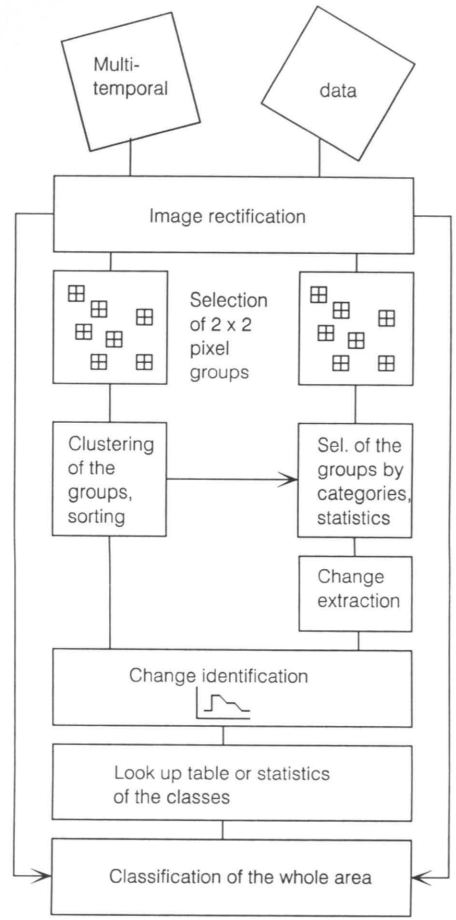

Fig. 50. Scheme for a fully automated change detection system.

6) The change is identified by applying prior information about the areas of the classes and the spectral properties of the categories of the unsupervised classification. For example, clustering of the first image has separated a category having intensities referring to pine dominated, midaged forest. New clustering to the second image within this category separates two new categories: a category which has 70 percent of the pixels, and another category which has the remaining 30 percent of the pixels and in which the red light intensities are higher and the near infrared intensities lower than in the larger category. The larger area class would be labeled "unchanged", and the smaller area class "damaged" (*Gremmeniella abietina* Lagerb. fungus).
7) A look-up table will be made of the intensities of the labeled classes, or spectral statistics are computed.
8) All pixels of the area will be classified.

The change monitoring system can be carried out by means of an expert system approach. A risk of this method is that incorrect labels are given to the classes. For instance, a changed class may be classified as unchanged and *vice versa*. Those errors are relatively easy to correct with simple testing, perhaps even with visual interpretation of the images. If the time between the images is long, or if the change is gradual, the identification of the change is more difficult. Setting proper standard deviation limits may need rough standardization of the images; or rather a mechanism that changes the deviation limits according to the spectral statistics of the images and circumstances during image acquisition.

The method has similarities to the Change Vector Analysis by Malila (1980); see Section 2.4.5. However, the images are not standardized carefully, but the spectral model is adjusted to the new images. The aim of using clustering to separate the changed and unchanged pixel groups is to try to avoid a weakness of the Change Vector Analysis: setting the parameters manually.

Future investigation needs

Study 1) The reflectance model as a function of time should be developed further. Tools for further development include spectrometer measurements of different canopy types. The ground truth should be comprehensive. The traditional measurements of forest stand characteristics are not adequate. The biomass of the canopy elements should be measured.

The topics which should be studied are:

a) The spectral characteristics of the incident radiation in the wavelength range of 400 — 2700 nm as a function of the above-ground biomass and plant species. The measurements should be made at the ground level.
b) The relationship between spectral characteristics of tree stem volume, needle (leaf) mass, and above-ground biomass. The spectral characteristics should be studied from above the canopy, using an imaging or nonimaging spectrometer.
c) Development of general reflectance model for tree stem volume, biomass variables, and canopy age. The data should be measured using imaging or nonimaging spectrometer. Even Landsat TM and Spot data can be used.
d) Spectral characteristics of carefully controlled treatments in the forest. The spectral data can be obtained using spectrometers or optical satellite images.
e) Spectral impact of solar angle and moisture changes. Spectrometer data should be obtained above the plant canopy.

Study 2) The automated forest change monitoring system should be completed and tested. The phases of the study are presented above. Study No. 1.

8. Summary

The basic aim of the study was to discover the spectral characteristics of rapid changes in forest and the spectral separability of change categories through the analysis of satellite scanner images. The change categories studied were: 1) clear cuttings; 2) selective thinning cuttings; 3) soil preparation for regeneration on clear cut areas; 4) deciduous shrub removals and/or conifer seedling thinnings on regeneration areas; 5) pine damage caused by the *Gremmeniella abietina* (Lagerb.) fungus; and 6) deciduous shrub growth on regeneration areas. Spectroradiometer measurements were applied to support the satellite image investigation. The study was divided into two parts. Part I concentrated on achieving the fundamental goal. Part II was a brief discussion about how a satellite image based change monitoring system should be constructed.

PART I

Theoretical background of spectral change detection

Opportunities to detect rapid changes are largely opposite to opportunities to detect growth. Successive observations within a short time increase the possibility to detect a rapid change. Thus, a shorter time span is best for all changes studied.

Four groups of sources for an intensity change in satellite images can be separated (Fig. 2):

1) Relationship between the reflecting and emitting elements of plant canopy
2) Angles between illumination source, canopy, and sensor
3) Atmosphere
4) Signal registration and processing

In vegetation studies, the only category of interest is the first, the other categories being disruptive.

The available information about the spectral properties of different canopy elements were applied to construct a model of the reflectance of a pine stand during a rotation (Table 1, Fig. 3a and b). The model suggested that the changes could be detected in the following order, from the easiest to the most difficult: 1) clear cuts; 2) soil preparation; 3) deciduous shrub removal and deciduous shrub growth; and 4) thinning cuts and damage.

The essential factors in the selection of the approach to the interpretation are:

1. Image acquisition
2. Preprocessing
3. Spectral features
4. Ground truth
5. Algorithms

Images should be acquired in the same season, if possible, to avoid the intensity differences caused by the seasonal cycle. In image rectification, the multitemporal images may overlap better if they are rectified first with each other and, after this phase, with the map coordinate system. Using a small pixel size in resampling reduces the intensity shift.

The original channels of a satellite contain all the spectral information; the problem is irrelevant information and a large amount of data.

Two basic types of ground truth are available in forest applications: stand and plot data. In forestry, stand data are collected for operational planning and plot data for strategic planning. The main benefit of the stand data is that an adequate number of observations for statistical spectral models are usually obtained. The plots represent a small area, but the measurements are usually very reliable because the objective of the sampling is to give trustworthy statistical information.

Most often, applied change interpretation methods should be placed in the category of supervised methods.

According to the earlier studies, more information is needed about the spectral properties of changes and the optimal spectral features used in change interpretation. According to the literature, the behavior of the near infrared radiation in conifer forests is not well understood. The main focus of the analyses was on the spectral behavior of the changes (Chart 1).

Materials

The study area, centered at 61°51' N, 24°22' E, covered a 40 km by 40 km square in boreal forest in Southern Finland. Scots pine (*Pinus sylvestris* L.) and Norway spruce (*Picea abies* (L.) Karst.) were the most common tree species.

Five satellite scanner images (three Landsat Thematic Mapper and two Spot HRV images) were used for interpretation. The images were acquired 1984 — 1987.

The ground truth data were obtained from three sources: 1) stands by the National Board of Forestry; 2) plots measured to estimate the *Gremmeniella* damage; and 3) twice-measured plots of the National Forest Inventory (NFI). The stand data included "unchanged" (only natural vegetative succession) reference stands for change categories. The intensities of the ground truth stands and plots were selected from satellite images.

Three topographic variables were employed as ancillary data. The intensities of Spot images had to be corrected due to radiometric errors.

The objectives of the spectroradiometer measurements were: 1) to study how *Gremmeniella abietina* (Lagerb.) damage changes the spectral reflectance of Scots pine needles; and 2) to investigate the relationship between needle biomass and reflectance.

Data analysis

The following spectral features were computed using arithmetic image operations:

- Difference channels with and without histogram matching
- Ratio Channels
- Principal components
- Canonical variables using canonical discriminant analysis

The differences of the spectral means of the classes were studied using Tukey's tests and discriminant analysis. Linear regression analysis was used to estimate the drain in thinning cuttings and the magnitude of damage.

Finally, the separability of the classes was tested by making classifications and testing them with external data. The classification methods were: Euclidean distance classification; maximum likelihood classification; and unsupervised clustering.

Image segmentation was utilized to generalize the result and bring the spatial aspect to the interpretation.

Results of intensity value analyses and classifications

Spectroradiometer measurements showed that the *Gremmeniella* damage increased the reflectance in the area of the visible light, but decreased the near infrared reflectance. The damaged needles differed from the healthy, mostly in the red light. The biomass measurements showed that, when the biomass increased, the values of the reflectance factor in the near infrared increased very steeply.

Near infrared intensities decreased when the drain in thinning cuttings increased. Regression analysis could be applied to some extent to estimate the drain if the thinned stands were already separated from their environment.

Damage grade and the near infrared intensities related closely until the damage grade exceeded a certain limit. The weakening of the relationship was due to the undergrowth and earlier damage in the most heavily damaged forests.

Absolute elevation was the only topographical variable which was related to the damage grade.

Tukey's tests indicated that usually the original channels separated changes better than did the transformed features. The most useful transformed features were the difference channels. The most important spectral ranges were the red light and near infrared radiation. The experimental discriminant models confirmed the results of the Tukey's tests. Also, the blue-green light and middle infrared channels of the Landsat Thematic Mapper were useful.

Following the intensities in the three year period indicated that the recovery of a rapid field change can result in an intensity change which is opposite to the original change. All rapid changes except the deciduous shrub growth increased the red light reflectance.

The analogous difference images, computed from bitemporal data, showed a big variation in intensities. A large part of the image area had intensity changes.

The best classification results were achieved using the original bitemporal channels and maximum likelihood classification, where the change classes had lower *a priori* probabilities than classes which represented unchanged forest. Thinning cuts were assigned to damage classes or their reference class, but not to their own class. Classifications where the time period between the images was three years gave very poor results. The main reasons were limited ground truth and vegetative succession. Clustering did not separate manmade changes but it separated the damage.

Map hardcopies of the classification results combined with other maps showed, among other things, that the closeness of the bedrock and the damage may have a relationship. Image segmentation was useful in finding boundaries of truly changed areas. Change classes also included areas with seasonal changes and manmade changes other than treatments for forestry.

Possibilities to detect changes

The results of the study gave information about spectral changes caused by the rapid field changes in a coniferous stand. Because the field changes occur at different times in the life of a stand, information about the general spectral behavior of stands was obtained. Furthermore, information about the opportunities to spectrally separate field change types was obtained.

An empirical model of the reflectance of a pine stand was constructed using class statistics. It was compared to the computational model (Fig. 46). The biggest difference between the models was in soil preparation, which showed much smaller spectral change in the empirical data than in the computational model.

The actual order of the separability of the change types was partially different in the empirical data from the computational reflectance data. Soil preparation could not be separated as well as the computational reflectances indicated. Damage could be separated better.

The poorer separability of soil preparation was partly due to the heterogeneity of the plowed areas, which increased the deviations of intensities. The damaged areas were separated better than assumed because they were spectrally homogeneous.

Predetermined changes were investigated. This made it possible to detect smaller spectral changes than could be done if satellite image interpretation were applied to update a general forest inventory.

The empirical studies supported the theory, presented in Section 2.2.2, that a slight decrease in the biomass will decrease the near infrared reflectance and a large decrease will increase the reflectance. The reflectance decrease is caused by changes in the spectral characteristics of the needles and by increased roughness of the surface. The reflectance increase occurs when the absorbing plant mass drops under a critical limit and the reflectance from the ground starts to control the total reflectance.

The correlation between the biomass and the near infrared radiation is negative in coniferous forests because their biomass is so much larger than the biomass of grasslands, where the correlation is positive.

A general conclusion of the feature testing was that an arithmetic image operation should not be done automatically, as is often the case in many remote sensing applications. Also, the same feature set seemed to be suitable for all classes. Consequently, all classes can be interpreted simultaneously.

Spectral changes by thinning cuttings, soil preparation and deciduous shrub removal were close to the radiometric resolution limit of the Landsat TM and Spot satellite images. It is likely that better sensitivity of the sensors could make the separation of those changes easier.

The use of existing ground truth made it possible to study all the most important rapid changes. The drawback of the existing data was their general nature.

PART II

On the practical use of satellite image aided change detection

Satellite image aided change detection can be used to: update forest map systems, help normal treatment planning, update sampling inventory results, and give information for ecological investigations.

The value of the interpretation is that field work is only checking instead of total inventory and that the whole area need not

be checked (Fig. 48). If the final requirement of a forest inventory operation is a map that is completely error-free, satellite image interpretation of changes is not useful. Total field inventory is required.

In sampling inventory, the interpretation results must be calibrated using field measurements (Fig. 49).

Maximum likelihood classification, either with original or difference channels, is the best of the commonly available methods to detect rapid small-area changes, according to the results of this study. Unsupervised methods should be applied in cases where the objective is to make a general change inventory, and where one is interested in changes over larger areas in which information on the changes is limited.

The reflectance model of this study and other knowledge about changes in forest could be applied to create a fully automated forest change detection system (Fig. 50). The system could be carried out using an expert system approach.

References

Ahern, F. J. 1988. Remote sensing of spruce budworm damage. Proc. Seminar on Remote Sensing of Forest Decline Attributed to Air Pollution, March 11—12, 1978, IIASA, Laxenburg, Austria. Palo Alto, Calif., Electric Power Research Institute. EA-5715. p. 17-1—17-2.

Ajai, Kamat, D. S., Khatuverdi, G. S., Singh, A. K. & Sinha, S. K. 1983. Spectral assessment of leaf area index, chlorophyll content, and biomass of chickpea. Photogrammetric Engineering and Remote Sensing 49(12): 1721—1727.

Alajärvi, P. 1987. Color infrared photographs in inventory of damages. Proc. Remote Sensing-Aided Forest Inventory. Hyytiälä, Finland, Dec. 10—12, 1986. University of Helsinki, Department of Forest Mensuration and Management, Research Notes 19. p. 191—197.

— 1991. Väri-infrakuvat ja Landsat TM-satelliittikuvat männynversosyöpätuhon arvioinnissa. Color infrared photographs and Landsat TM images in estimating of *Gremmeniella* damage to Scots pine. In Finnish. Helsinki, University of Helsinki, Department of Forest Mensuration and Management. Thesis for the Master of Science in Forestry Degree. 72 p.

Assman, E. 1970. The principles of forest yield study. Studies in the organic production, structure increment and yield of forest stands [Translation of Waldertragskunde 1961]. Oxford et al. XIV. 506 p.

Badhwar, G. D. & Henderson, K. E. 1982. A comparative study of the Thematic Mapper and Landsat spectral bands from field measurement data. Proc. Eighth International Symposium on Machine Processing of Remotely Sensed Data with Special Emphasis on Crop Inventory and Monitoring, July 7—9, 1982. West Lafayette, Indiana 47907, Purdue University, Laboratory for Applications of Remote Sensing. p. 266—272.

Barklund, P., Axelsson, G. & Unestam, T. 1984. Gremmeniella abietina in Norway Spruce, latent infection, sudden outbreaks, acid rain, predisposition. In: Manion, P. D. (ed.). 1984. Scleroderris canker of conifers. Martinus Nijhoff/Dr. W. Junk Publishers. p. 111—113.

Bernstein, R. 1976. Digital image processing of earth observation sensor data. IBM J. Res. Develop. 20(1): 40—57.

Boehnel, H.-J. 1976. Spectral field measurements of agricultural and forest crops. Proc.of the XIV IUFRO World Congress, Oslo, June 6—July 7, 1976. IUFRO. p. 110—119.

Bragg, R. J. & Manion, P. D. 1984. Evaluation of possible effects of acid rain on Scleroderris canker of red pine in New York. In: Manion, P. D. (ed.). 1984. Scleroderris canker of conifers. Martinus Nijhoff/Dr. W. Junk Publishers. p. 130—141.

Brockhaus, J., Campbell, M., Bruck, R. & Khorram, S. 1989. Analysis of forest decline in the Southern Appalachians with TM data. Proc. ASPRS/ACSM 1989 Annual Convention Agenda for the 90's, April 2—7, 1989/Baltimore. Falls Church, Virginia, American Society for Photogrammetry and Remote Sensing and American Congress on Surveying and Mapping. Volume 1. p. 227—236.

Burk, T. E., Bauer, M. E., Ek, A. R. & Ahearn, S. C. 1988. Satellite inventory of Minnesota's forest resources. In: Satellite imageries for forest inventory and monitoring; experiences, methods, perspectives. Proc. IUFRO Subject Group 4.02.05 Meeting in Finland, Aug. 29—Sept. 2. 1988. University of Helsinki, Department of Forest Mensuration and Management. Research Notes 21. p. 43—52.

Burns, G. S. 1985. Comparative evaluation of digital change detection methods in forestland and rangeland environments using Landsat multispectral data. In: Pecora 10, Remote Sensing in Forest and Range Resource Management. Proc. 10th William T. Pecora Symposium, August 20—22, Fort Collins, Colorado. Falls Church, Virginia, American Society for Photogrammetry and Remote Sensing. p. 200—207.

Buschmann, C., Kocsanyi, L. Nagel, E., Rang, S. & Stober, F. 1989. Reflexionsspektren von Blättern und Nadeln als Basis für die physiologische Beurteilung von Baumschäden — 2. Grundlegende Messungen. Presented in: 5. Statuskolloquium des Projektes Europäisches Forschungszentrum für Massnahmen zur Luftreinhaltung (PEF), March 7—9, 1989. Kernforschungszentrum, Karlsruhe, Germany. 11 p.

Cajander, A. K. 1913. Ueber Waldtypen. Acta Forestalia Fennica 1(1). 175 p.

Campbell, J.B. 1987. Introduction to remote sensing. New York, The Guilford Press. 551 p.

The catalogue of Spot products and services 1989. Toulouse-Cedex. Spot Image. 54 p.

Cinevan, M. E. 1979. Testing land use map accuracy: Another look. Photogrammetric Engineering and Remote Sensing 45(11): 1507—1512.

Colwell, R. N. 1970. Applications of remote sensing in agriculture and forestry. In: Remote sensing with special reference to agriculture and forestry. Washington D. C., National Academy of Sciences. p. 164—223.

Colwell, J. E. 1974. Vegetation canopy reflectance. Remote Sensing of Environment 3(3): 175—183.

Courtois, M. 1988. Le programme Spot. Proc. Spot 1, Image utilization, Assessment, Results, Paris, November 1987. Toulouse, Cepadues-Editions. p. 1473—1479.

Cunia, T. 1978. On the objectives and methodology of national forest inventory systems. Proc. Joint Meeting of the IUFRO Groups S4.02 and S4.04, Bucarest. IUFRO.

Denissoff, G. 1981. Ohjatun luokituksen menetelmat ja tietokoneohjelmat. Methods and computer programs for supervised classification. Technical Research Centre of Finland, Research Notes 48/1981. 41 p.

DISIMP 1987. Device-Independent Software for Image Processing. Version 4.0. Utilities Reference Manual. Canberra. Canberra ACT 2601, CSIRO Division of Information Technology, Centre for Spatial Information Systems.

Dottavio, C. L. & Dottavio, F. D. 1984. Potential benefits of new satellite sensors to wetland mapping. Photogrammetric Engineering and Remote Sensing 50(5): 599—606.

Duggin, M. J., Sakhavat, H. & Lindsay, J. 1985. The systematic and random variation of recorded radiance in a Landsat Thematic Mapper image. International Journal of Remote Sensing 6(7): 1257—1261.

Eyton, J. R. 1983. Landsat multitemporal color composites. Photogrammetric Engineering and Remote Sensing 49(2): 231—235.

Frank, T. D. 1984. Assessing change in the surficial character of a semiarid environment with Landsat residual images. Photogrammetric Engineering and Remote Sensing 50(4): 471—480.

Franssila, E., Hakala, J., Lahtinen, R., Paavilainen, J. & Peltola, J. 1982. Pienikaavainen maastokartoitus digitaalisesti parannetuista Landsat-kuvista. Abstract: The usability of digitally enhanced Landsat-imagery in small-scale terrain mapping. Valtion teknillinen tutkimuskeskus, Tiedotteita — Technical Research Centre of Finland, Research Notes 128. 38 p. + app. 11 p.

Gates, D. M. 1970. Physical and physiological properties of plants. In: Remote sensing with special reference to agriculture and forestry. Washington D. C., National Academy of Sciences. p. 224—252.

Genderen, J. L. & Lock, B. F. 1977. Testing land-use map accuracy. Photogrammetric Engineering and Remote Sensing 43(9): 1135—1137.

Geological map of Finland 1982. Quaternary deposits. Scale 1:100,000. No. 2142 Orivesi. Helsinki, Geological Survey of Finland.

Gibbs, J. N. 1984. Brunchorstia dieback in Europe. In: Manion, P. D. (ed.) 1984. Scleroderris canker of conifers. Martinus Nijhoff/Dr. W. Junk Publishers. p. 32—41.

Goldberg, M., Schlaps, D., Alvo, M. & Karam, G. 1982. Monitoring and change detection with Landsat imagery. Proc. 6th International Conference on Pattern Recognition, Munich, Germany, Oct. 19—22, 1982. IEEE Computer Society. p. 523—526.

Guyot, G. & Riom, J. 1988. Review of factors affecting remote sensing of forest canopies. Proc. Seminar on Remote Sensing of Forest Decline Attributed to Air Pollution, March 11—12, 1978, IIASA, Laxenburg, Austria. Palo Alto, California, Electric Power Research Institute EA-5715. p. 8-1—8-26.

Haavisto, M. (ed.) 1983. Maaperäkartan käyttöopas 1 : 20000, 1 : 50000 Summary: Basic mapping of quaternary deposits in Finland. Espoo, Geological Survey of Finland, Guide 10. 80 p.

Hall, R. J., Still, G. N. & Crown, P. H. 1983. Mapping the distribution of aspen defoliation using Landsat color composites. Canadian Journal of Remote Sensing 9(2): 86—91.

Hall, F. G., Strebel, D. E. & Sellers, P. J. 1988. Linking knowledge among spatial and temporal scales: Vegetation, atmosphere, climate and remote sensing. Landscape Ecology 2(1): 3—22.

Hay, A. M. 1979. Sampling designs to test land-use map accuracy. Photogrammetric Engineering and Remote Sensing 45(4): 529—533.

Hirvonen, R. A. 1971. Adjustment by least squares in geodesy and photogrammetry. Frederick Ungar Publishing Co., New York. 261 p.

Hopkins, P. F. & Abrahamsson, L. P. 1984. Scleroderris canker survey using aerial photography. In: Manion, P. D. (ed.). 1984. Scleroderris canker of conifers. Martinus Nijhoff/Dr. W. Junk Publishers. p. 226—235.

Hopkins, P. F., MacLean, A. L. & Lillesand, T. M. 1988. Assessment of Thematic Mapper imagery for forestry applications under Lake States conditions. Photogrammetric Engineering and Remote Sensing 54(1): 61—68.

Horler, D. N. H. & Ahern, F. J. 1986. Forestry information content of Thematic Mapper data. International Journal of Remote Sensing 7(3): 405—428.

Hyytiälän ympäristössä vuonna 1984 mitattujen pysyvien koealojen uudelleenmittaus kesällä 1987. Remeasurement of the 1984 grounded permanent sample plots "Hyytiälä" in summer 1987. In Finnish. Finnish Forest Research Institute, Department of Forest Inventory and Yield. 11 p. Stencil.

Häme, T. 1984a. Landsat-aided forest site type mapping 1984. Photogrammetric Engineering and Remote Sensing 50(8): 1175—1183.

— 1984b. Interpretation of deciduous trees and shrubs in conifer seedling stands from Landsat imagery. The Photogrammetric Journal of Finland 9(2): 209—217.

— 1987. Satellite image aided change detection. In: Remote sensing-aided forest inventory. Proc. Remote Sensing-Aided Forest Inventory. Seminars organized by SNS (Samarbetsnämden för Nordisk Skogsforskning) and Taksaattoriklubi (Forest Mensurationist Club), Hyytiälä, Finland, Dec. 10—12, 1986. University of Helsinki, Department of Forest Mensuration and Management, Research Notes 19. p. 47—60.

— 1988a. Interpretation of forest changes from satellite scanner imagery. In: Satellite imageries for forest inventory and monitoring; experiences, methods, perspectives. Proc. IUFRO Subject Group 4.02.05 Meeting in Finland, Aug. 29—Sept. 2. 1988. University of Helsinki, Department of Forest

Mensuration and Management, Research Notes 21. p. 119—133.
— 1988b. Landsat-aided detection of *Gremmeniella* damage to Scots pine. Proc. Seminar on Remote Sensing of Forest Decline Attributed to Air Pollution, March 11—12, 1978, IIASA, Laxenburg, Austria. Palo Alto, California, Electric Power Research Institute. EA-5715. p. 9-1—9-10.
— Tomppo, E. & Parmes, E. 1988. Stand-based forest inventory from Spot image. Proc. Spot 1, Image utilization, Assessment, Results, Paris, November 1987. Toulouse, Cepadues-Editions. p. 971—977.
— & Rantasuo M. 1988. Shuttered camera — Aerial color video imaging in the visible and near infrared. Photogrammetric Engineering and Remote Sensing 54(12): 1735—1738.
Joyce, A. T., Ivey, J. H. & Burns, G. 1980. The use of Landsat MSS data for detecting land use changes in forestland. Proc. Fourteenth International Symposium on Remote Sensing of Environment, San Jose, Costa Rica 23—30. Ann Arbor, Michigan, Environmental Research Institute of Michigan. Volume II. p. 979—988.
Kadro, A. & Hildebrant, G. 1980. Beobachtungen ueber das spektrale Reflexionsverhalten von Kiefern- und Fichtenbeständen. Proc. International Society for Photogrammetry, 14th Congress, Hamburg 13—25 July 1980. Hamburg, International Archives of Photogrammetry 23(B7), Commission VII. Committee of the XIV International Congress for Photogrammetry. p. 487—496.
Kalensky, R. & Wilson, D. A. 1975. Spectral signatures of forest trees. Proc. Third Canadian Symposium on Remote Sensing. Edmonton, Alberta. September 22—24. 18 p. Reprint.
Kalliola, R. 1973. Suomen kasvimaantiede. Werner Söderström Osakeyhtiö. 308 p.
Kauth, R. J. & Thomas, G. S. 1976. The tasselled cap — A graphic description of the spectral-temporal development of agricultural crops as seen by Landsat. Proc. Machine Processing of Remotely Sensed Data, West Lafayette, Indiana, June 29—July 1, 1976. West Lafayette Indiana, Purdue University, p. 4B-41—4B-51.
Kellomäki, S., Hari, P., Kanninen, M. & Ilonen P. 1980. Eco-physiological studies on young Scots pine stands: II. Distribution of needle biomass and its application in approximating light conditions inside the canopy. Silva Fennica 14(3): 243—257.
Kieffer, H. H., Cook, D. A., Eliason, E. M. & Eliason, P. T. 1985. Intraband radiometric performance of the Landsat Thematic mappers. Photogrammetric Engineering and Remote Sensing 51(9): 1331—1336.
Kilkki, P. 1988. Satelliittikuvat valtakunnan metsien inventoinnissa. In: Häme, T., Ihalainen, A. & Kanninen, M. (ed.) 1988. Kaukokartoitus metsätaloudessa. Seminaariesitelmät 7.6. 1988. Helsinki, Metsäntutkimuslaitoksen tiedonantoja 316. p. 17—20.
Kilpelä, E., Jaakkola, S., Kuittinen, R. & Talvitie, J. 1978. Automated earth resources surveys using satellite and aircraft scanner data. Helsinki, Technical Research Centre of Finland, Building Technology and Community Development. Publication No. 15. 174 s.
Kimes, D. S., Markham, B. L. & Tucker, C. J. 1980. Temporal relationships between spectral response and agronomic variables of a corn canopy. Remote Sensing of Environment 11(5): 401—411.
Kleman, J. 1986. The spectral reflectance of stands of Norway spruce and Scots pine, measured from a helicopter. Remote Sensing of Environment 20(3): 253—265.
Koch, B., Ammer, T., Schneider, T. & Wittmeier, H. 1990. Spectroradiometer measurements in the laboratory and in the field to analyse the influence of different damage symptoms on the reflection spectra of forest trees. International Journal of Remote Sensing 11(7): 1145—1163.
Kriebel, K. T. 1978. Measured spectral bidirectional reflection properties of four vegetated surfaces. Applied Optics 17(2): 253—259.
Kuittinen, R. 1988. Determination of areal snow water equivalent using satellite images and gamma ray spectrometry. Acta Polytechnica Scandinavica. Ci 91. 139 p.
Kurkela, T. 1984a. The growth of trees affected by *Gremmeniella abietina*. In: Manion, P. D. (ed.). Scleroderris canker of conifers. Martinus Nijhoff/Dr. W. Junk Publishers. p. 177—180.
— 1984b. Factors affecting the development of disease epidemics by *Gremmeniella abietina*. In: Manion, P. D. (ed.) Scleroderris canker of conifers. Martinus Nijhoff/Dr. W. Junk Publishers. p. 148—152.
Kuusela, K. & Poso, S. 1970. Satellite pictures in the estimation of the growing stock over extensive areas. The Photogrammetric Journal of Finland 4(1): 3—9.
Landsat 4 data users handbook 1984. U.S. Geological Survey, National Oceanic and Atmospheric Administration. US Geol. Survey, 604 South Pickett Street, Alexandria, VA 22304.
Lehto, E. 1981. Satelliittikuvien soveltuvuus maankäytön muutosten seurantaan seutukaavatasolla Abstract: The usability of satellite data in change detection for land use at the regional planning level. Espoo, Technical Research Centre of Finland, Research Reports 25/1981. 49 p.
Lillesand, T. M. & Kiefer, 1987. Remote Sensing and image interpretation. 2nd ed. John Wiley & Sons. 721 p.
Lozano-Garcia, D. F. & Hoffer, R. M. 1985. Evaluation of a layered approach for classifying multitemporal Landsat MSS data. In: Pecora 10, Remote Sensing in Forest and Range Resource Management. Proc. 10th William T. Pecora Symposium, August 20—22, Fort Collins, Colorado. Falls Church, Virginia, American Society for Photogrammetry and Remote Sensing. p. 189—199.
MacFarlane, M. & Robinson, I. S. 1984. Atmospheric correction of Landsat MSS data for a multidate suspended sediment algorithm. International Journal of Remote Sensing 5(3): 561—576.
Malila, W. A. 1980. Change vector analysis: An approach for detecting forest changes with Landsat. Proc. 6th Annual Symposium on Machine Processing of Remotely Sensed Data, Purdue University, Indiana 1980. IEEE. p. 326—335.
Manual of Remote Sensing. Second Edition 1983. Falls Church, Virginia. Vol. 1. American Society of Photogrammetry. 1232 p.
Mälkönen, E. 1974. Annual primary production and nutrient cycle in some Scots pine stands. Communicationes Instituti Forestalis Fenniae 84(5). 78 p.
Nagao & Matsuyama 1979. Edge preserving smoothing. CGIP 9(4): 394—407.
Narendra, P. M. & Goldberg, M. 1977. A non-parametric clustering scheme for Landsat. Pattern Recognition 9: 207—215.
Narendra, P. M. & Goldberg, M. 1980. Image segmentation with directed trees. IEEE Transactions on Pattern Analysis and Machine Intelligence, Vol. PAM-2, No. 2, p. 185—191.
Nelson, R. F. 1983. Detecting forest canopy change due to insect activity using Landsat MSS. Photogrammetric Engineering and Remote Sensing 49(9): 1303—1314.
Nilson, T. & Kuusk, A. 1989. A reflectance model for the homogeneous plant canopy. Remote Sensing of Environment 27(2): 157—167.
O'Brien, J. T. 1984. Historical and current Scleroderris situations in the United States. In: Manion, P. D. (ed.) Scleroderris canker of conifers. Martinus Nijhoff/Dr. W. Junk Publishers. p. 26—31.
Oke, T.R. 1987. Boundary layer climates. Methuen: London and New York. 435 p.
Olsson, H. 1989. Relative calibrated Landsat-TM data for standwise change detection in forestry — A pilot study on Scots pine infected by *Gremmeniella abietina*. Proc. 9th EARSeL Symposium, Espoo, Finland, 27 June—1 July 1989. Commission of the European Communities, EUR 12827 EN. p. 299—305.
— 1990. Spectral response from thinning cuttings measured by multitemporal satellite data. Proc. ISPRS Commission VII Mid-Term Symposium, Victoria, Canada, Sept. 17—21, 1990. International Society of Photogrammetry and Remote Sensing. 6 p. In press.
— 1991. Jämförelse av regressionsfunktioner för relativ calibrering av Landsat TM data över skog Abstract: Comparison of regression functions for multitemporal image normalization of Landsat TM data over forest. Umeå. Remote Sensing Laboratory, Swedish University of Agricultural Sciences, Report 6. 38 p. ISSN 1100—777X.
Parmes, E. & Kuittinen, R. 1988. Image segmentation in unsupervised and supervised land cover classification from satellite images. Proc. 16th Congress of the International Society for Photogrammetry and Remote Sensing, Kyoto, July, 1988. International Archives of Photogrammetry and Remote Sensing, Vol. 27, Part B10. p. III-237—III-243.
Peng Shikui. 1987. On the combination of multitemporal satellite and field data for forest inventories. Acta Forestalia Fennica 200. 95 p.
Peterson, U. 1989. Seasonal reflectance profiles for forest clearcut communities at early stages of secondary succession. Tartu, Academy of Sciences of the Estonian SSR, Preprint A-5 (1989). 70 p.
Poso, S., Häme, T. & Paananen, R. 1984. A method of estimating the stand characteristics of a forest compartment using satellite imagery. Silva Fennica 18(3): 261—292.
— Paananen, R. & Similä, M. 1987. Forest inventory by compartments using satellite imagery. Silva Fennica 21(1): 69—94.
— 1988. Seeking for an optimal path for using satellite imageries for forest inventory and monitoring. In: Satellite imageries for forest inventory and monitoring; experiences, methods, perspectives. Proc. IUFRO Subject Group 4.02.05 Meeting in Finland, Aug. 29—Sept. 2. 1988. Helsinki. University of Helsinki, Department of Forest Mensuration and Management, Research Notes 21. p. 181—203.
Päivinen, R. & Rautiainen, S. 1990. Spectral reflectance of forest stands. Paper presented at the SNS/IUFRO Remote Sensing and Forest Inventory Workshop, 26—28 February, Umeå, Sweden. 6 p.
Ranson, K. J., Daughtry, C. S. T. & Biehl, L. L. 1986. Sun angle, view angle, and background effects on spectral response of simulated balsam fir canopies. Photogrammetric Engineering and Remote Sensing 52(5): 649—658.
Rauste, Y. 1983. Korkeustiedon kayttö keilainaineiston numeerisessa luokituksessa Abstract: The use of height information in numeric classification of scanner data. Thesis for M. Sc. degree. Helsinki University of Technology, Department of Surveying. 80 p.
Richards, J. A. 1980. Thematic mapping from multitemporal image data using the principal components transformation. Remote Sensing of Environment 16(1): 35—46.
Ritari, A. 1987. Lumipeitteen sulamisen riippuvuus eräista metsikkö- ja kasvupaikkatunnuksista Kivalon tutkimusalueella Summary: Ablation of late snow-cover in relation to some stand and site characteristics in Kivalo, Northern Finland. Folia Forestalia 691. 16 p.
— & Saukkola, P. 1985. Spectral reflectance as an indicator of ground vegetation and soil properties in Northern Finland. Communicationes Instituti Forestalis Fenniae 132. 37 p.
Robinson, V. B., Coiner, J. C. & Barringer, T. H. 1982. Dynamic modeling of vegetation change in arid lands. Proc. First Thematic Conference, International Symposium on Remote Sensing of Environment, Cairo, Egypt, 19—25 January 1982. Ann Arbor, Michigan, Environmental Research Institute. p. 121—131.
Rosengren, M. & Ekstrand, S. 1988. A method aiming at monitoring of large-area forest decline using satellite imagery. Proc. Seminar on Remote Sensing of Forest Decline Attributed to Air Pollution, March 11—12, 1978, IIASA, Laxenburg, Austria. Palo Alto, California, Electric Power Research Institute. EA-5715. p. 2-1—2-20.
Rouge, B. 1987. Outil d'Analyse d'Image Multispectrale a Partir de Classification Automatique (Methode de Partition de l'Histogramme Multispectral). Summary: Analysis of Spot multispectral images by a new automatic clustering. Proc. MARI 87, Machines, Reseaux Intelligents/Intelligent Networks and Machines. Paris, La Villette, 18—22 May 1987. 2 p.
Sader, S. A. Remote sensing investigations of forest biomass and change detection in tropical regions. Proc. IUFRO Subject Group 4.02.05 Meeting in Finland, Aug. 29. -Sept. 2, 1988. University of Helsinki, Department of Forest Mensuration and Management, Research Notes No. 21. p. 31—42.
SAS Institute Inc. 1985. SAS User's Guide: Basics, Version 5 Edition. Cary, North Carolina, SAS Institute Inc. 1290 p.
SAS Institute Inc. 1988. SAS/STAT User's Guide, Release 6.03 Edition. Cary, North Carolina, SAS Institute Inc. 1028 p.
Saukkola, P. 1977. Metsikön spektrinen heijastussäteily eräitten metsikkötunnusten ilmentäjänä. Relationships between some stand characteristics and reflected radiation. In Finnish. University of Helsinki, Department of Forest Mensuration and Management. Thesis for the Master of Science in Forestry Degree. 88 p.
— 1982. Uudistushakkuiden seuranta satelliittikuvista. Abstract: Monitoring regeneration fellings by satellite imagery. Technical Research Centre of Finland, Research Reports 89. 108 p.
— 1983. Ominaisspektrin mittaaminen kuvatulkinnan perusselvityksenä. Abstract: Spectral signature measurements in remote sensing. Technical Research

Centre of Finland, Research Notes 169. 31 p.
Saukkola, P. & Jaakkola, S. 1983. Numeerinen kuvatulkinta metsäalueen ja metsikön tunnusten arvioinnissa. Numerical image interpretation in forest inventory and mensuration. Valtion teknillinen tutkimuskeskus — Technical Research Centre of Finland, Tutkimuksia — Research Reports 151. 101 p. + app. 8 p.
Seal, H. L. 1964. Multivariate statistical analysis for biologists. John Wiley & Sons Inc. 207 p.
Singh, A. 1989. Digital change detection techniques using remotely-sensed data. International Journal of Remote Sensing 10(6): 989—1003.
Singh, A. & Harrison, A. 1985. Standardized principal components. International Journal of Remote Sensing 6(6): 883—896.
Sirén, G. 1955. The development of spruce forest on raw humus sites in Northern Finland and its ecology. Acta Forestalia Fennica 62(4). 408 p.
Sterner, T. E. 1984. Scleroderris canker, *Gremmeniella abietina* (Lagerb.) Morelet, in Canada — An overview. In: Manion, P. D. (ed.) Scleroderris canker of conifers. Martinus Nijhoff/Dr. W. Junk Publishers. p. 8—10.
Strahler, A. H. 1980. The use of prior probabilities in maximum likelihood classification of remotely sensed data. Remote Sensing of Environment 10: 135—163.
Swain, P. H. 1980. Image data analysis in remote sensing. In: Haralick, R. M. & Simon, J. C. (ed.). Issues in digital image processing. Sijthoff & Noordhoff. p. 313—339.
Tomppo, E. 1988. Standwise forest variate estimation by means of satellite images. In: Satellite imageries for forest inventory and monitoring; experiences, methods, perspectives. Proc. IUFRO Subject Group 4.02.05 Meeting in Finland, Aug. 29. -Sept. 2, 1988. University of Helsinki, Department of Forest Mensuration and Management, Research Notes 21. p. 103—111.
Tucker, C. J. 1979. Red and photographic infrared linear combinations for monitoring vegetation. Remote Sensing of Environment 8: 127—150.
— 1980. Remote sensing of leaf water continent in the near infrared Remote Sensing of Environment 10: 23—32.
— Miller, L. D. & Pearson, R. L. 1975. Shortgrass prairie spectral measurements. Photogrammetric Engineering and Remote Sensing 41(9): 1157—1162.
Uotila, A. 1988. Mitä uutta versosyövästä. Metsä ja Puu 10/1988. p. 14—15.
Valtakunnan metsien 8. inventointi. Kenttätyön ohjeet 1986. Helsinki, The Finnish Forest Research Institute, Department of Forest Inventory. Stencil. 86 p. + app.
Vogelman, J. & Rock, B. 1986. Assessing forest decline in coniferous forests of Vermont using NS-001 Thematic Mapper simulator data. International Journal of Remote Sensing 7(10): 1303—1321.
— Defeo, N. & Rock, B. 1989. Detection of forest change in the eastern United States using multitemporal remote sensing data sets. Proc. ASPRS/ACSM 1989 Annual Convention Agenda for the 90's, April 2—7, 1989/Baltimore. Falls Church, Virginia, American Society for Photogrammetry and Remote Sensing and American Congress on Surveying and Mapping. Volume 1. p. 217—226.
Wastenson, L., Boresjö, L. & Alm, G. 1981. Hyggeskartering från satellit. Svensk Lantmäteritidskrift 1981:3, p. 220—226.
Wastenson, L., Alm, G., Kleman, J. & Wastenson, B. 1988. Swedish experiences of forest damage inventory by remote sensing. Proc. Seminar on Remote Sensing of Forest Decline Attributed to Air Pollution, March 11—12, 1978, IIASA, Laxenburg, Austria. Palo Alto, California, Electric Power Research Institute. EA-5715. p. 16-1—16-31.
Wharton, S. W. 1983. A generalized histogram clustering scheme for multidimensional image data. Pattern recognition 16(2): 193—199.
Williams, D. L. 1988. The use of quantitative remote sensing techniques to assess forest decline damage in Vermont. Proc. Remote Sensing Applications for Acid Deposition session of the 1988 ACSM/ASPRS Convention, St. Louis, Missouri 1988. Las Vegas, Nevada, U.S. Environmental Protection Agency. p. 37—55.
— 1991. A comparison of spectral reflectance properties at the needle, branch, and canopy level for selected conifer species. Remote Sensing of Environment 35(2 & 3): 79—93.
Yokota, S. 1984. Pathogenity and host range of races of *Gremmeniella abietina* in Hokkaido. In: Manion, P. D. (ed.). Scleroderris canker of conifers. Martinus Nijhoff/Dr. W. Junk Publishers. p. 47—53.

Total of 129 references

Seloste

Metsän muutosten spektrinen tulkinta satelliittikeilainkuvien avulla

JOHDANTO

Kasvipeitteen suksessio on luonnon perustapahtuma, jossa metsän biomassa ja kasvilajien runsaussuhteet muuttuvat. Ihminen vaikuttaa suksessioon esimerkiksi tekemällä hakkuita ja metsänhoitotöitä. Ihmisen vaikutusta voidaan kutsua suksession häiriöiksi. Myös eläimet, sienet ja eloton luonto häiritsevät normaalin suksession kulkua. Häiriötyyppisten muutosten aikajänne on lyhyt verrattuna suksession aiheuttamiin muutoksiin. Ilmaston ja maaperän muutoksien aikajänne on yleensä kaikkein pisin.

Metsätalous tarvitsee tietoa yleisistä kasvuolosuhteista, metsävaroista ja niiden muutoksista. Kasvipeitteen suksessiota ja siihen liittyvää runkopuun kasvua kyetään ennustamaan laskennallisesti. Tiedon saaminen äkillisistä muutoksista vaatii erillisiä havaintoja.

Metsätalouden suunnittelun tarpeet voidaan jakaa kahteen ryhmään: strategisen ja operatiivisen suunnittelun tarpeisiin. Strateginen suunnittelu vaatii ennen muuta luotettavia tilastotietoja laajoista metsäalueista. Operatiivista suunnittelua varten metsävaratiedot on paikannettava maastoon. Tiedot muutoksista on näihin asti kerätty vertaamalla perättäisten inventointien tietoja toisiinsa. Viime aikoina on operatiivisessa suunnittelussa otettu käyttöön numeerisia karttajärjestelmiä, joissa on aiempaa helpompi päivittää tietoja.

Kenttähenkilökunnan raportointiin perustuva päivitysjärjestelmä tarvinnee tuekseen kontrollijärjestelmän. Kontrollijärjestelmän avulla kyetään havaitsemaan ja korjaamaan tavanomaisen järjestelmän puutteita sekä rekisteröimään häiriöitä, jotka eivät suoranaisesti riipu ihmisen toimista, esimerkiksi tuhoja.

Satelliittikeilainkuvat ovat yksi mahdollinen tapa saada aineistoa metsävaratietojen päivittämiseksi, koska kuvien intensiteettiarvojen ja metsää kuvaavien tunnusten välillä on havaittu olevan riippuvuus. Luonnonvarasatelliittien kuvia on ollut saatavissa vuodesta 1972 lähtien.

Tutkimuksen tavoite on saada selville metsässä esiintyvien nopeiden muutosten spektriset ominaisuudet sekä muutostyyppien spektrinen erottuvuus satelliittikeilainkuvien avulla. Tutkitaan kuutta nopeiden muutosten tyyppiä: 1) avohakkuut, 2) kasvatushakkuut, 3) maanmuokkaus uudistusaloilla 4) taimistonhoito, 5) männynversosyöpä (versosurma, *Gremmeniella abietina* Lagerb.) ja 6) uudistusalojen vesottuminen.

Neulasten spektrisiä ominaisuuksia mitataan lisäksi spektroradiometrillä. Mittauksilla tuetaan satelliittikuvien tulkintaa. Tutkimuksen Osa I keskittyy saavuttamaan perustavoitteen. Osa II on lyhyt katsaus, kuinka satelliittikuviin pohjaava muutosten seurantajärjestelmä tulisi rakentaa.

Tutkimuksessa keskitytään spektrisiin ominaisuuksiin, koska ne ovat kaiken kaukokartoitukseen perustuvan muutosten seurannan lähtökohta. Muutosten spektriset ominaisuudet tunnetaan puutteellisesti.

OSA I

MUUTOSTEN SPEKTRISEN TULKINNAN TEOREETTINEN LÄHTÖKOHTA

Äkilliset muutokset havaitaan ja tunnistetaan sitä helpommin, mitä lähempänä toisiaan ennen muutosta ja sen jälkeen tehdyt havainnot ovat. Biomassan kasvu taas on helpompi todeta, jos havaintojen välinen aikajänne on pitkä.

Moniaikaisissa satelliittikuvissa havaittavat intensiteettien muutokset voivat johtua neljästä päätekijästä (kuva 2):

1) Heijastavien ja emittoivien elementtien keskinäiset suhteet,
2) Säteilylähteen, kasvuston ja ilmaisimen väliset kulmat
3) Ilmakehä
4) Signaalin tallennus ja käsittely

Ensimmäiseen ryhmään kuuluvat sekä tämän tutkimuksen kannalta kiinnostavat muutokset että esimerkiksi vuodenaikaisvaihtelu, joka aiheuttaa kaikkein suurimmat intensiteettimuutokset pohjoisissa havumetsissä.

Kirjallisuudesta saatua tietoa maastotyyppien heijastussäteilystä käytettiin kehitettäessä mallia, joka kuvaa männikön heijastussäteilyä kiertoaikana (kaava 2, taulukko 1, kuva 3a ja b).

Sekä punaisen valon että lähi-infrapunasäteilyn heijastussuhde laskee, kun metsikkö kehittyy aukeasta uudistuskypsäksi metsäksi ja kun kokonaisbiomassa lisääntyy. Heijastussuhteen lasku myös lähi-infrapunasäteilyn alueella osoittaa päinvastaista riippuvuutta kuin on havaittu ruoho- ja heinäkasvustoilla. Laskeva lähi-

infrapunasäteilyn heijastussuhde johtunee siitä, että varttunut puusto pystyy pidättämään sen osan tulosäteilystä, joka ei heijastu heti kasvuston yläosista.

Nopeat muutokset yleensä nostavat heijastussuhdetta, koska niissä biomassa laskee. Maastomuutosten vaikutus lähi-infrapunasäteilyyn oli kuitenkin epäselvä käytettävissä olleen tiedon perusteella.

Mallin mukaan tutkitut muutokset erottuvat seuraavassa järjestyksessä parhaimmasta erottuvuudesta huonoimpaan: 1) avohakkuut, 2) maanmuokkaus, 3) vesakon perkaus ja vesakoituminen, 4) harvennushakkuu ja versosyöpätuho.

Tulkintatekniikan valinta

Optimaalinen tulkintamenetelmä säilyttää kiinnostuksen kohteena olevien muutosten aiheuttamat intensiteettierot, mutta minimoi muiden intensiteettimuutosten vaikutukset tulkinnan tulokseen. Tulkinnan tulokseen vaikuttavat:

1) Kuvien tallennuksen ajankohta ja kuvauskulma
2) Kuvien esikäsittely
3) Spektriset piirteet
4) Maastoaineisto
5) Algoritmit

Valittu tulkintatekniikka selviää kaaviosta 1. Tulkintaan valittiin useita vaihtoehtoja, koska käytettävissä olevan tiedon perusteella ei pystytty suoraan valitsemaan parasta lähestymistapaa. Pääpaino oli erilaisten spektraalipiirteiden testauksessa tutkimuksen tavoitteen mukaan.

AINEISTO

Tutkimusalue, 40 km x 40 km, sijaitsi Pohjois-Hämeessä (keskipiste 61°51' N, 24°22' E, kuva 6, taulukko 2) ja käsitti metsähallituksen Korkeakosken hoitoalueen ympäristöineen. Tutkimusalue kuuluu Etelä-Suomen keskeisiin metsätalousalueisiin. Puuston keski-ikä metsämaalla oli 57,0 vuotta ja keskitilavuus 59,8 m^3/ha. Mänty oli valtapuuna 52,2 %:lla pinta-alasta ja kuusi 43,1 %:lla. Moreeni käsitti noin 90 % maa-alasta ja lajittuneet maalajit, lähinnä hiekka, noin 10 %. Peruskallio oli korkeintaan metrin syvyydessä suurimmassa osassa moreenialuetta. Korkeusvaihtelu ulottui 85 m:stä 190 m:iin merenpinnasta.

Tulkinnoissa käytettiin viittä satelliittikeilainkuvaa, joista kolme oli Landsat TM -kuvia (Thematic Mapper) ja kaksi Spot-kuvia (taulukko 3). Ensimmäinen TM-kuva, vuodelta 1984, oli taltioitu kasvipeitteen ollessa osittain syysväreissään. Viimeisessä TM kuvassa (1986) oli paikoin pilviä. Vuoden 1985 kuvan taltioinnin aikaan alueella riehui versosyöpäepidemia.

Kuvat oikaistiin yhtenäiskoordinaatistoon. Lineaarisen affiinisen muunnoksen tarvitsemat tukipisteet poimittiin peruskartoista ja satelliittikuvista. Oikaisuvaiheessa käytettiin lähimmän naapurin menetelmää. Kuvat, yhtä Spot-kuvaa lukuun ottamatta, oikaistiin toistensa päälle ennen kuin ne oikaistiin karttakoordinaatistoon. Kaksivaiheisella oikaisulla haluttiin saada kuvat niin hyvin päällekkäin kuin mahdollista.

Spot-kuvan intensiteettejä jouduttiin korjaamaan havaitun radiometrisen virheen vuoksi.

Maastoaineistoa oli kolmea tyyppiä (taulukko 4): 1) metsähallituksen metsiköt, 2) versosyöpätuhojen ilmakuvatulkintaa varten mitatut koealat, 3) kahdesti (1984 ja 1987) mitatut valtakunnan metsien inventoinnin koealat.

Metsähallituksen kenttähenkilökunta oli rajannut karttoihin metsiköt, joissa oli tehty hakkuu tai metsänhoitotoimenpide annettujen aikarajojen välillä sekä muutosmetsiköiden kanssa mahdollisimman samanlaiset vertailumetsiköt.

Versosyöpäaineistossa neulaskato oli mitattu yhdistetyistä ympyrä- ja relaskooppikoealoista puittain. Kato laskettiin kullekin koealalle pohjapinta-alalla painottaen.

Metsikköjen rajat digitoitiin ja niiden intensiteettiarvot poimittiin satelliittikuvista. Intensiteettiarvoista laskettiin metsiköittäiset keskiarvot. Versosyöpäkoealat paikannettiin satelliittikuviin visuaalisen tulkinnan avulla ja koealaa ja sen lähiympäristöä edustava alue rajattiin kuviin. Alueita vastaavat intensiteettiarvot poimittiin satelliittikuvasta ja niille laskettiin alueittaiset keskiarvot kuten metsikköaineistossa. Valtakunnan metsien inventoinnin koealaa vastaavan kuvanalkion ja lähimpien neljän kuvanalkion intensiteettiarvot poimittiin satelliittikuvasta. Jokaiselle koealalle laskettiin intensiteettiarvo poimitun viiden kuvanalkion intensiteettien keskiarvona.

Metsikköaineistoa ja valtakunnan metsien inventoinnin aineistoa jouduttiin karsimaan seuraavista syistä:

— pilvet
— ilmeinen virhe maastotiedoissa
— koeala liian lähellä kuvion rajaa
— hyvin harvinainen muutos

Metsikköaineisto sisälsi jokaista muutosluokkaa vastaavan vertailuluokan. Valtakunnan metsien inventoinnin aineistosta oli mahdollista erottaa kaksi vertailuluokkaa, yksi nuorille ja yksi vanhoille metsille. Versosyöpäaineistossa ei ollut täysin tervettä metsää edustavia koealoja lainkaan.

Saatua intensiteettiaineistoa analysoitiin tilastollisen ohjelmiston avulla. Analyysiin otettiin kaikki metsiköt ja koealat, paitsi karsitut, mutta luokituksia varten arvottiin luokitusmalliin otettavat ja testaukseen käytettävät metsiköt ja koealat.

Versosyöpätulkinnoissa käytettiin apuaineistona numeerista maaston korkeusmallia, josta laskettiin myös kaksi johdettua topografista muuttujaa, normalisoitu neliöllinen korkeusgradientin suuruus ja paikallinen korkeus.

Spektroradiometrimittausten avulla hankittiin versosyövän ja kasvatushakkuiden tulkintaa tukevaa tietoa. Tutkittiin neulasnäytteistä, miten versosyöpä muuttaa neulasten heijastusominaisuuksia näkyvän valon ja lähi-infrapunasäteilyn alueella. Mittauksen aallonpituusalue oli 400 — 1000 nm ja aallonpituuskaistan leveys 20 nm. Vastaavasti selvitettiin neulasmassan ja heijastussäteilyn välisiä suhteita.

Taimet olivat mittaushetkellä, toukokuussa 1986, kaksivuotiaita. Mittausnäytteisiin irrotettiin edellisen vuoden neulasia välittömästi ennen mittausta (kuva 9). Versosyöpämittauksia varten mitatut näytteet olivat kaikki noin kahden senttimetrin korkuisia kasoja, joissa neulaset olivat satunnaisessa järjestyksessä. Tuhomittauksissa oli neljä neulasluokkaa (taulukko 7).

Neulasmassamittauksia varten tuore neulasmassa aina kaksinkertaistettiin mittausten välillä. Näytteistä mitattu radianssi muutettiin heijastussuhteeksi eli reflektanssiksi käyttämällä radianssimittauksia $BaSO_4$-näytteestä, jonka heijastusominaisuudet tunnettiin. Heijastussuhde saatiin neulasnäytteen radianssin ja tulosäteilyksi muutetun $BaSO_4$-radianssin suhteena.

AINEISTON ANALYYSI

Analyyseissä käytetyt spektriset muunnokset (kaavio 2) olivat:

— Erotuskanavat
— Suhdekanavat
— Pääkomponentit
— Kanoniset muuttujat

Eriaikaisten kuvien intensiteettien histogrammit sovitettiin toisiinsa ennen joidenkin erotuskuvamuunnosten laskemista (kaava 13 ja kaava 14). Histogrammien sovituksella myös kalibroitiin kuvia samanlaisiksi testattaessa, voidaanko kuvaparia varten kehitetty luokitusmalli siirtää toiseen kuvaparii.

Luokkien keskiarvojen eroja tutkittiin Tukey'n testien ja diskriminanttimallien avulla. Vaihtelevilla spektristen piirteiden yhdistelmillä (kaavio 3) lasketut mallit testattiin syöteaineistollaan.

Lineaarisen regressioanalyysin avulla estimoitiin poistumaa harvennushakkuissa sekä versosyöpätuhon ankaruutta.

Muutosluokkien erottumista testattiin lopulta luokittamalla koko tutkimusalue ja testaamalla luokitukset (kaavio 4) aineistolla, joka oli jätetty ulkopuolelle estimoitaessa luokitusmallin parametreja. Luokituksissa käytettiin kahta ohjattua menetelmää, lähimmän keskiarvon menetelmää (euklidinen etäisyys) ja maximum likelihood -luokitusta sekä yhtä ohjaamatonta menetelmää, moniulotteisen histogrammin segmentointia.

Segmentointia sovellettiin myös alkuperäisiin kuviin. Segmentoinnin avulla kuva jaettiin keskimäärin vajaan puolen hehtaarin osiin, joita käytettiin suodatusikkunoina. Kuvanalkio kuvanalkiolta -luokituksen jälkeen laskettiin luokkien frekvenssit segmenteittäin ja segmentit täytettiin yleisimmällä luokalla eli moodiluokalla. Segmentointia ja suodatusta tarvittiin erityisesti luokitustulosten karttatulostukseen.

INTENSITEETTIARVOJEN ANALYYSIEN JA LUOKITUSTEN TULOKSET

Spektroradiometrimittaukset

Versosyöpä nosti neulasten heijastussuhdetta näkyvän valon, varsinkin punaisen valon, alueella (kuvat 10a, 10b, 11). Lähi-infrapunasäteilyn heijastussuhde laski versosyövän vuoksi. Lähi-infrapunasäteily ja sinivihreä valo olivat suunnilleen samanarvoisia vaurioituneiden ja terveiden neulasten erottamisessa ja selvästi heikompia kuin punainen valo. Heikoimpia aallonpituuksia olivat vihreä valo sekä lähi-infrapunasäteilyn pisimmät aallonpituudet, lähellä 1000 nm.

Biomassan logaritmi ja heijastussuhde olivat suoraan verrannollisia vihreän valon ja lähi-infrapunasäteilyn alueella. Lähi-infrapunasäteilyn heijastussuhde nousi erittäin jyrkästi biomassan kasvaessa.

Muutosten spektriset ominaisuudet

Kasvatushakkuiden poistumalla ja lähi-infrapunasäteilyllä oli heikko riippuvuus siten, että poistuman kasvaessa lähi-infrapunasäteilyn intensiteetit laskivat (taulukko 10, kuva 13). Punaisen valon intensiteetit saattoivat nousta poistuman kasvaessa. Poistuman määrää pystyttiin estimoimaan regressioanalyysin avulla, jos kasvatushakkuut on ensin erotettu muusta metsästä (kaava 26). Regressioanalyysi ei kyennyt erottamaan hakattuja alueita hakkaamattomista. Parhaat aallonpituuskanavat poistuman ennustamiseen olivat lähi-infrapunasäteilyn ja punaisen valon erotuskanavat laskettuina ilman histogrammien sovitusta.

Absoluuttinen korkeus oli ainoa topografinen muuttuja, jolla oli merkitsevä korrelaatio ($r = -0,48$) tuhoasteen kanssa (taulukko 11, kuva 15).

Tuhoaste ja spektrisistä muuttujista etenkin lähi-infrapunasäteily olivat riippuvuussuhteessa. Tuhoasteen pahetessa lähi-infrapunasäteilyn intensiteetit laskivat 30 prosentin tuhoasteeseen saakka. Tämän jälkeen riippuvuussuhde ei ollut selvä. Versosyöpätuhosta erotettiin

kaksi luokkaa luokituksia varten, koska riippuvuus heikkeni 30 prosentissa. Tuhoja 30 prosentin tuhoasteeseen saakka kutsuttiin lieviksi tuhoiksi ja korkeamman tuhoprosentin tuhoja vakaviksi tuhoiksi.

Todennäköisin syy riippuvuuden heikkenemiseen oli aluskasvillisuus, joka rehevöityy kasvuston harvennuttua riittävästi, ja heijastaa tehokkaasti lähi-infrapunasäteilyä.

Vuoden 1984 TM-kuvan intensiteettiarvoista voitiin havaita, että myös monet lievien tuhojen ryhmään kuuluneet koealat olivat vaurioituneet jo vuoden 1982 epidemian aikana. Erotuskuvissa suurimmat muutokset havaittiin kaikkein terveimmissä koealoissa. Vain näissä koealoissa tuho lienee alkanut vasta vuonna 1985. Puissa on ollut paljon neulasia tuhon alkaessa ja tuho on siten voinut aiheuttaa suuren muutoksen neulasmassassa (taulukot 12 ja 13, kuvat 16 — 20).

Spektrisiä muuttujia mallinnettiin metsikkömuuttujilla ja tuhon asteella. Mallinnuksen tavoitteena oli saada selville, kuinka suuri osa intensiteettien vaihtelusta kyetään selittämään maastomuuttujilla. Lisäksi haluttiin tietää, mikä on metsässä mitattujen muuttujien keskinäinen merkitys malleissa.

Tuhoastetta puolestaan mallinnettiin spektrisillä muuttujilla. Menetelmänä molemmissa mallinnuksissa oli regressioanalyysi. Mallit laskettiin 61 versosyöpäkoealalle.

Lähi-infrapunasäteilyä kyettiin mallintamaan parhaiten tuhoprosentin avulla. Muille aallonpituusalueille parhaat selittävät muuttujat olivat runkoluku ja puuston keskiläpimitta (taulukko 14). Myös regressioanalyysi vahvisti, että lievät tuhot olivat alkaneet jo 1982 (kaava 27).

Tukey'n testit (taulukot 15 — 17, liite 1) osoittivat, että yleensä alkuperäiset kanavat erottivat muutoksia paremmin kuin muunnetut piirteet. Erotuskanavat, jotka oli laskettu ilman histogrammien sovitusta, antoivat parempia tuloksia kuin erotuskanavat, jotka oli laskettu histogrammien sovituksen jälkeen. Tärkeimmät aallonpituusalueet olivat punainen valo ja lähi-infrapunasäteily. Punainen valo oli hyödyllinen miltei kaikkien muutostyyppien erottamisessa. Lähi-infrapunasäteily erotti varsinkin tuhoja, taimistonhoito- ja maanmuokkausluokkia. Erotuskanavat olivat parempia kuin samoista syötekanavista lasketut suhteet. Talvikuva ei auttanut muutosten erottamisessa.

Yleistulos Tukey'n testeistä oli, että ainoastaan avohakkuut voitiin selvästi erottaa muista luokista yhden spektrisen piirteen avulla.

Piirteiden testaus diskriminanttianalyysillä vahvisti Tukey'n testien tulokset. Parhaat tulokset saatiin pareittaisilla alkuperäisillä aallonpituuskanavilla (taulukot 18 ja 19). Landsat TM -kuvien Spot-kuvia paremmasta spektrisestä erotuskyvystä oli hyötyä.

Muutosten vaikutuksia intensiteetteihin tarkasteltiin myös kolmen vuoden ajanjaksona (kuva 21a ja b ja kuva 22a ja b). Kasvatushakkuu ja versosyöpätuho nostivat hieman punaisen valon intensiteettejä. Vuoden-puolentoista kuluttua hakkuusta seurasi päinvastainen muutos: intensiteettien lasku. Kahdessa tai kolmessa vuodessa hävisi lievän tuhon ja harvennushakkuun vaikutus heijastussäteilyyn. Intensiteettimuutokset olivat kuitenkin vähäisiä.

Avohakkuu nosti rajusti punaisen valon intensiteettejä. Intensiteetit laskivat hieman, kun hakkuusta oli kulunutrunsas vuosi. Maanmuokkauksen vuoksi ne nousivat uudelleen samalle tasolle kuin välittömästi hakkuun jälkeen.

Taimistonhoito aiheutti samantapaisen muutoksen kuin maanmuokkaus. Taimistonhoitoalueet erosivat maanmuokkauksista korkeampien lähi-infrapunasäteilyn intensiteettien vuoksi.

Kuva 23a, b ja c havainnollistaa, että eri luokkien maastohavaintojen intensiteettiarvot olivat usein limittäin.

Analogiset kuvat

Erotuskanavista tehdyt analogiset kuvat (kuva 24a, b ja c, kuva 25a ja b, sekä kuva 26a ja b) havainnollistavat, että eri vuosien kuvat eroavat yllättävän paljon toisistaan. Kuvasta 26 havaitaan, kuinka kasvipeitteen suksessio on edennyt uudistusaloilla avohakkuun jälkeen. Värikuviin erotuskanavat laskettiin osin eri lailla kuin testejä varten, jotta saatiin aikaan mahdollisimman värikäs lopputulos ja haluttu visuaalinen vaikutelma.

Luokitukset

Intensiteettien hajonnat nousivat muutosten vuoksi (taulukko 21).

Osaan luokituksista sovellettiin alempia ennakkotodennäköisyyksiä muutosluokille kuin muille luokille. Syynä oli, että muutosten pinta-ala oli pienempi kuin muiden luokkien pinta-ala ja että luokkien intensiteettijakaumat peittivät toisiaan. Ennakkotodennäköisyyksien valinnassa testattiin niiden laskemista luokkien olettettujen pinta-alojen mukaan (kaava 31). Menetelmä ei ottanut huomioon luokkien intensiteettien sekoittumista. Lopulta päädyttiin todennäköisyyksien valitsemiseen päättelyn sekä yrityksen ja erehdyksen avulla (kaava 32).

Luokitusten (kaavio 4) pinta-alajakaumat (kuvat 28 30) viittaavat muun muassa siihen, että versosyöpätuho ei juuri ollut jatkunut vuoden 1985 epidemian jälkeen. Kun muutosluokille annettiin alemmat ennakkotodennäköisyydet kuin muille luokille, niiden pinta-ala oli noin 70 prosenttia siitä, mitä muutosluokkien pinta-ala oli yhtä suuria ennakkotodennäköisyyksiä soveltaneissa luokituksissa. Kuvasegmenteittäin tehty moodisuodatus

alensi muutosluokkien pinta-alan noin puoleen suodattamattomiin kuviin verrattuna (kuva 31). Kuvien segmentointi oli löytänyt tasakoosteiset alueet hyvin, sillä segmentit, joissa moodiluokan pinta-ala oli vähintään 50 prosenttia, käsittivät 96,3 prosenttia koko kuva-alasta.

Luokkakohtainen tarkkuus oli kaikissa luokituksissa melko alhainen (kuvat 33 ja 34). Paljon paremmin erottuivat muutosta edustaneet luokat yhtenä ryhmänä muuttumatonta metsää edustaneista luokista. Tarkkuuden arvioinnissa on otettava huomioon, että luokkien osuudet testiaineistoissa eivät vastanneet luokkien osuuksia todellisuudessa.

Parhaat tulokset saatiin maximum likelihood -luokituksella, jossa oli käytetty alkuperäisiä kanavia ja jossa muutosluokkien ennakkotodennäköisyydet olivat pienemmät kuin muiden luokkien. Myös erotuskanavaluokitusten antamat tulokset antoivat kohtuullisen hyviä tuloksia. Tekstuurikanava ei parantanut tuloksia. Kolmen ajankohdan aineiston käytöstä näytti olevan hyötyä. Luokitusmenetelmien arvottaminen tulkinnan tavoitteesta ja inventointiin käytettävissä olevista varoista.

Muutosten erottuvuusjärjestys empiirisessä aineistossa oli: 1) avohakkuut, 2) versosyöpä, 3) maanmuokkaus, 4) harvennushakkuu, vesakon perkaus ja vesakoituminen. Maanmuokkaus siis erottui heikommin kuin malli antoi olettaa tuhot erottuivat paljon paremmin. Tuhoalueiden hyvä erottuvuus johtui niiden intensiteettien pienistä hajonnoista. Harvennushakkuiden luokat eivät edustaneet harvennushakkuita vaan hakkuut luokittuivat usein spektrisesti samankaltaisiin, mutta pienempihajontaisiin tuholuokkiin (taulukot 23 — 26). Tuhoja (ja harvennushakkuita) edustaneet luokat erottuivat todennäköisesti paremmin kuin testimatriisit osoittavat, sillä osassa harvennushakkuiden referenssiluokan koealoista oli versosyöpää.

Luokitukset, joissa kuvien taltioinnin väli oli kolme vuotta, antoivat hyvin huonoja tuloksia. Luokitusmallien opetusaineistona käytetty valtakunnan metsien inventoinnin koeala-aineisto oli liian pieni ja kasvipeitteen suksessio oli osin ehtinyt hävittää äkillisten muutosten jäljet. Myöskin luokitusmallin siirto kuvaparista toiseen antoi huonoja luokitustuloksia. Kuvien kalibrointimenetelmä oli ilmeisesti liian karkea ja vuodenaikaismuutokset haittasivat kalibrointia.

Käytetyllä ohjaamattoman luokituksen menetelmällä aineistosta löytyi yli tuhat luokkaa. Varsinkin alueet, jotka edustivat vain osittain sulkeutunutta puustoa, olivat pirstoutuneet usein kymmeniin ohjaamattoman tulkinnan luokkiin. Edes avohakkuut eivät erottuneet. Klusteroinnilla sen sijaan näytti löytyvän uusia versosyöpäalueita. Nämä alueet eivät olleet tulleet esille ohjatuissa tulkinnoissa, koska ohjattujen tulkintojen opetusaineisto oli keskittynyt nuorehkoihin metsiin. Klusteroinnin löytämille tuholuokille oli tyypillistä keski-infrapunasäteilyn intensiteettien jyrkkä nousu, jota ei ollut tavattu yhtä selkeänä ohjatuissa luokituksissa.

Karttatulostukset muutoksista

Metsätuhoiksi tulkittujen alueiden (kuvat 37, 38 ja 39) maantieteellinen jakauma on samanlainen kuin laaja-alaisten intensiteettimuutosten sijainti analogisissa kuvissa. Tuhoiksi tulkitut alueet sijaitsivat ylängöillä, mutta eivät kaikkein korkeimmilla paikoilla (kuva 40).

Suuri osa taimistonhoitoluokkaan lukeutuneesta alueesta edusti vuodenaikaismuutoksia soilla. Myös maanmuokkausluokassa oli muuta aluetta kuin uudistusalojen maanmuokkausta (kuvat 42 ja 43). Kuvasegmenteittäin tehty moodisuodatus erotti todelliset avohakkuut paremmin ympäristöstään kuin alkuperäinen luokitus (kuva 44a ja b). Moodisuodatuksella yleistetty tulkintatulos voidaan muuntaa vektorimuotoon ja siirtää numeeriseen karttajärjestelmään (kuva 45).

MUUTOSTEN HAVAITSEMISEN MAHDOLLISUUDET

Tutkimus antoi tietoa spektrisistä muutoksista, joita havupuumetsiköissä tapahtuvat maastomuutokset aiheuttivat. Koska maastomuutokset esiintyvät metsikön elinkaaren eri vaiheissa, saatiin tietoa metsiköiden yleisestä spektrisestä käyttäytymisestä. Myös muutostyyppien spektrinen erottuvuus selvitettiin.

Taulukossa 21 esiintyvien luokkien intensiteettiarvojen avulla laskettiin empiirinen malli männikön heijastussäteilyksi kiertoaikana (kuva 46a ja b sekä kuva 47a, b ja c). Malli oli samankaltainen kuin aiemmin esitetty laskennallinen malli. Suurimmat erot ovat maanmuokkauksen luokassa sekä heijastussuhteen alenemisen nopeudessa puuston vanhetessa. Maanmuokkaus nosti empiirisessä aineistossa paljon vähemmän punaisen valon heijastussuhdetta kuin laskennallisessa mallissa. Heijastussuhteen aleneminen ei ole lineaarista, vaan suhde alenee nopeasti puuston sulkeutumiseen asti, jolloin se on jo hyvin lähellä uudistuskypsän metsikön intensiteettejä.

Tulkinnassa oli mahdollista erottaa intensiteeteiltään vähäisempiä muutoksia, kun muutokset nimettiin etukäteen, kuin jos olisi yritetty havaita muutoksia satelliittikuviin pohjautuvassa yleisinventoinnissa.

Empiiriset havainnot tukivat luvussa 2.2 esitettyä teoriaa havumetsien ja lähi-infrapunasäteilyn suhteista. Lievä harvennushakkuu tai tuho saattaa alentaa lähi-infrapunasäteilyn heijastussuhdetta ja satelliittikuvien intensiteettejä. Lasku johtuu neulasten heijastusominaisuuksien muutoksista sekä kasvuston rakenteen muuttumisesta aiempaa epätasaisemmaksi. Epätasaisuus lisää kasvuston varjoisuutta. Voimakkaampi hakkuu tai

tuho nostavat heijastussuhdetta, kun absorboiva biomassa alittaa tietyn kynnysarvon. Kynnysarvo alittuu, kun merkittävä osa heijastuneesta lähi-infrapunasäteilystä tulee muualta kuin puustosta. Viljelysmaat poikkeavat lähi-infrapunasäteilyn heijastusominaisuuksiltaan metsistä, koska niiden biomassa voi olla vain noin kolmaskymmenesosa metsien biomassasta. Viljelysmailla osa heijastuneesta lähi-infrapunasäteilystä on aina peräisin muualta kuin kasveista.

Teorian mukaan havumetsien heijastussäteily vakiintuisi havumetsissä korkeammalla biomassatasolla kuin lehtimetsissä. Ero johtuu monien havupuiden latvusten muodosta. Tulosäteily pääsee tunkeutumaan syvemmälle kasvustoon havumetsissä kuin epätasaisissa lehtimetsissä. Havumetsien biomassan estimointi heijastussäteilyn avulla tulisi onnistua paremmin kuin lehtimetsien. Havupuiden latvusten muoto aiheuttaa myös niiden alhaisen heijastavuuden lähi-infrapuna-alueella.

Tuhoalue sijaitsi karuhkolla ylängöllä, joka oli osittain niin sanottua vedenkoskematonta aluetta. Avokallio oli useissa kohden lähellä pintaa (kuvat 38 ja 39).

Parhaat spektriset piirteet muutosten havaitsemiseksi olivat punainen valo, lähi-infrapunasäteily sekä keski-infrapunasäteily. Kuvissa oli niin paljon muuta kuin muutoksista johtuvaa vaihtelua, että pääkomponenttimuunnokset ja kanoniset muunnokset eivät toimineet hyvin. Samasta syystä ohjatut luokitusmenetelmät antoivat parempia tuloksia kuin ohjaamaton menetelmä. Talvikuvat eivät osoittautuneet hyödyllisiksi, koska lumen heijastussuhde on niin paljon suurempi kuin kasvipeitteen.

Kuvien radiometrisen herkkyyden parantumisesta olisi todennäköisesti hyötyä muutosten erottamiselle, samoin maastonerotuskyvyn. Nykyisten satelliittikeilainkuvien spektrinen erotuskyky ei näytä olevan kriittisin tekijä muutosten tulkinnan kannalta.

Vaikka maximum likelihood -luokitus näyttää parhaalta yleisesti käytettävissä olevalta muutosten tulkintamenetelmältä, sen puutteena on korkeat vaatimukset maastoaineistolle. Maastohavaintoja täytyy olla paljon ja intensiteeteiltään läheisten luokkien hajontojen tulisi olla samankaltaisia.

Maastoaineisto oli alun perin kerätty muihin tarkoituksiin kuin kuvatulkintaan. Se oli tästä syystä osittain epätarkka. Toisaalta aineisto oli monipuolinen ja mahdollisti kokonaiskuvan saamisen muutosten spektrisistä vaikutuksista.

OSA II

SATELLIITTIKUVIIN PERUSTUVAN MUUTOSTEN TULKINNAN KÄYTÄNNÖN SOVELTAMISESTA

Muutosluokkien pinta-ala oli valtakunnan metsien inventoinnin aineistossa noin 10 prosenttia vuodessa. Vain puolet muutoksista oli hakkuita.

Satelliittikuviin perustuvaa muutosten seurantaa voidaan käyttää metsätaloussuunnitelman päivityksessä, metsän käsittelyn suunnittelussa, otantainventoinnin päivityksessä sekä ekologiseen tutkimukseen.

Kuvien taltioinnin ajoituksessa voidaan noudattaa samoja periaatteita kuin muidenkin mittausten ajoituksessa. Kuvien aikajänteen tulee olla lyhyt, jos ollaan kiinnostuneita äkillisistä muutoksista ja pitkä, jos halutaan havaita kasvua. Kuvien tulee olla kesäajalta, mieluiten heinä-elokuulta.

Maastoaineisto on syytä kerätä erikseen kuvatulkintaa varten, kun halutaan seurata muutoksia, joiden vaikutukset intensiteetteihin ovat vähäisiä, kuten kasvatushakkuita tai taimistonhoitoa. Paras maastoaineisto koostuu muutosta edustavista metsiköistä ja muuttumattomista referenssimetsiköistä, kuten tässä tutkimuksessa. Metsikkötiedot voidaan kerätä normaalin taloustoiminnan yhteydessä. Muutosmetsikön viereinen metsikkö voidaan usein ottaa vertailuluokkaa edustavaksi metsiköksi. Intensiteettiarvot on syytä poimia pienemmältä alalta kuin metsikön todelliset rajat.

Muutosten tulkintaan lasketaan maximum likelihood -luokittelumalli käyttäen joko alkuperäisiä kanavia tai ilman histogrammien sovitusta laskettuja erotuskanavia. Erotuskanavien etuna on, että kasvustojen biomassa- ja kasvupaikkaerojen merkitys vähenee, jolloin luokkia tarvitaan vähemmän ja selvitään vähemmällä maastoaineiston keruulla. Haittana on muutosluokkien sekoittuminen keskenään. Ohjaamaton tulkinta on syytä yhdistää muutosten tulkintaan, jos kaikkia muutostyyppejä ei tunneta hyvin ennalta.

Muutosten estimointimenetelmän harhaisuutta pystytään vähentämään antamalla pienemmät ennakkotodennäköisyydet muutosta edustaville luokille kuin muille luokille, jos muutosluokkien oletettu pinta-ala on pienempi kuin muiden luokkien. Harhaisuuden minimoiminen tulkintavaiheessa ei kuitenkaan ole aina järkevää. Mikäli esimerkiksi tavoitteena on tehdä tarkka kartta muutoksista ja hankkeeseen on käytettävissä runsaasti varoja, kannattaa pyrkiä siihen, että kaikki muutokset lukeutuvat muutosluokkiin, vaikka näihin luokkiin lukeutuisi paljon muuttumatontakin metsäaluetta. Maastotarkastukset voidaan silloin keskittää muutoksiksi tulkittuihin alueisiin.

Keskipitkän aikavälin operatiivista suunnittelua varten muutostiedot saadaan visuaalisen tai numeerisen tulkinnan tai näiden yhdistelmän avulla. Hyväksi käytetään paikkatietojärjestelmäohjelmistoa. Useimmat muutosta edustavat tulkintaluokat on tarkastettava maastossa tai ilma-aluksesta esimerkiksi videokuvauksen avulla (kuva 48).

Tulkintatulos voidaan kalibroida valtakunnan metsien inventointi -tyyppistä inventointia varten esimerkiksi mittaamalla maastossa suurehkoilta, otannalla valituilta alueilta, muutosten todelliset pinta-alat ja korjaamalla tulkintatulosta maastoinventoinnin mukaan (kuva 49). Päivitetyt tulokset voidaan laskea mille tahansa maastossa mitatulle muuttujalle tulkintatuloksen avulla. Tulosten luotettavuus riippuu maastomuuttujien ja tulkintaluokkien välisen riippuvuuden kiinteydestä.

Tutkimuksessa kehitettyä männikön spektrisen elinkaaren mallin ja muun metsän muutoksia koskevan tiedon avulla voidaan kehittää täysin automaattinen muutosten tulkinnan järjestelmä. Menetelmän vaiheet ovat (kuva 50):

1) Kuvien oikaisu
2) Homogeenisten 2 x 2 -kuvanalkioryhmien etsiminen
3) Kuvanalkioryhmien järjestäminen klusteroinnilla
4),5) Muutoksen havaitseminen klusteroinnin tuottamien ryhmien hajontoja tarkastelemalla
6) Muutoksen tunnistaminen mallin avulla
7),8) Luokituksen teko

APPENDIX 1

RESULTS OF TUKEY'S STUDENTIZED RANGE TESTS

An asterisk * means that the intensity means of classes have considered significantly different with the significance level of 5 percent. Description of spectral features in the end of Table 1.

Table 1. Tukey's studentized range tests to image pair TMI84/TMI85.

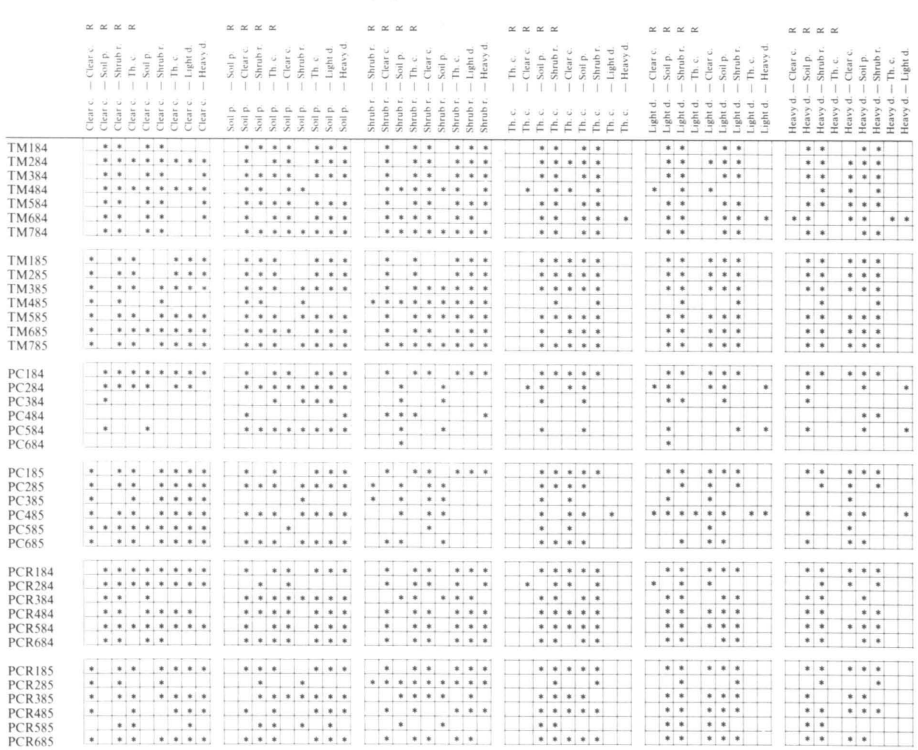

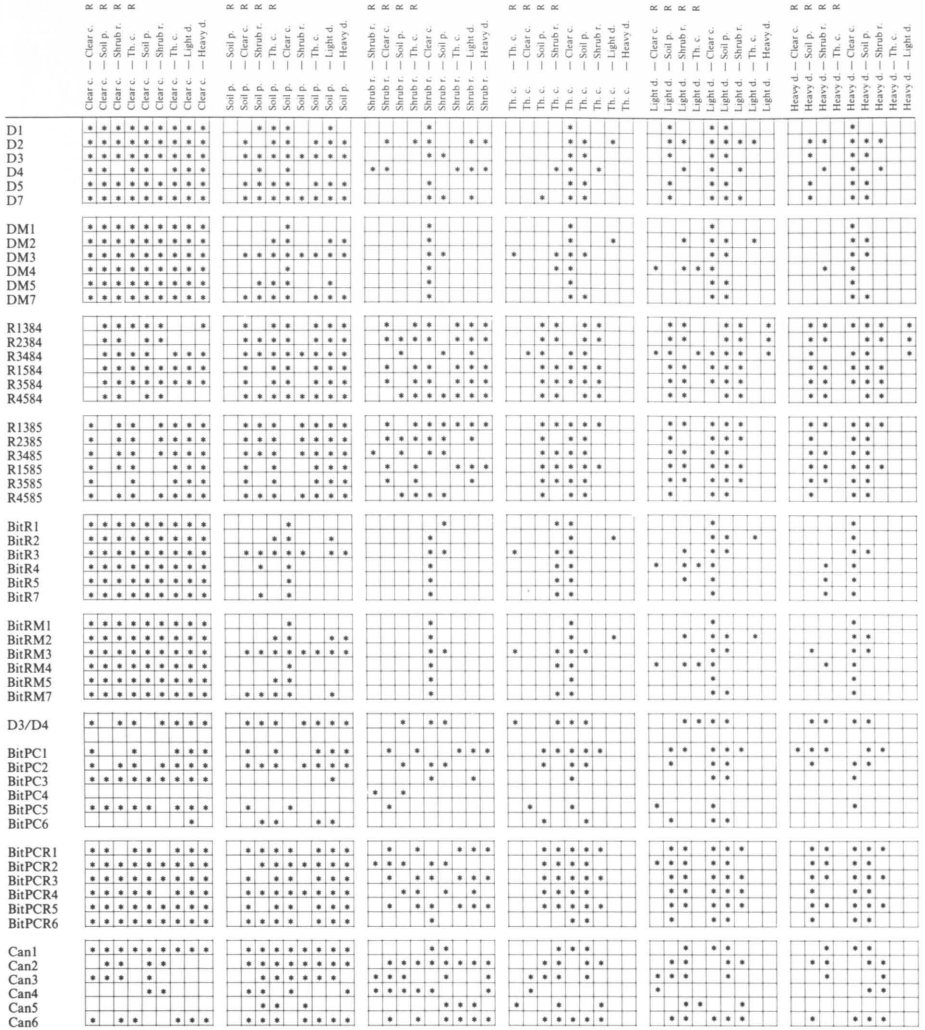

Data: Set1 and Dam. No. of observations: 256

Legend:

TMkyr	Channel k (1—7) of a Landsat Thematic Mapper image. Optional yr stands for the last two digits of the year of the image acquisition. It is used with all abbreviations but only when the context does not tell the year.
SSk	Channel k (1—3) of the Spot summer image.
Dk	Difference channel k calculated from paired bitemporal channels without histogram matching.
DMk	Difference channel k calculated with histogram matching.
Rkl	Ratio feature from channels k and l of monotemporal TM image.
BitRk	Ratio feature from bitemporal paired original channels k.
BitRMk	Ratio feature from bitemporal matched channels k.
DTex	Local variance channel of D3. Window size for variance calculation 3 x 3 pixels. Used only in one final classification.
PCk	k'th principal component computed from covariance matrix of a monotemporal TM image.
PCRk	k'th principal component computed from correlation matrix of a monotemporal TM image.
BitPCk	k'th principal component computed from covariance matrix of a merged bitemporal TM image pair.
BitPCRk	k'th principal component computed from correlation matrix of a merged bitemporal TM image pair.
Cank	k'th canonical variable computed from a merged bitemporal TM image pair.
DGreen	SS1-TM284 without histogram matching
DRed	SS2-TM384 without histogram matching
DNIR	SS3-TM484 without histogram matching
DMGreen	SS1-TM284 with histogram matching
DMRed	SS2-TM384 with histogram matching
DMNIR	SS3-TM484 with histogram matching

Table 2. Tukey's studentized range tests to image pair TMI85/TMI86.

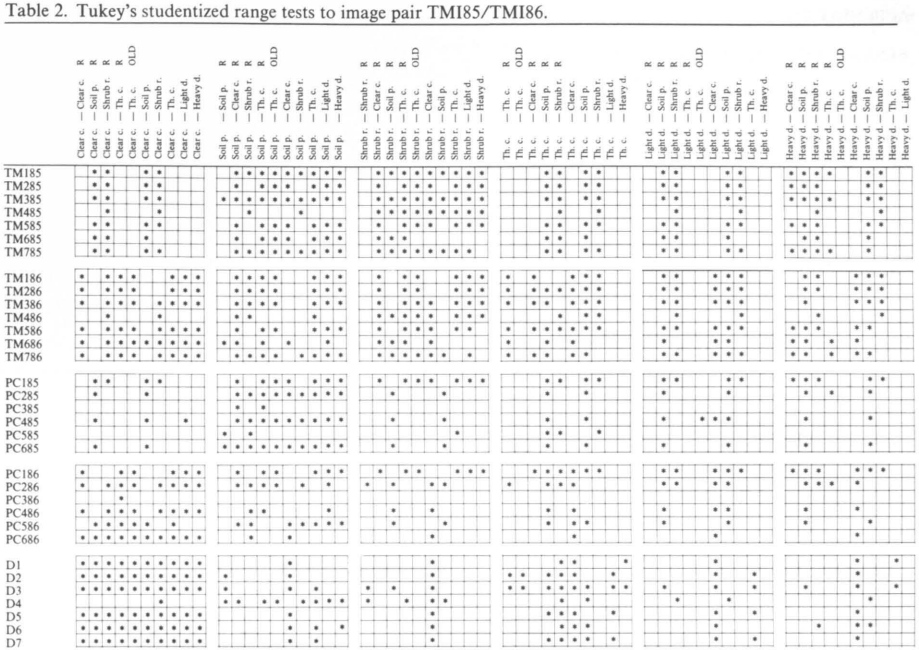

Data: Set2, Dam, from Set1 21 stands where the thinning cutting had been made between images TMI84 and TMI85. No. of observations: 201

Table 3. Tukey's studentized range tests to image pair TMI84/SSI87.

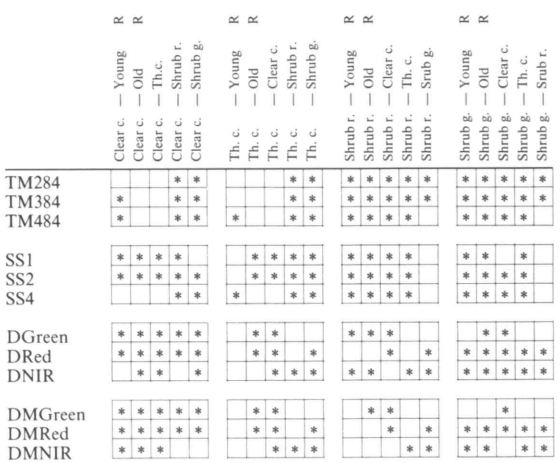

Data: PNFI
No. of observations: 176

APPENDIX 2

RESULTS OF SUPERVISED CLASSIFICATIONS

Table 1. Test result of the MLOrigAltF -classification to image pair TMI84/TMI85.

Field observation	Interpretation: Corresponding class in interpretation						
	C	T	D	S	P	N	Tot.
Clear c.	**6**	0	0	0	0	3	9
Clear c.R	0	0	1	0	0	**7**	8
Th. c.	1	**0**	7	0	0	19	27
Th. c. R	0	0	2	0	0	**17**	19
Light d.	0	0	**16**	0	0	4	20
Heavy d.	0	0	**6**	0	0	4	10
Shrub r.	0	0	0	**0**	0	0	0
Shrub r. R	0	0	0	0	0	**16**	16
Soil p.	0	0	0	0	**2**	7	9
Soil p. R	0	0	0	0	0	**3**	3
Total	7	0	32	0	2	80	121

Test data: Set1T, DamT
Legend:
D — combined light and heavy damage classes
N — combined reference classes
Other legend in the end of the Appendix

Table 2. Test result of the MLDiffEqF -classification to image pair TMI84/TMI85.

Field observation	Interpretation: Corresponding class in interpretation						
	C	T	D	S	P	N	Tot.
Clear c.	**6**	0	0	0	0	3	9
Clear c. R	0	0	1	0	0	**7**	8
Th. c.	0	**0**	14	0	0	13	27
Th. c. R	0	0	8	0	0	**11**	19
Light d.	0	0	**18**	0	0	2	20
Heavy d.	0	0	**7**	0	0	3	10
Shrub r.	0	0	0	**0**	0	0	0
Shrub r. R	0	0	2	0	0	**14**	16
Soil p.	0	0	0	0	**2**	7	9
Soil p. R	0	0	0	0	0	**3**	3
Total	7	0	32	0	2	80	121

Test data: Set1T, DamT
Legend:
D — combined light and heavy damage classes
N — combined reference classes
Other legend in the end of the Appendix

Table 3. Test result of the MLDiffTexEq -classification to image pair TMI84/TMI85.

Field observation	Interpretation: Corresponding class in interpretation										
	C	CR	T	TR	L	H	S	SR	P	PR	Tot.
Clear c.	**8**	0	0	0	0	0	1	0	0	0	9
Clear c. R	1	**6**	0	0	1	0	0	0	0	0	8
Th. c.	2	0	**0**	0	16	5	0	0	0	4	27
Th c. R	0	0	0	**4**	9	1	1	3	0	1	19
Light d.	0	0	0	1	**15**	4	0	0	0	0	20
Heavy d.	0	0	0	0	5	**1**	0	2	0	2	10
Shrub r.	0	0	0	0	0	0	**0**	0	0	0	0
Shrub r. R	0	2	0	0	2	0	0	**12**	0	0	16
Soil p.	3	0	0	0	0	0	0	0	**3**	3	9
Soil p. R	0	0	0	0	0	0	0	0	0	**3**	3
Total	14	8	0	5	48	11	2	17	3	13	121

Test data: Set1T, DamT
Legend: in the end of the Appendix

Table 4. Test result of the Euclidean classification to image pair TMI85/TMI86.

Field observation	Interpretation: Corresponding class in interpretation											
	C	CR	T	TR	L	H	S	SR	P	PR	Tot.	
Clear c.	**6**	0	0	0	0	0	0	0	0	0	6	
Clear c. R	0	**4**	0	0	0	0	0	1	0	0	5	
Th. c.	1	1	**4**	2	1	6	0	0	0	0	15	
Th c. R	0	14	2	**10**	9	2	0	4	1	0	42	
Light d.	0	2	1	3	**10**	4	0	0	0	0	20	
Heavy d.	0	2	1	1	1	**4**	0	1	0	0	10	
Shrub r.	0	0	0	0	0	0	**0**	1	0	0	1	
Shrub r. R	0	1	0	1	2	0	2	**13**	2	0	21	
Soil p.	0	0	1	0	1	0	0	1	**5**	0	8	
Soil p. R	0	0	0	0	0	0	0	0	0	**0**	0	
Total	7	25	9	17	24	16	2	21	8	0	128	

Classified to clouds: 0 stands.

Test data: Set2T, DamT, from Set1 20 thinning cuts where the cutting had been made before acquisition of image TMI85. Were added to Th c. R class.
Legend: in the end of the Appendix

Table 5. Test result of the MLOrigEq -classification to image pair TMI85/TMI86.

Field observation	Interpretation: Corresponding class in interpretation										
	C	CR	T	TR	L	H	S	SR	P	PR	Tot.
Clear c.	**5**	0	1	0	0	0	0	0	0	0	6
Clear c. R	0	**4**	0	1	0	0	0	0	0	0	5
Th. c.	1	4	**1**	1	0	5	0	2	0	0	14
Th c. R	0	21	0	**4**	9	3	1	4	0	0	42
Light d.	0	3	0	0	**13**	4	0	0	0	0	20
Heavy d.	0	1	0	1	3	**4**	0	1	0	0	10
Shrub r.	0	0	0	0	0	0	**0**	1	0	0	1
Shrub r. R	0	1	1	1	0	0	1	**17**	0	0	21
Soil p.	0	0	0	0	1	0	0	1	**6**	0	8
Soil p. R	0	0	0	0	0	0	0	0	0	**0**	0
Total	6	34	3	8	26	16	2	26	6	0	127

Classified to clouds: 1 stand.

Test data: Set2T, DamT, from Set1 20 thinning cuts where the cutting had been made before acquisition of image TMI85. Were added to Th c. R class.
Legend: in the end of the Appendix

Table 6. Test result of the MLOrigAlt -classification to image pair TMI85/TMI86.

Field observation	Interpretation: Corresponding class in interpretation										
	C	CR	T	TR	L	H	S	SR	P	PR	Tot.
Clear c.	**6**	0	0	0	0	0	0	0	0	0	6
Clear c. R	0	**4**	0	1	0	0	0	0	0	0	5
Th. c.	1	4	**0**	2	0	4	0	3	0	0	14
Th c. R	0	21	0	**6**	5	3	1	5	0	1	42
Light d.	0	3	0	0	**13**	4	0	0	0	0	20
Heavy d.	0	1	0	1	3	**4**	0	1	0	0	10
Shrub r.	0	0	0	0	0	0	**0**	1	0	0	1
Shrub r. R	0	1	1	1	0	0	0	**18**	0	0	21
Soil p.	0	0	0	0	1	0	0	1	**6**	0	8
Soil p. R	0	0	0	0	0	0	0	0	0	**0**	0
Total	7	34	1	11	22	15	1	29	6	1	127

Classified to clouds: 1 stand.

Test data: Set2T, DamT, from Set1 20 thinning cuts where the cutting had been made before acquisition of image TMI85. Were added to Th c. R class.
Legend: in the end of the Appendix

Table 7. Test result of the MLDiffEq -classification to image pair TMI85/TMI86.

Field observation	Interpretation: Corresponding class in interpretation										
	C	CR	T	TR	L	H	S	SR	P	PR	Tot.
Clear c.	**6**	0	0	0	0	0	0	0	0	0	6
Clear c. R	0	**1**	0	0	3	1	0	0	0	0	5
Th. c.	1	0	**0**	0	0	11	2	0	0	0	14
Th c. R	0	9	0	**0**	20	7	0	2	2	1	41
Light d.	0	3	0	0	**12**	4	0	0	1	0	20
Heavy d.	0	3	0	0	2	**4**	0	0	1	0	10
Shrub r.	0	0	0	0	0	0	**1**	0	0	0	1
Shrub r. R	0	2	0	1	3	0	0	**12**	1	2	21
Soil p.	0	1	0	1	0	1	0	2	**3**	0	8
Soil p. R	0	0	0	0	0	0	0	0	0	**0**	0
Total	17	19	0	2	40	28	3	16	8	3	126

Classified to clouds: 2 stands.

Test data: Set2T, DamT, from Set1 20 thinning cuts where the cutting had been made before acquisition of image TMI85. Were added to Th c. R class.
Legend: in the end of the Appendix Table 8. Test result of the MLOrigAlt -classification to image pair TMI84/SSI87.

Legend for all tables:

Clear c.	Clear cut
Clear c. R	Clear cut reference
Th. c.	Thinning cut
Th. c. R	Thinning cut reference
Light d.	Light damage
Heavy d.	Heavy damage
Shrub r.	Shrub removal
SAhrub r. R	Shrub removal reference
Soil p.	Soil preparation
Soil p. R	Soil preparation reference

Table 8. Test result of the MLOrigAlt -classification to image pair TMI84/SSI87.

Field observation	Interpretation: Corresponding class in interpretation							
	C	R1	T	R2	S	G	Rej	Tot.
Clear c.	**1**	3	0	5	3	0	11	23
Reference 1	0	**56**	11	9	3	5	2	86
Th. c.	0	40	**12**	10	0	2	0	64
Reference 2	0	21	4	**8**	13	5	4	55
Shrub r.	0	2	0	3	**7**	10	0	22
Shrub g.	0	0	0	0	0	**0**	0	0
Total	1	122	27	35	26	22	17	250
Soil p.	0	0	0	2	0	15	0	17
Light d.	0	7	9	1	0	1	2	20
Heavy d.	0	2	1	5	0	1	1	10
Total	1	131	37	43	26	39	20	297

Performance (from 250 observations)

Overall: 34 %
Changed classified to changed: 21 % from changed
Unchanged classified to unchanged: 67 % from unchanged
Test data: Set1A (changed), Set2A (changed), DamT, PNFIT

Reference 1 — unchanged, stem volume ≥ 40 m^3/ha, from PNFI
Reference 2 — unchanged, stem volume 0 — 39 m^3/ha, from PNFI
Shrub g. — Shrub growth
Other legend in the end of the Appendix

Instructions to authors — Ohjeita kirjoittajille

Submission of manuscripts

Manuscripts should be sent to the editors of the Society of Forestry as three full, completely finished copies, including copies of all figures and tables. Original material should not be sent at this stage.

The editor-in-chief will forward the manuscript to referees for examination. The author must take into account any revision suggested by the referees or the editorial board. Revision should be made within a year from the return of the manuscript. If the author finds the suggested changes unacceptable, he can inform the editor-in-chief of his differing opinion, so that the matter may be reconsidered if necessary.

Decision whether to publish the manuscript will be made by the editorial board within three months after the editors have received the revised manuscript.

Following final acceptance, no fundamental changes may be made to manuscript without the permission of the editor-in-chief. Major changes will necessitate a new submission for acceptance.

The author is responsible for the scientific content and linguistic standard of the manuscript. The author may not have the manuscript published elsewhere without the permission of the publishers of Acta Forestalia Fennica. The series accepts only manuscripts that have not earlier been published.

The author should forward the final manuscript and original figures to the editors within two months from acceptance. The text is best submitted on a floppy disc, together with a printout. The covering letter must clearly state that the manuscript is the final version, ready for printing.

Form and style

For matters of form and style, authors are referred to the full instructions available from the editors.

Käsikirjoitusten hyväksyminen

Metsäntutkimuslaitoksesta lähtöisin olevien käsikirjoitusten hyväksymismenettelystä on ohjeet Metsäntutkimuslaitoksen julkaisuohjesäännössä.

Muista käsikirjoituksista lähetetään Suomen Metsätieteellisen Seuran toimitukselle kolme täydellistä, viimeisteltyä kopiota, joihin sisältyvät myös kopiot kaikista kuvista ja taulukoista. Originaaliaineistoa ei tässä vaiheessa lähetetä.

Vastaava toimittaja lähettää käsikirjoituksen valitsemilleen ennakkotarkastajille. Tekijän on otettava huomioon ennakkotarkastajien ja toimituskunnan korjausesitykset. Korjaukset on tehtävä vuoden kuluessa siitä, kun käsikirjoitus on palautettu tekijälle. Jos tekijä ei voi hyväksyä korjausesityksiä, hänen on ilmoitettava eriävä mielipiteensä vastaavalle toimittajalle tai toimituskunnalle, joka tarvittaessa ottaa asian uudelleen käsittelyyn.

Acta Forestalia Fennican toimituskunta päättää kirjoituksen julkaisemisesta ennakkotarkastajien lausuntojen ja muiden ilmenneiden seikkojen perusteella. Päätös tehdään kolmen kuukauden kuluessa siitä, kun käsikirjoituksen lopullinen korjattu versio on saapunut toimitukselle.

Hyväksymisen jälkeen käsikirjoitukseen ei saa tehdä olennaisia muutoksia ilman vastaavan toimittajan lupaa. Suuret muutokset edellyttävät uutta hyväksymistä.

Tekijä vastaa kirjoituksen tieteellisestä asiasisällöstä ja kieliasusta. Tekijä ei saa julkaista kirjoitusta muualla ilman Acta Forestalia Fennican julkaisijoiden suostumusta. Acta Forestalia Fennicaan hyväksytään vain aiemmin julkaisemattomia kirjoituksia.

Tekijän tulee antaa lopullinen käsikirjoitus ja kuvaoriginaalit toimitukselle kahden kuukauden kuluessa hyväksymispäätöksestä. Käsikirjoituksen saatteesta pitää selvästi ilmetä, että käsikirjoitus on lopullinen, painoon tarkoitettu kappale. Teksti otetaan mieluiten vastaan mikrotietokoneen levykkeellä, jonka lisäksi tarvitaan paperituloste.

Käsikirjoitusten ulkoasu

Käsikirjoituksen asun tulee noudattaa sarjan kirjoitusohjeita, joita saa toimituksesta.

219 **Heliövaara, Kari, Väisänen, Rauno & Immonen, Auli.** Quantitative biogeography of the bark beetles (Coleoptera, Scolytidae) in northern Europe. Seloste: Pohjois-Euroopan kaarnakuoriaisten kvantitatiivinen eliömaantieteellinen analyysi.

220 **Kuusela, Kullervo & Salminen, Sakari.** Suomen metsävarat 1977–1984 ja niiden kehittyminen 1952–1980. Summary: Forest resources of Finland in 1977–1984 and their development in 1952–1980.

221 **Pohjonen, Veli.** Selection of species and clones for biomass willow forestry in Finland. Tiivistelmä: Biomassan viljelyyn sopivien pajulajien ja -kloonien valinta Suomessa.

222 **Häme, Tuomas.** Spectral interpretation of changes in forest using satellite scanner images. Seloste: Metsän muutosten spektrinen tulkinta satelliittikeilainkuvien avulla.

223 **Finér, Leena.** Effect of fertilization on dry mass accumulation and nutrient cycling in Scots pine on an ombrotrophic bog. Seloste: Lannoituksen vaikutus männyn kuivamassan kertymään ja ravinteiden kiertoon ombrotrofisella rämeellä.

224 **Heikkilä, Risto.** Moose browsing in a Scots pine plantation mixed with deciduous tree species. Tiivistelmä: Hirven ravinnonkäyttö lehtipuusekoitteisessa mäntytaimikossa.

ISBN 951-651-092-2
ISSN 0001-5636